DEGRADATION MODELING OF INK FADING AND DIFFUSION OF PRINTED IMAGES

by

ZIYI WANG

A dissertation submitted to the

School of Graduate Studies

Rutgers, The State University of New Jersey

In partial fulfillment of the requirements

For the degree of

Doctor of Philosophy

Graduate Program in Industrial and Systems Engineering

Written under the direction of

Elsayed A. Elsayed

And approved by

_____

_____

_____

_____

New Brunswick, New Jersey

JANUARY, 2020

ABSTRACT OF THE DISSERTATION

Degradation Modeling of Ink Fading and Diffusion of Printed Images

By ZIYI WANG

Dissertation Director:

Elsayed A. Elsayed

Color printing plays an important role in the modern society. It is known that the color of printed images degrades gradually due to the fading and diffusion of the inks. Color degradation leads to a distortion or loss of the original information in printed images. Therefore, it is desirable to understand how the color of printed images changes over time. In this dissertation, we present degradation models to predict the characteristics of the ink fading and diffusion of printed images.

We begin by modeling the ink degradation from a physics-based perspective. Color images are printed by projecting small ink dots on medium, usually paper. This technique is called halftone printing. Halftone printing of color images results in a variety of ink mixtures and subsequently their potential catalytic fading. For the most commonly used Cyan-Magenta-Yellow-Black (CMYK) ink set, sixteen possible ink mixtures are generated during printing. A state transition diagram is then proposed for the ink fading in this multi-ink printing scenario. The ink area coverage is used as the performance indicator. Assuming constant fading and diffusion rates, we develop an ink fading model based on the differential

equations according to the state transition diagram and an autoregressive ink diffusion model by discretizing the two-dimensional diffusion equation. The two models are then integrated into a single degradation model.

Further examination of the developed degradation models reveals that the fading or diffusion rate is equivalent to the hazard rate in reliability engineering. It is known that the hazard rate of the exponential failure time distribution is constant. Hence, the developed degradation model with constant fading and diffusion rates is equivalent to the multistate Markov process model with exponential transition time distribution. By using non-exponential transition time distributions, the fading and diffusion rates become time-varying and a more general semi-Markov process degradation model is developed accordingly.

Moreover, stochastic process models are investigated to provide stochastic area coverage prediction for the ink degradation. We first model the ink fading using the Hull-White/Vasicek (HWV) stochastic process. The HWV ink fading model considers that the variance of the ink area coverage shrinks as it approaches zero. Besides, spatial convolution is used to model ink diffusion. The two models are integrated into a spatio-temporal stochastic degradation model for the ink fading and diffusion of printed images. The cases of recurrent and non-recurrent time-varying fading and diffusion rates are investigated.

Inks on the paper degrade, so does the paper. The degradation of paper condition may in turn affect the degradation of the inks. Therefore, the investigation of the degradation

modeling of ink fading and ink diffusion with ink-paper interactions is needed. Two aspects of the ink-paper interactions are considered, i.e., the effect of paper aging such as depolymerization and yellowing, and the fiber orientation of the paper.

The degradation process of printed images usually takes a very long time. An accelerated degradation model and the optimal design of accelerated degradation test planning is developed for accurate degradation prediction of printed images. The effects of three constant environmental stresses: temperature, humidity, and illumination (intensity), are investigated, and experimental data are used to validate the proposed model. The results show strong agreements between the proposed ink fading and ink diffusion prediction model and the actual experimental data.

ACKNOWLEDGMENTS

I would like to express my deepest gratitude to my adviser Dr. Elsayed A. Elsayed for his patient guidance and caring support throughout the years of my PhD study. It would not have been possible to complete this dissertation without his great effort and devotion. The education and training I received at Rutgers set high standards for me to follow in the future days of my life. My gratitude is extended to the committee members of my dissertation, Dr. Hoang Pham, Dr. Weihong Guo, and Dr. Minge Xie, for their valuable comments and advice. Besides, my special thanks go to Design Specialist Joe Lippencott for his help on the experimental set-up of this research. I would also like to thank my friends who accompanied me in the bittersweet days at this school. Finally, I sincerely thank my parents for their unconditional standing-by my side.

TABLE OF CONTENTS

LIST OF TABLES

LIST OF ILLUSTRATIONS

CHAPTER 1

INTRODUCTION

1.1 Motivation of the Work

The modern color printing method is based on the color mixing theory. The first color photograph was taken in 1861 to demonstrate Maxwell's principle of three color synthesis. Color photographic films were first introduced by Kodak in 1935 (Wilhelm and Brower 1993). Since then, new color printing products have been continuously introduced into the mass market.

Unlike the long-lasting life of black-and-white photographs that are made of permanent metallic silver, early color photographs usually fade rapidly. The discoloration of colorant particles induced by the inherent instability of early chromogenic dyes leads to easily observed fading of printed color photographs in just a few months or years. Kodacolor, a color negative film introduced by Kodak in 1942, is known for causing "The Totally Lost Kodacolor Era of 1942-1953." (Nash *et al.* 2007)

Color printers are now widely used in printing color photographs, posters, and brochures. The printing industry is especially concerned with the durability of printed images. In addition, fading of printed color materials would be a major concern to museums, galleries, and archives since their collections are intended to be preserved for decades or hundreds of years. Understanding the degradation process of printed images would help in both the preservation and the restoration of their collections. Therefore, the permanence of printed

images has received considerable research attention (Wilhelm and Brower 1993, Wilhelm and McCormick-Goodhart 2000, Wilhelm 2004, Medley 2009, Kimmel *et al.* 2013, Kimmel and Baranoski 2016). However, the question regarding the expected life of printed images remains incompletely addressed. Traditional lifetime estimations of photographic inks are often simple linear extrapolations from accelerated degradation tests (Bugner and Lindstrom 2006, Campbell *et al.* 2007). As color printers are widely used today, there is an urgent need to accurately predict the longevity of printed images.

The motivation of this research is to investigate new approaches for predicting the degradation of printed images while considering the effect of the paper and the environmental stresses on the image degradation process. Such a prediction method would be beneficial for manufacturers in improving the quality of their products.

1.2 Color Printing Technologies

As photography moved into the digital printing era, a great variety of printing devices, papers, and inks were developed to meet consumers' needs. In this section, we present a brief introduction to modern color printing technologies (Image Permanence Institute 2004).

1. *Traditional Silver-Halide Prints*

The light-sensitive silver halide is used to form color dyes in this printing process. Silver-halide paper has three color emulsion layers (cyan, yellow, magenta) on top of the paper. The emulsion layers include either light-sensitive dyes or color

couplers which react with color developers to produce color dyes. Traditionally, color photographs are printed by exposing the photographic paper to light passing through a negative via an optical enlarger. Today, laser or light-emitting diodes (LEDs) are used instead to print digital images.

2. *Inkjet Prints*

In inkjet printing, small ink droplets are projected onto paper to create the image. Coated papers are preferred to print high-quality inkjet photographs since coating prevents the ink from spreading and creates the look and feel of traditional photographs. In general, two types of coated papers are used: swellable and porous. The ink-receiving layer of swellable paper is a moisture-sensitive polymer which swells in contact with the water-based ink and absorbs the colorants carried in the ink, whereas the surface of porous paper is composed of small pores in which colorants are deposited. Lacking a protective polymer layer in porous paper makes colorants more susceptible to environmental stresses, but the porous structure has the advantage of drying the printed photograph more quickly and reducing the possibility of smearing the image while the photograph is still wet.

The color of colorants is the result of the absorption of certain wavelengths of light. In general, the colorants used in inkjet printing are divided into two groups: dyes and pigments. Dyes are usually small-sized soluble molecules. Historically, dye-based inks produce more brilliant colors and larger color gamut than pigment-based inks and have better scratch resistance because dyes are absorbed by the paper due

to their small size. Beyond the merits, dye-based inks suffer from inferior stability under environmental stresses and potential catalytic fading problem. Pigments are large, insoluble aggregation of particles. Due to their larger size than dye particles, pigments are more stable than dyes, yet such property makes pigments less resistant to abrasion, since pigment particles stay on the surface of the paper, rather than being absorbed by it. From the perspective of image quality, pigments also offer less color brilliance and smaller color gamut than dyes. However, the problems with the two types of colorants are being mitigated or resolved as technology develops.

3. *Dye Diffusion Thermal Transfer Prints* (*Dye-Sublimation Prints*)

Dye diffusion thermal transfer printing, commonly known as dye sublimation printing, is frequently used for snapshot-size photo printers or in instant-photo kiosks. This printing technique uses heat to transfer colorants from a donor ribbon to the paper. The amount of dyes is controlled by varying the temperature on the printer head. A clear coating is usually applied during printing to protect the image from rubbing and environmental stresses.

4. *Electrophotographic Prints* (*Laser Prints*)

In this process, powdered inks are deposited on the paper by electrostatic charges (laser) and bound to the paper by heat and/or pressure. This is the technology used in laser printers and photocopiers. Usually, uncoated plain papers are used to print text documents. Although this technology can be used to print photographs, it cannot achieve high photo-quality printing.

Most, if not all, modern color printers use a small ink set to reproduce a wide range of colors. The most basic and the most commonly used ink set is the CMYK ink set, which is composed of cyan, magenta, yellow and black inks. Other ink sets may be used to expand the color gamut and enhance the color printing quality. During the printing process, inks are projected onto the paper as small dots. This technique is called halftone printing. Figure 1.1 shows some microscopic photos of halftone printed colors.

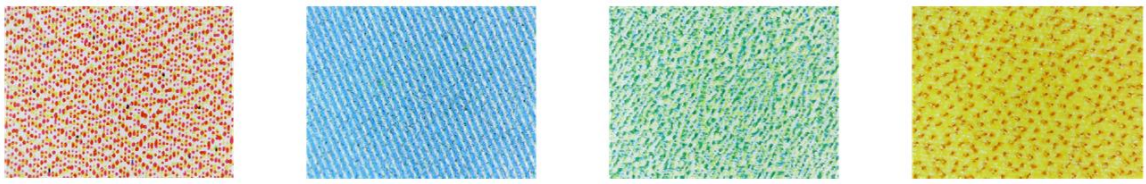

Figure 1.1 Microscopic photos of halftone printed colors

1.3 Color Measurement

An object appears colored because it absorbs certain wavelengths of visible light projected onto it and reflects or transmits the remaining; the light that enters human eyes would be perceived as color. Color can be defined by various color models that emulate human color perception. A color space is the set of all the colors that a color model defines. Color models do not have the same color space. Loss of color may happen when a color being converted from one color space lies outside the color space to which it is converted. Except for the colorimetric description of a color, densitometric measurements are traditionally used in the printing industry. Past research on the degradation of printed images focuses on taking colorimetric and/or densitometric measurements of printed images. Another color-

measuring method that has gained popularity in recent years is measuring the light spectrum. In this section, we discuss these three color-measuring methods.

1.3.1 *Colorimetry*

1. *RGB Color Model*

The RGB color model shown in Figure 1.2 is usually used in digital display devices such as televisions and computer monitors. The RGB color model is an additive model with three primary colors: red, green, and blue. Other colors are obtained by mixing the primary colors and represented in this color model as different integer values of the three primary colors, each ranging from 0 to 255. For example, black is defined as [R G B] = [0 0 0], and white is defined as [R G B] = [255 255 255]. Digital photos of printed images taken by a camera or a scanner are usually saved in the RGB format.

Figure 1.2 RGB color model

2. *CMY*(*K*) *Color Model*

The CMY（K) color model shown in Figure 1.3 is mainly used in the printing industry. Before printing a digital color image, the image is converted into the CMY(K) color model.

The CMY color model is composed of three primary colors of cyan, magenta, and yellow. It is called a subtractive color model because each of its three colors absorbs one primary color of the RGB color model. For example, the amount of cyan controls how much red light is absorbed. Theoretically, combining the three colors absorbs all the light and produce a black color. However, mixing the inks of the three colors cannot produce the desired black color in real-life printing, but a dark muddy brown. Therefore, the fourth color, black, is added. Moreover, using one black ink instead of three color inks not only saves on ink expenses but also dries more quickly.

Figure 1.3 CMY color model

3. *Lab Color Model*

The *Lab* color model is established by Commission internationale de l'éclairage (International Commission on Illumination). The color difference in this model is designed to match the difference perceived by human eyes. The *Lab* color model defines a color by its luminance and chrominance. The luminance is defined by *L*, with 0 representing complete darkness and 100 representing full brightness. The chrominance is defined by the red-green *a* and the yellow-blue *b*, each ranging from -128 to 127. The difference between two colors is mostly calculated in this perceptually uniform color space as

$$\Delta E = \sqrt{(L_1 - L_2)^2 + (a_1 - a_2)^2 + (b_1 - b_2)^2}$$

Above all, color is a human perception of visible light, colorimetric change in the *Lab* color space provides insufficient information in understanding the physical degradation process of printed images. McCormick-Goodhart and Wilhelm (2003b) address the problems with colorimetric measurements.

1.3.2 *Densitometry*

CMYK ink densities have traditionally been measured in the printing industry for quality control. Ink densities are measured using different filters and calculated from the percentage of the light reflected from the color as

$$\text{Density} = \log_{10} \frac{1}{\%\text{Reflectance}}$$

Table 1.1 shows the relationship between reflectance and ink density. The more inks are printed on the paper, the more light would be absorbed by the ink and the less light would be reflected, the higher the density is. As the paper gradually develops a yellowish color, the density of the paper should be subtracted from the ink density measurements to determine the absolute density loss of the inks.

Table 1.1 Relationship between reflectance and density

%Reflectance	Density
100%	0.0
10%	1.0
1%	2.0
0.1%	3.0
0.01%	4.0

Traditionally, ink density is collected using standard optical filters optimized for silver halide images. Since the modern color printing process is different from the silver halide printing process, the use of these filters in measuring non-silver halide color images is criticized for generating incorrect density measurements (Oldfield *et al.* 2004). For example, it is inappropriate to measure the CMYK ink densities for inks of other colors.

1.3.3 *Spectrum*

The spectral reflectance of color images has been measured for accurate color reproduction (Burns and Berns 1996, Tzeng and Berns 1998, Tzeng 1999, Wyble and Berns 2000). Such a method can be used in the image degradation test (Wilhelm *et al.* 2011) to determine the ink amount on paper. The spectral reflectance is measured every 5 or 10 nm across the visible light spectrum, roughly 400 to 700 nm in wavelength. Spectrum provides a higher level of accuracy than colorimetric or densitometric measurements. For example, measuring spectral reflectance helps minimize metamerism, which is a phenomenon that two different spectra result in the same color in human eyes. Figure 1.4 shows examples of the spectral reflectance of CMYK inks and white paper.

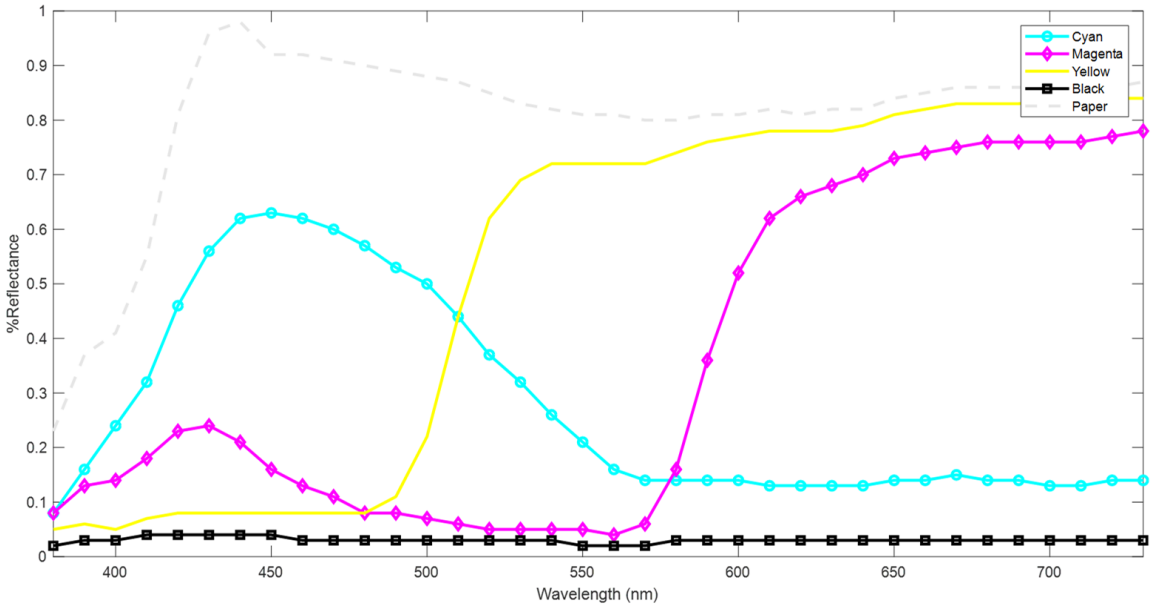

Figure 1.4 Examples of spectral reflectance of CMYK inks and white paper

1.4 Problem Definition

Color degradation of printed images can be the result of many chemical or physical causes. In this dissertation, we focus on two types of image degradation induced by inks (Image Permanence Institute 2009).

1. *Ink Fading*

   Ink fading results in two types of color degradation: overall fading and hue shift. In overall fading, inks fade at similar rates and the image appears somewhat bleached. While in hue shift, inks fade at different rates and the image gains the tone of the inks that fade slower.

Sometimes, the fading rate of an ink changes if it is overprinted with other inks. This phenomenon is called catalytic fading. One explanation is the energy absorbed by one ink transfers to another ink at a lower energy level, making it fades at an accelerated rate (Fryberg 2005). Moreover, under light fading, prints having multiple ink-receiving layers exhibit more pronounced catalytic fading than prints having ink mixture in a single layer, since each ink layer absorbs some wavelengths of light that would harm other inks (Wilhelm and Brower 1993). Today, ink sets with even twelve color inks are readily available to provide photo-quality printing. This makes catalytic fading a more difficult problem in image degradation prediction.

2. *Ink Diffusion*

Ink diffusion happens mostly when printed images are kept under high humidity conditions. The results are color change and loss of image sharpness.

Paper, the substrate on which inks are printed, as well undergoes degradation. Paper is a stochastic network of fibers that are primarily attached to each other by hydrogen bonds (Mao 2001). The fibers for papermaking chiefly come from wood. Wood-derived fibers are mainly composed of three components: cellulose, hemicellulose, and lignin (Roberts 2007). Lignin can easily develop a yellowish color, together with hemicellulose, which is not practically usable, should be removed during the pulping process to produce high-quality paper. In addition to fibers, various additives are added in most papers to improve the mechanical, chemical, and optical properties of the final paper. As the main component

of paper, cellulose has much longer molecular chains than hemicellulose and lignin. The breakage of the long cellulose chains into shorter ones is called depolymerization process, which reduces the strength and durability of paper. Besides, the fiber orientation distribution, as a result of the manufacturing process, is also an important parameter of the paper structure (Yang *et al.* 1987, Drouin and Gagnon 1993). Therefore, the ink-paper interactions: the effect of paper aging and fiber orientation on the fading and diffusion rates, is of great interest and should be studied.

Temperature, humidity, illumination, and air pollutants are four major environmental factors that affect the color degradation of printed images (Image Permanence Institute 2009). Ink fading and diffusion are accelerated at high temperature. Humidity is the main cause for ink diffusion; it is also indispensable in the chemical reactions that deteriorate the printed image. Illumination is characterized by two properties: spectral distribution and light intensity. Light at shorter wavelength (higher frequency) carries more energy. Generally, light deteriorates printed images by decomposing the ink molecules and heating up the print. Another frequently discussed environmental stress is the air pollutants in the atmosphere, especially ozone. These air pollutants are found to have detrimental effects on printed images. In this dissertation, we only consider three environmental stresses: temperature, humidity, and illumination (intensity only). The effect of the environmental stresses on the fading and diffusion rates, as well as the optimal design of accelerated degradation test planning, need to be investigated.

Current research lacks mathematical models that predict the degradation of printed images. This problem is addressed in this dissertation. We limit our research to ink fading and ink diffusion, while considering the effect of ink-paper interactions and environmental stresses. The objective is to develop a series of mathematical models for the two types of ink degradation under the multi-ink printing scenario, in order to predict the color degradation of printed images. The traditional CMYK ink set is chosen to study. To develop appropriate degradation models, we investigate the ink fading and diffusion from a physics-based perspective. Halftone printing of the CMYK ink set results in $2^4 = 16$ possible states, which are CMYK, CMY, MYK, CYK, CMK, MY, CY, CM, CK, MK, YK, C, M, Y, K, W (white paper). The assumption that ink dots on paper are of uniform concentration is often used in the field of color science for accurate image reproduction (Taplin 2001). Under this assumption, the ink amount is equivalent to its area coverage. We adopt this assumption and use area coverage as the performance indicator in this dissertation.

1.5 Organization of the Dissertation

The remainder of the dissertation is organized as follows. In Chapter 2, we review the degradation modeling of ink fading and diffusion of printed images as well as its degradation behavior under different environmental stresses. In addition, we provide a brief literature review of the general degradation models and accelerated degradation tests in reliability engineering. In Chapter 3, we present a state transition diagram for halftone-printed images and develop physics-based degradation models of ink fading and ink diffusion with constant fading and diffusion rates. In Chapter 4, we explore the equivalent Markov model and propose a more general semi-Markov degradation model to relax the

assumption of constant fading and diffusion rates. In Chapter 5, we investigate the statistics-based degradation modeling of ink fading and ink diffusion of printed images. In Chapter 6, the degradation modeling of ink-paper interactions is studied. In Chapter 7, accelerated degradation model is developed and the optimal accelerated degradation test planning is designed. In Chapter 8, conclusions and future research are discussed.

CHAPTER 2

LITERATURE REVIEW

In this chapter, we first present a literature review of the degradation of printed images, including the degradation mechanisms and models of ink fading and ink diffusion, ink-paper interactions of printed images, and accelerated testing of ink fading and ink diffusion. We then provide a literature review of the general degradation models and accelerated degradation tests in reliability engineering that are relevant to the topic of study.

2.1 Literature Review of Degradation of Printed Images

2.1.1 *Degradation Models of Printed Images*

To develop the degradation models of printed images, it is very important to understand the degradation behavior of inks. Ink fading can be thought of as a reaction process and be modeled from a kinetic perspective. Honda (1998) represents the fading of silver images as a first-order kinetic model

$$A \xrightarrow{k} B$$

where A is the non-discolored state, B is the discolored state, and k is the fading rate. Other research (Johnston-Feller *et al.* 1984, Pugh and Guthrie 2002, De Rossi *et al.* 2003) also confirm that the degradation of colorants can be described as a first-order reaction and the slowdown of the ink fading is attributed to the reduction of the remaining ink amount. The first-order reaction kinetic model has also been applied in the color degradation of food (Ahmed *et al.* 2002) and fresco (Shi and Lu 2005). In the field of reliability, kinetic models

have been developed for lifetime prediction in accelerated life tests (LuValle *et al.* 1988, Meeker and LuValle 1995).

Industry standards and systematic mathematical models of the degradation of printed images are still lacking. Most of the degradation models only deal with ink fading. Medley (2009) develops a semi-empirical kinetic model for light-induced magenta ink fading. The proposed model predicts the surface covered by the magenta ink as a function of time,

$$\theta_D = \theta_{D_0}\left[\alpha + (1-\alpha)e^{-(1-\theta_{D_0})\beta t}\right]$$

where θ_D is the fraction of the total surface occupied by the magenta ink, $\theta_D = \theta_{D_0}$ at time $t = 0$, and α and β are constant parameters for a given ink/paper combination. Kimmel *et al.* (2013, 2016) present a physical model of the absorptive properties of inks for spectral change prediction under light-induced fading. Gschwind (1989) investigates the digital restoration of faded color photographs and proposes that the faded ink density is the product of a bleach matrix and the original ink density,

$$\begin{bmatrix} Y' \\ M' \\ C' \end{bmatrix} = \begin{bmatrix} a_{11} & a_{12} & a_{13} & a_{14} \\ a_{21} & a_{22} & a_{23} & a_{24} \\ a_{31} & a_{32} & a_{33} & a_{34} \end{bmatrix} \begin{bmatrix} Y \\ M \\ C \\ 1.0 \end{bmatrix}$$

where *Y*, *M* and *C* are the original optical densities of the inks, *Y'*, *M'* and *C'* are the optical densities of the bleached inks, and the matrix coefficients are unknown parameters to be estimated.

Limited research has been carried out on ink diffusion of printed images. Kunii *et al.* (1995) simulate the diffusion of ink paintings using diffusion equation, which is a partial differential equation that describes the behavior of diffusing substances. Discretizing the diffusion equation in both time and space using finite difference method results in discrete-time discrete-space autoregressive models (Wikle 2003, Hooten and Wikle 2008, Malmberg *et al.* 2008). There is a significant research that focuses on autoregressive models. These models are either solved under a hierarchical Bayesian framework (Wikle *et al.* 1998, Sahu *et al.* 2007, Cameletti *et al.* 2013) or by making use of Kalman filter (Wikle 1999, Xu and Wikle 2007, Stroud *et al.* 2010). Besides, spatio-temporal models are widely studied and applied in fields like weather forecasting and ecological processes. Discrete-time continuous-space convolution-based models are proposed to model the spatio-temporal data (Wikle 2002, Xu *et al.* 2005, Dewar *et al.* 2009, Scerri *et al.* 2009, Sigrist *et al.* 2011, Sigrist *et al.* 2012). Brown *et al.* (2000) develop a model with non-separable space-time covariance function for blurring effect by applying a spatial Gaussian kernel to random field data. Its equivalent stochastic differential equation is also derived. Sigrist *et al.* (2015) develop a spatio-temporal model by solving the stochastic partial differential equation for the convection-diffusion process using Fourier transform. Liu *et al.* (2016) extend Brown's model by considering the spatial degradation generation and a Gaussian kernel with time-varying stress-dependent parameters. They establish the relationship between the proposed statistics-based degradation model and the physical convection-diffusion partial differential equation. Wu and Berland (2008) use a power law diffusion rate for time-dependent anomalous diffusion,

$$D_{ins}(t) = \frac{\alpha}{2n}\Gamma t^{\alpha-1}$$

and a multi-variate Gaussian function as the diffusion propagator,

$$f\left(\mathbf{r}',(t+\tau)\,|\,\mathbf{r},t\right)=\frac{1}{\left(2\pi\Gamma\tau^{\alpha}/n\right)^{n/2}}\exp\left(\frac{-|\mathbf{r}'-\mathbf{r}|^{2}}{2\Gamma\tau^{\alpha}/n}\right)$$

where $D_{ins}(t)$ is the instantaneous diffusion rate at time *t*, α is a constant, Γ is referred to as transport factor, *n* is the number of dimension, and $\mathbf{r}$ and $\mathbf{r}'$ are locations of the particle. If $\alpha>1$, the phenomenon is called super-diffusion; if $\alpha<1$, the phenomenon is called sub-diffusion.

Cellulose molecules are the building blocks of paper. Many studies confirm that there is a correlation between the physical properties of paper and the average length of cellulose chains, expressed by Degree of Polymerization (DP) (Zou *et al.* 1994, Hill *et al.* 1995, Emsley *et al.* 1997, Emsley *et al.* 2000, Ding and Wang 2008). During the depolymerization process, the long cellulose chains break into shorter ones under the reactions of hydrolysis, oxidation, and photo-deterioration, and the paper gradually loses its strength and becomes brittle. Almost all research on paper aging characterizes the degradation of paper by the depolymerization of its cellulose. The breakage of cellulose chains is assumed to follow a first-order reaction, which can be approximated by a zero-order reaction in its early stage. Under this assumption, the cellulose degradation model in terms of degree of polymerization is derived as

$$\frac{1}{DP(t)}-\frac{1}{DP(0)}=kt$$

Although systematic research and publications on how paper-ink interactions affect the long-term stability of printed images are lacking, it has been found that ink permanence is

affected by the strength of the ink-fiber bond: The stronger the ink is attached to the fiber, the easier the ink transfers its absorbed energy to the fiber, resulting in improved ink permanence (Clifton and Nugent 2000, Vikman 2004). Such ink-fiber bond is believed to degrade with the depolymerization process of cellulose. Besides, diffusion rate in Einstein relation (Einstein 1905) is related to the dynamic viscosity, from which the degree of polymerization is calculated (Immergut *et al.* 1953).

Another aspect of paper aging is the generation of chromophores, or yellowing of paper, as a consequence of the degradation of nearly every constituent of the paper. Lignin, when a considerable amount of this substance is contained in paper, is the most important contributor to this type of paper degradation. The chemistry of the yellowing of paper is discussed in (Carter 1996a, Carter 1996b). Wilhelm (2003a, 2003b) provides a description of light-induced as well as thermally-induced yellowish stain formation in inkjet prints and traditional silver-halide color photographs. A review of the kinetics of paper aging and the stress dependence of its degradation rate is given in (Menart *et al.* 2011). A degradation model that describes the spectrum of paper as a function of time is developed in (Blayo *et al.* 2003) as

$$R(t,\lambda) = R(0,\lambda)\exp\left(-\mu(\lambda)t^{\alpha(\lambda)}\right)$$

where $R(t,\lambda)$ is the spectrum of paper, t is the exposure time, λ is the wavelength of light in nanometer, and μ and α are constants that depend on wavelength.

2.1.2 *Accelerated Testing of Printed Images*

Modern printed images are so stable that under the normal displaying condition, they take several years to show noticeable color degradation. This process can be easily extended to decades if the images are well kept under proper environmental conditions. Therefore, accelerated tests are performed to gather meaningful degradation data in a short period of time. Extensive studies have been carried out on accelerated testing of printed images to investigate their degradation behaviors under different environmental stresses. Basically, printed images are subjected to four types of environmental stresses, namely, temperature, humidity, illumination, and air pollutants. A review of the accelerated testing methods for the permanence prediction of digitally printed photographs is given in Wilhelm (2004). A survey of environmental conditions relative to the display of photographs in consumer homes is provided in Bugner *et al*. (2005, 2006).

Temperature accelerated degradation is frequently predicted by the well-known Arrhenius equation, which describes the relationship between temperature and the rate of a chemical reaction. De Rossi *et al.* (2003) investigate the activation energy of dye degradation with consideration of the influence of humidity, reporting a dye-amount dependent fading rate. Bugner and Lindstrom (2005) study the influence of humidity on Arrhenius equation for inkjet photographic prints. Their result shows that yellowing of paper can also be well described by the Arrhenius equation.

McCormick-Goodhart and Wilhelm (2000, 2001) study humidity-induced fading behavior and use a logarithmic function to fit the color change. Such a model is partially confirmed

by Guo *et al.* (2002). Humidity is also the major cause of ink diffusion that results in loss of image sharpness. Significant research on humidity-induced color degradation has been conducted with a focus on ink diffusion (Hill *et al.* 2000, McCormick-Goodhart and Wilhelm 2003a, McCormick-Goodhart and Wilhelm 2005, Salesin and Burge 2014). Ink density gain is discussed in (Hodgson and Jackson 2004b) and is attributed to the increase of ink coverage caused by ink diffusion. Hofmann and Reber (2009) show that ink diffusion tends to slow down as ink migrates to lighter areas.

Generally, printed images exposed to light undergo two types of photo-degradation: photolysis and photo-oxidation (Image Permanence Institute 2010). Photolysis is the chemical reaction in which colorant molecules are broken down by light photons and turned into colorless products, while photo-oxidation is the chemical reaction of inks in the presence of light. More details on the theory of light-induced fading is provided in (Pugh and Guthrie 2001). The effect of illumination on printed images is determined by two properties: spectral distribution and light intensity. Based on the wavelength, the light spectrum is divided into three parts: ultraviolet (UV), visible, and infrared. UV light has the highest frequency and is the most destructive part of light. Frequently considered light sources in image permanence tests include glass-filtered or UV-filtered sunlight, incandescent light, fluorescent light, LED, and xenon light. Light intensity is usually quantified in Lux, which measures the luminous flux per unit area. The equivalency of different light sources is investigated in (Baumann and Hofmann 2004). A reciprocity relationship is often assumed in accelerated light-induced fading tests to predict image life under normal illumination condition as

$$image\ life = \frac{test\ condition \times test\ duration}{normal\ condition}$$

It is often observed that for the same lux-hour exposure, incorrect extrapolations could be made. This phenomenon is called reciprocity failure. One explanation is that oxygen involved in photo-degradation might be depleted under high-intensity light fading, resulting in a slowdown of photochemical reaction. In addition, photo-degradation by-products may be congested around the reaction site, further slowing down the light fading process (Wilhelm and Brower 1993). Wilhelm and McCormick-Goodhart (2001) conduct light fading tests at two light intensities: a high intensity at 35 klux and a low intensity at 1 klux. Results from the low-intensity test are used to correct the prediction from the high-intensity test suffered from potential reciprocity failure. Light-induced fading is also studied in (Guo and Miller 2001, Wilhelm 2002, Hodgson and Jackson 2004b, Bugner and Lindstrom 2006).

Air pollution in the atmosphere is another factor that poses a threat to the stability of printed images. Ozone, among all the air pollutants, is the most detrimental on image permanence. The reciprocity relationship is also assumed to predict the image life under normal condition in accelerated gas fading tests. Reciprocity failure likewise exists. The ozone resistance of printed images is studied in (Berger and Wilhelm 2003, Berger and Wilhelm 2004, Wilhelm *et al.* 2007). Hodgson and Jackson (2004a) compare the difference between the fading characteristics of printed images subjected to gas and light fading.

The point at which an image reaches an unacceptable degradation is called endpoint. Apparently, the endpoint is very subjective and depends on use application of the image.

Accelerated image permanence tests usually adopt densitometric endpoint criteria. For example, ISO (2006) specifies the endpoint as 30% density loss for any ink. Wilhelm (2002) proposes endpoint criteria considering both density loss and color imbalance. Assessment of the existing endpoint criteria is presented in (Oldfield *et al.* 2004, Shibahara *et al.* 2004).

The literature review in this section reveals that existing degradation models of printed images are limited and insufficient to capture the sophisticated characteristics of the degradation of printed images. In the next section, we provide a literature review of the general degradation models in reliability engineering that are applicable to the degradation modeling of printed images.

2.2 General Degradation Models

2.2.1 *Regression Models*

Regression is a commonly used tool in degradation estimation and prediction (Nelson 1990, Meeker and Escobar 1998). When applying the regression method, the degradation observations are fitted to a linear or non-linear deterministic function. Lu and Meeker (1993) introduce a general path regression model with random coefficients as

$$y_{ij} = \eta\left(t_j; \mathbf{\Phi}, \mathbf{\Theta}_i\right) + \varepsilon_{ij}$$

where y_{ij} is the j^{th} measurement of the i^{th} unit, $\eta\left(t_j; \mathbf{\Phi}, \mathbf{\Theta}_i\right)$ is the actual degradation path of the i^{th} unit, t_j is the time of the j^{th} measurement, $\mathbf{\Phi}$ is the vector of fixed-effect parameters for all the units, $\mathbf{\Theta}_i$ is the vector of random-effect parameters of the i^{th} unit, and

$\varepsilon_{ij} \sim N\left(0, \sigma_{\varepsilon}^{2}\right)$ is the measurement error. The degradation prediction is used to estimate the failure time distribution. Stress factors are incorporated into the model by Meeker *et al.* (1998).

Regression degradation models are also studied in the literature by other researchers (Lu *et al.* 1997, Zuo *et al.* 1999, Crk 2000, Robinson and Crowder 2000, Bae and Kvam 2004, Chen and Zheng 2005, Bae *et al.* 2007, Yuan and Pandey 2009). McPherson (2010) summarizes three time-dependent forms for degradation: power-law, exponential, and logarithmic. Quadratic function is another option for the parametric form of degradation path (Li and Nilkitsaranont 2009). Boulanger and Escobar (1994) consider a degradation process with an asymptotic maximum value. Bae *et al.* (2008) model the degradation path of plasma display panels with a bi-exponential model. Zhou *et al.* (2014) use spline functions as the degradation path. Regression degradation models with measurement errors of non-constant variance are investigated in (Lu *et al.* 1997, Yuan and Pandey 2009). Yu (2006) develops optimal accelerated degradation test plan with a reciprocal Weibull degradation rate. Robinson and Crowder (2000) estimate the parameters of the general path model using the Bayesian method. Parameter update by the Bayesian method is studied in (Gebraeel *et al.* 2005, Gebraeel 2006, Gebraeel and Pan 2008, Gebraeel *et al.* 2009).

2.2.2 *Markov Models*

Markov models have been widely exploited in degradation modeling and prediction, especially for multistate systems (Lisnianski and Levitin 2003). The Markov models are based on the memoryless property, i.e., the state transition is independent of the history of

the degradation process. The Markov model with a discrete-state and discrete-time space is called the Markov chain model. Marseguerra *et al.* (2002) model the degradation of a multi-component system and investigate its maintenance optimization using the Markov chain model. When the time space is continuous, the Markov model is referred as the Markov process model. The sojourn time of the system in each state in the Markov process model is exponentially distributed. Elsayed and Zebib (1979) investigate the probability of failure and the availability of a multistate reparable device using the Markov process model. Eryilmaz (2015) uses the phase-type distribution for the dynamic assessment of a multistate system modeled by a Markov process. The degradation modeling of multistate systems as a non-homogeneous Markov process is investigated in (Liu and Kapur 2008, Liu and Huang 2010, Shu *et al.* 2010, Sheu and Zhang 2013, Liu *et al.* 2015). More research on the Markov process model can be found in (Xue and Yang 1995, Liu and Kapur 2006, Soro *et al.* 2010, Yin *et al.* 2013, Eryilmaz 2016).

The semi-Markov process model is used when the sojourn time is not exponential. The semi-Markov process model is only Markovian at the jump instants. Lisnianski (2007) models the degradation of a repairable multistate system as a semi-Markov process and obtains its solution using the universal generating function technique. Veeramany and Pandey (2011) compare the homogeneous Markov process model and the semi-Markov process model in estimating the reliability of a nuclear piping system. Compare *et al.* (2017) use the Bayesian method in estimating the model parameters for a semi-Markov process with Weibull-distributed transition times. The degradation modeling of multistate systems

using the discrete-time semi-Markov process is investigated in (Kao 1973, Chryssaphinou *et al.* 2011).

2.2.3 *Stochastic Process Models*

The stochastic process models represent another important class of degradation models (Si *et al.* 2011, Ye and Xie 2015). Among the stochastic processes, the Brownian motion with drift, also termed as Gaussian or Wiener process, receives the widest applications in degradation data analysis (Zhang *et al.* 2018). Doksum and Hoyland (1992) model the degradation as a Wiener process and analyze the failure time data with the inverse Gaussian distribution. Whitmore and Schenkelberg (1997) model the degradation using a Wiener process with a time scale transformation. A typical state transformation is the log-transformation of an exponential model (Gebraeel *et al.* 2005). Measurement error is considered in the inference of the Wiener process in (Whitmore 1995, Peng and Hsu 2012, Si *et al.* 2013a, Ye *et al.* 2013). To account for the unit-to-unit variation, the random effects of the model parameters are incorporated in the Wiener process in (Peng and Tseng 2009, Wang 2010, Peng and Tseng 2013, Wang *et al.* 2014b). The residual life distribution prediction of an individual unit requires updating the parameters of the Wiener process and is investigated in (Wang *et al.* 2011, Bian and Gebraeel 2012, Liao and Tian 2013, Si *et al.* 2013b, Si *et al.* 2013c, Ye *et al.* 2015). Multivariate Wiener process models are developed by assuming a multivariate normal distribution for the parameters of the correlated Wiener processes (Whitmore *et al.* 1998, Jin and Matthews 2014, Feng *et al.* 2016) or through copula functions (Sari *et al.* 2009, Pan *et al.* 2011, Wang *et al.* 2014a, Wang *et al.* 2015a, Peng *et al.* 2016a).

The gamma process is more appropriate when the degradation is monotonically increasing (van Noortwijk 2009). Park and Padgett (2005, 2006) investigate the lifetime distribution for gamma process degradation models. The non-stationary gamma process model is investigated in (Wang *et al.* 2000, Nicolai *et al.* 2004, Nicolai *et al.* 2007, van Noortwijk *et al.* 2007, Kuniewski *et al.* 2009) by assuming a time-dependent shape parameter and a constant scale parameter. The parameters estimation of gamma processes with measurement errors is investigated in (Kallen and van Noortwijk 2005, Zhou *et al.* 2011, Lu *et al.* 2013, Son *et al.* 2016). Lawless and Crowder (2004) consider the random effects on the scale parameter of the gamma process and incorporate covariates in the model. Pan and Balakrishnan (2011) use a bivariate Birnbaum-Saunders distribution to approximate the reliability function of a bivariate gamma process. Wang *et al.* (2015b) develop a bivariate gamma process model using copula functions.

The inverse Gaussian process is another alternative for degradation modeling (Wang and Xu 2010). The physical interpretation of using the inverse Gaussian process to model degradation is explored in (Ye and Chen 2014). Peng (2015) investigates the lifetime distribution of the inverse Gaussian process with random effects. Zhang *et al.* (2013) develop an inverse Gaussian process corrosion growth model for energy pipelines. Measurement error is considered in their model and the Bayesian method is used to update the model parameters. The Bayesian analysis of the inverse Gaussian process model is also investigated in (Peng *et al.* 2014, Pan *et al.* 2016, Peng *et al.* 2017). Peng *et al.* (2016b) develop a bivariate inverse Gaussian process degradation model using copula functions.

2.3 Accelerated Degradation Tests

Traditionally, accelerated life tests (ALT) are conducted to predict the lifetime distribution at the normal operating conditions. The ALT models can be classified into three categories: statistics-based models, physics-statistics-based models, and physics-experimental-based models (Elsayed 2012). The statistics-based models can be further classified into parametric models and semiparametric/nonparametric models. For highly reliable products, it is difficult to gather enough lifetime data in a short period of time for the traditional time-to-failure analysis. In this case, accelerated degradation tests (ADT) become a viable alternative in which degradation data are collected under higher levels of stresses and extrapolated to the normal operating conditions (Meeker *et al.* 1998). The degradation rate or model parameters are commonly modeled as physics/experiment-based functions, for example, the Arrhenius model, the Eyring model, and the inverse power model, or empirical functions of the stresses (Nelson 1990, Meeker and LuValle 1995, Escobar and Meeker 2006). In some applications, the degradation variation may also change with the stresses (Joseph and Yu 2006, Liao and Elsayed 2006). Besides, when the degradation is affected by more than one stress, the interactions between stresses need to be carefully considered (Escobar and Meeker 2006).

We review three acceleration stresses that are relevant to the degradation of printed images, that are temperature, humidity, and illumination. Arrhenius model is widely used when temperature is the acceleration stress. The Arrhenius equation describes the temperature dependence of the rate of a chemical reaction. In accelerated degradation tests, it is used as the acceleration factor on the reaction rate of kinetic models (Escobar and Meeker 2006,

McPherson 2010). The Arrhenius relationship is also used on the diffusion rates of various processes in different applications (Bahadori *et al.* 2015, Gagliardi *et al.* 2017). Humidity is another commonly used acceleration stress. It is frequently studied together with temperature and a variety of humidity models, mostly empirical, are proposed (Peck 1986, McPherson 2010). The effect of temperature and humidity on the degradation rate in kinetic models is investigated in (Li *et al.* 2011, Park *et al.* 2013, Naversnik and Jurecic 2016). Photodegradation is a type of degradation induced by light. A comprehensive mathematical model for photodegradation is proposed in (Escobar and Meeker 2006) as

$$\mathrm{D}_{\mathrm{Tot}}(t)=\int_0^t\int_{\lambda_1}^{\lambda_2} E_0(\lambda,\tau)\left\{1-\exp\left[-A(\lambda)\right]\right\}\phi(\lambda)\,d\lambda\,d\tau$$

where $\mathrm{D}_{\mathrm{Tot}}(t)$ is the total effective dosage of ultraviolet light up to time *t*, $E_0(\lambda,\tau)$ is the spectral irradiance (or intensity) of the light source at wavelength λ at time τ, $\left\{1-\exp\left[-A(\lambda)\right]\right\}$ is the spectral absorbance of the material, and $\phi(\lambda)$ is a quasi-quantum efficiency of the absorbed radiation. In many researches on kinetic models of photodegradation, the spectrum of the light source is less concerned. The dependence of the kinetic rate on light intensity is usually modeled as a power law function (Chen and Ray 1998, Chang *et al.* 2000, Mehrotra *et al.* 2003, Manzocco *et al.* 2012).

To achieve accurate prediction of the image at normal use conditions, an optimal design of ADT planning is needed. The objective of the test is to minimize the asymptotic variance of reliability characteristics of interest or minimize testing costs. Various optimality criteria include A-optimality and D-optimality. The test planning variables usually include testing stresses, number of units allocated to each stress, frequency of degradation measurements,

and the test duration. Optimal design of ADT planning for different degradation models has been studied. Boulanger and Escobar (1994) investigate ADT planning for a general path model by minimizing the asymptotic variance of the estimated degradation path. Optimal design of ADT planning for Wiener process by minimizing the asymptotic variance of the estimated *q*th percentile of the product's lifetime distribution is studied in (Liao and Tseng 2006, Lim and Yum 2011, Xiao and Ye 2016). Tsai *et al.* (2012) design ADT planning for a Wiener process with two stress factors and their interaction terms.

2.4 Summary and Conclusions

In this chapter, we first present a literature review of the degradation of printed images including the degradation models and accelerated testing of the ink fading, ink diffusion, and paper aging of printed images. We then provide a literature review of the general degradation models and accelerated degradation tests in reliability engineering relevant to the topic of study. The literature review shows that the research on degradation modeling and prediction of printed images is limited and the design of ADT for image "quality" prediction need further investigation.

CHAPTER 3

PHYSICS-BASED DEGRADATION MODEL OF PRINTED IMAGES WITH CONSTANT FADING AND DIFFUSION RATES

In this chapter, we investigate the degradation modeling of printed images with constant fading and diffusion rates. After presenting the estimation method of the performance indicator used in this research, we develop degradation models for ink fading and ink diffusion using a physics-based approach. The two models are further integrated into a single degradation model to predict the degradation characteristics of printed images.

3.1 Performance Indicator

The area coverages of the sixteen states of the CMYK ink set cannot be measured directly. One possible way is to use the Neugebauer equation (Neugebauer 1937). In this equation, the states are called Neugebauer primaries. The Neugebauer equation states that the reflectance of a halftone-printed area is calculated as the sum of the reflectance of the Neugebauer primaries weighted by their fractional area coverage. A factor *n* is added to correct the optical dot gain effect resulting in the Yule-Nielsen Spectral Neugebauer equation (YNSN) (Yule and Neilsen 1951),

$$\hat{R}(\lambda)^{1/n} = \sum_{i=1}^{16} a_i R_i(\lambda)^{1/n}$$

where $\hat{R}(\lambda)$ is the predicted spectral reflectance of the halftone-printed area, a_i and $R_i(\lambda)$ are the fractional area coverage and the spectral reflectance of the i^{th} Neugebauer primary, respectively, and λ is the wavelength of light.

Inversion of the Neugebauer equation gives the estimated area coverages of the sixteen states and is investigated in (Mahy and Delabastita 1996, Mahy 1998, Urban *et al.* 2007, Deshpande *et al.* 2014). Direct analytical inversion of the YNSN model is not possible. One solution is to use an iterative method of constrained nonlinear optimization by minimizing the difference between the measured and predicted spectral reflectance,

$$\min \sqrt{\sum_{\lambda}\left(R(\lambda)-\hat{R}(\lambda)\right)^2}$$

$$s.t.\ \sum_{i=1}^{16} a_i = 1,\ 0 \le a_i \le 1,\ for\ i = 1,...,16$$

where $R(\lambda)$ and $\hat{R}(\lambda)$ are the measured and predicted spectral reflectance of a halftone-printed area, respectively.

3.2 Degradation Model of Ink Fading

Catalytic fading is the phenomenon that the fading rate of an ink changes if it is overprinted with other inks. Therefore, we propose a multi-layered state transition diagram for ink fading under the halftone-printing scenario, as shown in Figure 3.1. The sixteen states are numbered in the state transition diagram. It is assumed that when one ink fades in a state in an infinitesimal area, the area covered by that state would then be covered by the state of the residual inks.

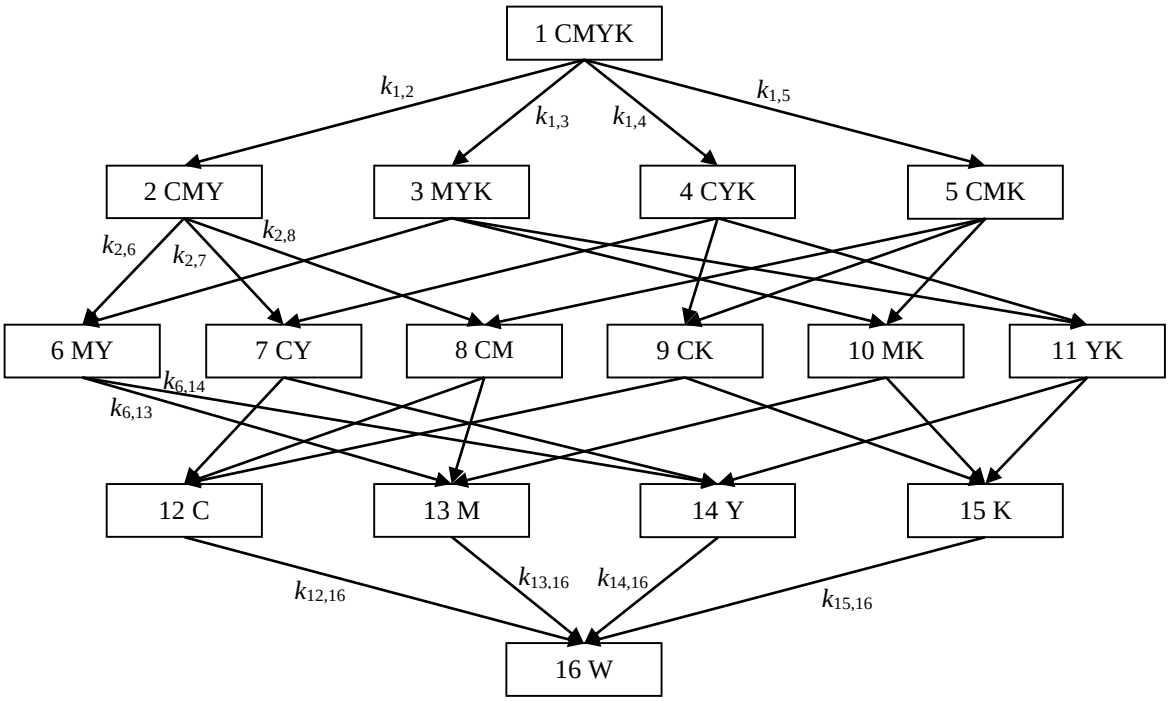

Figure 3.1 State transition diagram of the sixteen states of CMYK ink set by ink fading

The fractional area coverage of the sixteen states of a halftone-printed area is denoted as $a_i, i = 1, 2, \ldots, 16$. We model ink fading as a first-order kinetic process, thus the more surface area is covered by inks, the more amount of ink is exposed to the environment and the faster is the ink degradation. The area coverage transition rate from state *i* to state *j* is the product of the area coverage of state *i*, a_i, and the state-to-state fading rate $k_{i,j}$, which is assumed to be constant in this chapter. For better understanding in this dissertation, $k_{i,j}$ is sometimes denoted as $k_{ink}^{(state)}$, which means the fading rate of an ink in a state. The overall fading rate of state *i* to other states is the sum of all the state-to-state fading rates of state *i* and is denoted as κ_i or κ_{state}.

Based on the proposed state transition diagram, we develop the ink fading model using differential equations. The degradation rate of state *i* is given in Eq. (3.1),

$$\frac{da_i(t)}{dt} = \sum_j k_{j,i} a_j(t) - \kappa_i a_i(t) \tag{3.1}$$

We denote the area coverage transition rate into state *i* as $r_i(t) = \sum_j k_{j,i} a_j(t)$. A list of $r_i(t)$ is shown in Appendix. The matrix form of the differential equations is given in Eq. (3.2),

$$\frac{d\boldsymbol{a}(t)}{dt} = \boldsymbol{A}\boldsymbol{a}(t) \tag{3.2}$$

where $\boldsymbol{a}(t) = \begin{bmatrix} a_1(t) & a_2(t) & \cdots & a_{15}(t) \end{bmatrix}^{\mathrm{T}}$, and $\boldsymbol{A}$ is the differential equation matrix as shown in Appendix.

The solution of Eq. (3.2) using matrix exponential method is given in Eq. (3.3),

$$\boldsymbol{a}(t) = e^{\boldsymbol{A}t}\boldsymbol{a}(0) \tag{3.3}$$

The analytical solution of the differential equations is expressed in matrix form in Eq. (3.4),

$$\boldsymbol{a}(t) = \boldsymbol{c}\boldsymbol{e}^{-\boldsymbol{\kappa}t} \tag{3.4}$$

where $\boldsymbol{\kappa} = \begin{bmatrix} \kappa_1 & \kappa_2 & \cdots & \kappa_{15} \end{bmatrix}^{\mathrm{T}}$, and $\boldsymbol{c}$ is a coefficient matrix whose elements are calculated from the fading rates and the initial area coverages of the states. The predicted area coverages of the states and the coefficient matrix $\boldsymbol{c}$ are shown in Appendix. The differential equations can also be solved in discrete time given in Eq. (3.5),

$$\boldsymbol{a}(t + \Delta t) = \boldsymbol{p}\boldsymbol{a}(t) \tag{3.5}$$

where $\boldsymbol{p}$ is the fading transition matrix as shown in Appendix.

We denote the area coverage of an ink as $a_{ink}(t)$, $ink \in \{cyan, magenta, yellow, black\}$, and calculate it as the sum of the area coverage of the states that have this ink, as shown in Eq. (3.6),

$$a_{ink}(t) = \sum_{i \in \Omega_{ink}} a_i(t) \tag{3.6}$$

where $\Omega_{cyan} = \{1,2,4,5,7,8,9,12\}$, $\Omega_{magenta} = \{1,2,3,5,6,8,10,13\}$, $\Omega_{yellow} = \{1,2,3,4,6,7,11,14\}$, and $\Omega_{black} = \{1,3,4,5,9,10,11,15\}$ are the sets of the states that contain the CMYK inks respectively as shown in Figure 3.1. When no catalytic fading exists, the degradation model reduces to Eq. (3.7),

$$a_{ink}(t) = a_{ink}(0) e^{-\kappa_{ink} t} \tag{3.7}$$

where κ_{ink} is the fading rate of an individual ink. ($\kappa_{cyan} = \kappa_{12}$, $\kappa_{magenta} = \kappa_{13}$, $\kappa_{yellow} = \kappa_{14}$, and $\kappa_{black} = \kappa_{15}$)

3.2.1 *Parameters Estimation*

It is intuitive to print "pure" ink (one color ink) to estimate its fading rate. Therefore, to estimate the fading rates of a state, we only print inks of this state to avoid area coverage transition from other states into this state. By doing so, this state would become the practical top state in the state transition diagram. We first estimate the overall fading rate of each state by printing the state as the top state and then estimate the state-to-state fading rates using the estimated overall fading rates. The least squares method is chosen to

estimate the fading rates for its simplicity and the assumption of a constant variance in the residuals is only mildly violated due to the slow fading of inks.

Assuming that there are N samples and $M+1$ area coverage measurements at time $t_m,\ m=0,1,...,M,\ t_0=0$. By printing state i as the top state, the predicted area coverage of state i is

$$a_i(t)=a_i(0)e^{-\kappa_i t}$$

The least squares estimation of the overall fading rate $\hat{\kappa}_i$ is

$$\hat{\kappa}_i=-\frac{1}{N\sum_{m=1}^{M}t_m^2}\sum_{n=1}^{N}\sum_{m=1}^{M}\left[\ln x_{i;n}(t_m)-\ln x_{i;n}(t_0)\right]t_m$$

where $x_{i;n}(t_m)$ is the measured area coverage of state i of the n^{th} sample at time t_m.

Assuming state i is the top state and state j is one of the transition states from state i, the state-to-state fading rate from state i to state j is estimated using the estimated overall fading rates of states i and j. The predicted area coverage of state j is

$$a_j(t)=c_{j,i}e^{-\kappa_i t}+c_{j,j}e^{-\kappa_j t}$$

where $c_{j,i}=\dfrac{k_{i,j}a_i(0)}{\kappa_j-\kappa_i}$, and $c_{j,j}=a_j(0)-c_{j,i}$. The least squares estimation of the state-to-state fading rate $\hat{k}_{i,j}$ is

$$\hat{k}_{i,j}=\left(\hat{\kappa}_j-\hat{\kappa}_i\right)\frac{\sum_{n=1}^{N}\sum_{m=1}^{M}\left[x_{i;n}(t_0)\left(e^{-\hat{\kappa}_i t_m}-e^{-\hat{\kappa}_j t_m}\right)\left(x_{j;n}(t_m)-x_{j;n}(t_0)e^{-\hat{\kappa}_j t_m}\right)\right]}{\sum_{n=1}^{N}\sum_{m=1}^{M}\left[x_{i;n}(t_0)\left(e^{-\hat{\kappa}_i t_m}-e^{-\hat{\kappa}_j t_m}\right)\right]^2}$$

where $x_{i;n}(t_m)$ and $x_{j;n}(t_m)$ are the measured area coverages of states *i* and *j* of the n^{th} sample at time t_m, respectively.

3.2.2 *Numerical Examples*

In this section, we provide numerical simulations using the physics-based ink fading model. The proposed model is applied to the 3 × 3 color pixels defined in Table 3.1. The colors are assumed to be printed with the three color inks. The initial area coverages of the states are approximated using the Demichel equations given in Eq. (3.8) and shown in Table 3.2.

Table 3.1 Initial area coverage of inks in 3 × 3 color pixels

	a_{cyan}	$a_{magenta}$	a_{yellow}
(1,1) Cyan	1	0	0
(1,2) Magenta	0	1	0
(1,3) Yellow	0	0	1
(2,1) Red	0	1	1
(2,2) Green	1	0	1
(2,3) Blue	1	1	0
(3,1) Orange	0	0.5	1
(3,2) Purple	0.5	1	0.5
(3,3) Maroon	0.5	1	1

$$
\begin{aligned}
a_{CMY} &= a_{cyan}a_{magenta}a_{yellow} \\
a_{MY} &= \left(1-a_{cyan}\right)a_{magenta}a_{yellow} \\
a_{CY} &= a_{cyan}\left(1-a_{magenta}\right)a_{yellow} \\
a_{CM} &= a_{cyan}a_{magenta}\left(1-a_{yellow}\right) \\
a_{C} &= a_{cyan}\left(1-a_{magenta}\right)\left(1-a_{yellow}\right) \\
a_{M} &= \left(1-a_{cyan}\right)a_{magenta}\left(1-a_{yellow}\right) \\
a_{Y} &= \left(1-a_{cyan}\right)\left(1-a_{magenta}\right)a_{yellow} \\
a_{W} &= \left(1-a_{cyan}\right)\left(1-a_{magenta}\right)\left(1-a_{yellow}\right)
\end{aligned}
\tag{3.8}
$$

Table 3.2 Initial area coverage of states in 3 × 3 color pixels

	a_{CMY}	a_{MY}	a_{CY}	a_{CM}	a_{C}	a_{M}	a_{Y}
(1,1) Cyan	0	0	0	0	1	0	0
(1,2) Magenta	0	0	0	0	0	1	0
(1,3) Yellow	0	0	0	0	0	0	1
(2,1) Red	0	1	0	0	0	0	0
(2,2) Green	0	0	1	0	0	0	0
(2,3) Blue	0	0	0	1	0	0	0
(3,1) Orange	0	0.5	0	0	0	0	0.5
(3,2) Purple	0.25	0.25	0	0.25	0	0.25	0
(3,3) Maroon	0.5	0.5	0	0	0	0	0

The fading rates used in the simulation are shown in Table 3.3. Different fading rates are used to illustrate the catalytic fading phenomenon.

Table 3.3 Selected fading rates

$k_{cyan}^{(CMY)}$	0.008	$k_{cyan}^{(CY)}$	0.005	$k_{cyan}^{(CM)}$	0.008	$k_{cyan}^{(C)}$	0.005
$k_{magenta}^{(CMY)}$	0.002	$k_{magenta}^{(MY)}$	0.002	$k_{magenta}^{(CM)}$	0.002	$k_{magenta}^{(M)}$	0.002
$k_{yellow}^{(CMY)}$	0.03	$k_{yellow}^{(MY)}$	0.03	$k_{yellow}^{(CY)}$	0.01	$k_{yellow}^{(Y)}$	0.02

The predicted area coverages of the states are plotted in Figure 3.2. The area coverages of the states are not necessarily monotonically decreasing because of the area coverage transition. When the area coverage transition rate into a state is larger than the area coverage transition rate out of it, the area coverage of the state would increase.

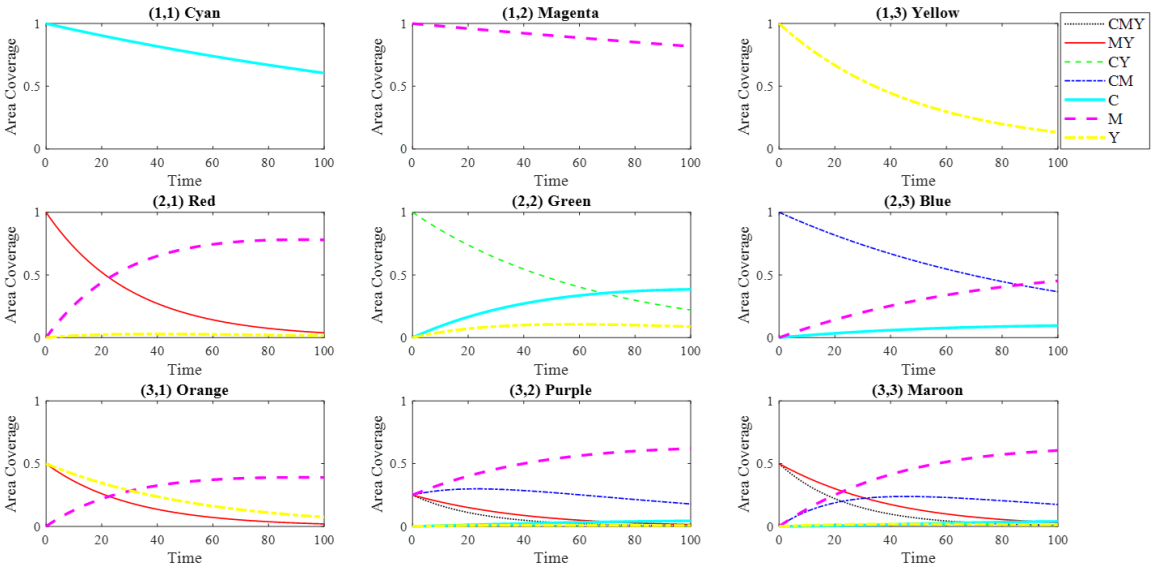

Figure 3.2 Predicted area coverages of states using physics-based ink fading model

The predicted area coverages of the CMY inks are plotted in Figure 3.3. Because of catalytic fading, the cyan or yellow ink starting with same initial area coverage in these colors end up with different area coverages.

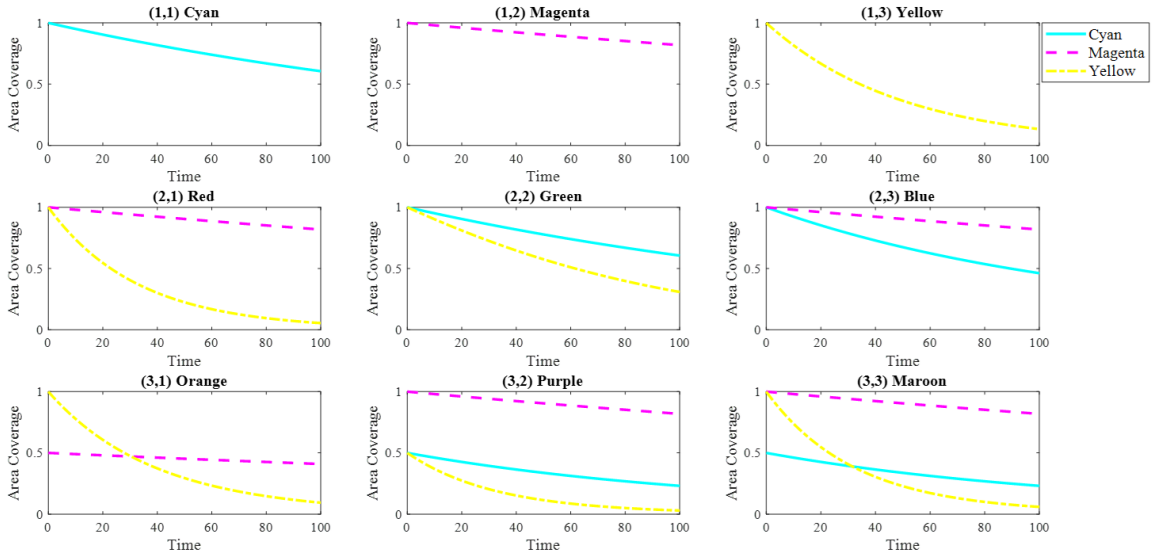

Figure 3.3 Predicted area coverages of inks using physics-based ink fading model

The color degradation of the 3 × 3 color pixels is shown in Figure 3.4. The area coverages of the CMY inks are converted into RGB values for display using Eq. (3.9),

$$\begin{bmatrix} Red \\ Green \\ Blue \end{bmatrix} = 255 \times \begin{bmatrix} 1-Cyan \\ 1-Magenta \\ 1-Yellow \end{bmatrix} \tag{3.9}$$

As the inks fade, the colors appear to be bleached out. In addition, colors like red, orange, and maroon that have a large proportion of yellow ink exhibit obvious hue shift due to the imbalanced ink fading.

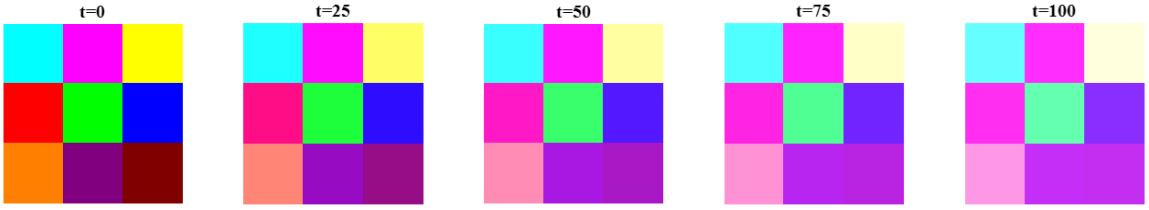

Figure 3.4 Color degradation using physics-based ink fading model

The same fading rates are used in a degradation simulation of an image of 500×500 pixels. The result is shown in Figure 3.5. Since the magenta ink fades slower than the other two inks, the faded image gradually gains a magenta tone.

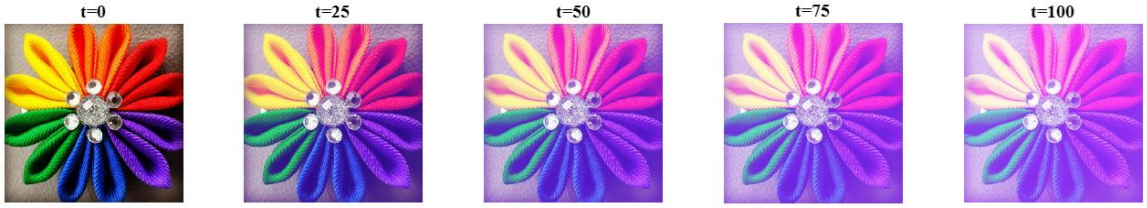

Figure 3.5 Image degradation using physics-based ink fading model

(Original image from https://www.etsy.com)

A real-life case study is used to demonstrate the application of the proposed model. The greenish color images in Figure 3.6 are the photographs of the cover of a book that was kept on a bookshelf for 32 years. The color fading of the book cover is shown in the figure (image size is 30×30 pixels). We estimate the ink fading rates using the data from the first 15 years. Observations and predictions of the ink fading are plotted in Figure 3.7 as dots and dashed lines, respectively. The model predictions match well with the observations except for a small deviation for the magenta ink.

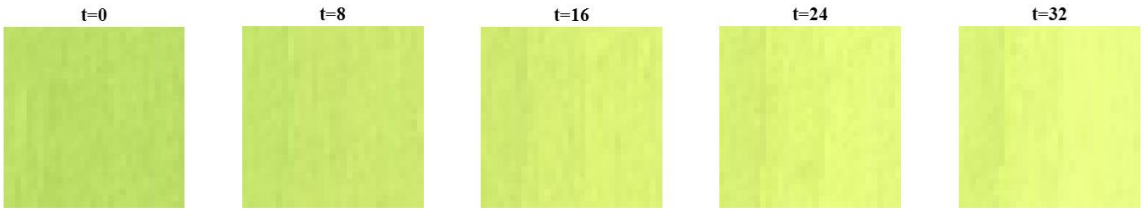

Figure 3.6 Color fading of a book cover

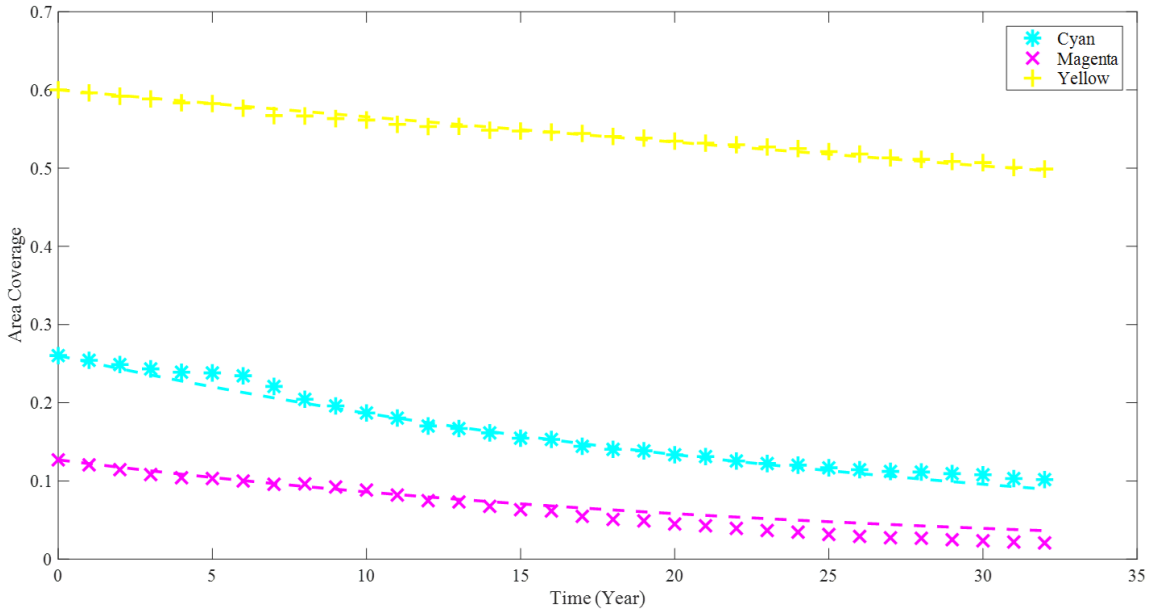

Figure 3.7 Degradation prediction of ink area coverages of a book cover

3.3 Degradation Model of Ink Diffusion

The degradation model of ink diffusion is based on the two-dimensional diffusion equation

$$\frac{\partial c(x,y,t)}{\partial t} = \delta\left(\frac{\partial^2 c(x,y,t)}{\partial x^2} + \frac{\partial^2 c(x,y,t)}{\partial y^2}\right)$$

where $c(x,y,t)$ is the concentration of a substance at location (x, y) at time t, and δ is its diffusion rate. The diffusion equation is derived from the Fick's laws of diffusion. Fick's first law states that the diffusion flux, or the amount of the substance that diffuses through a unit area in a unit time, is opposite and proportional to the gradient of the concentration. In two dimensions, the diffusion flux is written as

$$\begin{aligned} J &= -\delta \nabla c(x,y,t) \\ &= -\delta\left(\frac{\partial c(x,y,t)}{\partial x} e_x + \frac{\partial c(x,y,t)}{\partial y} e_y\right) \end{aligned}$$

where ∇ is the gradient operator, and e_x and e_y are orthogonal unit vectors along the axes. Fick's second law relates the diffusion over space to the concentration change over time. The two-dimensional diffusion equation is then derived as

$$\begin{aligned} \frac{\partial c(x,y,t)}{\partial t} &= -\nabla \cdot J \\ &= -\left(\frac{\partial}{\partial x}, \frac{\partial}{\partial y}\right) \cdot J \\ &= -\left(\frac{\partial}{\partial x}, \frac{\partial}{\partial y}\right) \cdot \left(-\delta\left(\frac{\partial c(x,y,t)}{\partial x} e_x + \frac{\partial c(x,y,t)}{\partial y} e_y\right)\right) \\ &= \delta\left(\frac{\partial^2 c(x,y,t)}{\partial x^2} + \frac{\partial^2 c(x,y,t)}{\partial y^2}\right) \end{aligned}$$

where $\nabla \cdot$ is the divergence operator.

By assuming each state has its own diffusion rate, we apply the diffusion equation to a state as shown in Eq. (3.10),

$$\frac{\partial a_i(x,y,t)}{\partial t} = \delta_i \left(\frac{\partial^2 a_i(x,y,t)}{\partial x^2} + \frac{\partial^2 a_i(x,y,t)}{\partial y^2} \right) \tag{3.10}$$

where $a_i(x,y,t)$ is the area coverage of state i at pixel (x, y) at time t, and δ_i is the diffusion rate of state i. We solve Eq. (3.10) using finite difference method. Applying first-order forward differences in time and centered differences in space (Haberman 1987) yields the discretization result in Eq. (3.11),

$$a_i(x,y,t+\Delta t) = \left(1 - \frac{4\delta_i \Delta t}{(\Delta s)^2}\right) a_i(x,y,t) + \frac{\delta_i \Delta t}{(\Delta s)^2} \begin{pmatrix} a_i(x+\Delta s,y,t) + a_i(x-\Delta s,y,t) + \\ a_i(x,y+\Delta s,t) + a_i(x,y-\Delta s,t) \end{pmatrix} \tag{3.11}$$

where Δs is the spacing in both horizontal and vertical directions.

We set the boundary condition to solve Eq. (3.11) for the pixels at the edges of the image. Possible boundary conditions include fixed values (Wikle 2003) and stochastic processes (Wikle *et al.* 2003). In this dissertation, we set the boundary value to be the same as the value of its adjacent pixel on the edge of the image. In this scenario, no ink loss would be induced by ink diffusion. Considering the slow ink diffusion rate, this is a minor assumption since the image size could be very large so that the ink diffusion on the boundary would have little effect on the main body of the image. We then rewrite Eq. (3.11) as Eq. (3.12),

$$a_{i;s}(t+\Delta t) = \left(1 - n_s \frac{\delta_i}{(\Delta s)^2} \Delta t\right) a_{i;s}(t) + \frac{\delta_i}{(\Delta s)^2} \Delta t \sum_{d(s,s')=\Delta s} a_{i;s'}(t) \tag{3.12}$$

where $s = 1, 2, \ldots, S$ is the pixel number after vectorizing the image, $a_{i;s}(t)$ is the area coverage of state *i* at pixel *s* at time *t*, n_s is the number of inside-image adjacent pixels of pixel *s*, and $d(s, s')$ is the Euclidean distance between pixels *s* and *s'*.

A vector autoregressive model for the diffusion of state *i* is given in Eq. (3.13),

$$\boldsymbol{a}_i(t + \Delta t) = \mathbf{H}_i \boldsymbol{a}_i(t) \tag{3.13}$$

where $\boldsymbol{a}_i(t) = \begin{bmatrix} a_{i;1}(t) & a_{i;2}(t) & \ldots & a_{i;S}(t) \end{bmatrix}^{\mathrm{T}}$ is the column vector of the area coverage of state *i* at time *t*, and $\mathbf{H}_i$ is the diffusion transition matrix of state *i* with diagonal values of $1 - n_s \frac{\delta_i}{(\Delta s)^2} \Delta t$ and values of $\frac{\delta_i}{(\Delta s)^2} \Delta t$ for pixel *s'* satisfying $d(s, s') = \Delta s$ in the s^{th} row of the matrix. Though there is no transition between different states, we write the autoregressive ink diffusion model for all the states as Eq. (3.14),

$$\boldsymbol{a}(t + \Delta t) = \mathbf{H}\boldsymbol{a}(t) \tag{3.14}$$

where $\boldsymbol{a}(t) = \begin{bmatrix} \boldsymbol{a}_1^{\mathrm{T}}(t) & \boldsymbol{a}_2^{\mathrm{T}}(t) & \cdots & \boldsymbol{a}_{15}^{\mathrm{T}}(t) \end{bmatrix}^{\mathrm{T}}$ is the column vector of the area coverage of all the states at time *t*, and **H** is the overall diffusion transition matrix as shown in Appendix.

3.3.1 *Numerical Examples*

In this section, we provide numerical simulations using the physics-based ink diffusion model. The spacings in time and space are $\Delta t = \Delta s = 1$ throughout the dissertation. For better illustration, we first provide a degradation simulation of a black ink dot on a white

paper, as shown in Figure 3.8. The diffusion rate used in the simulation is δ = 0.05. The ink in the simulation gradually diffuses to the surrounding area.

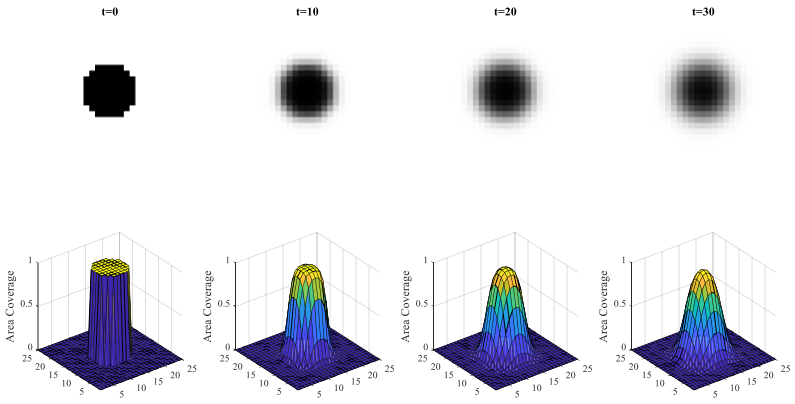

Figure 3.8 Ink dot degradation using physics-based ink diffusion model

The proposed model is applied to the 3 × 3 color pixels given in Table 3.1. The diffusion rates are δ_i = 0.005 for all the states. The predicted area coverages of the states and the CMY inks are plotted in Figure 3.9 and Figure 3.10, respectively. The area coverage change in this simulation is induced by ink diffusion alone. The color degradation is shown in Figure 3.11. The degradation induced by ink diffusion is not only affected by the diffusion rates but also by the spatial location of the pixels.

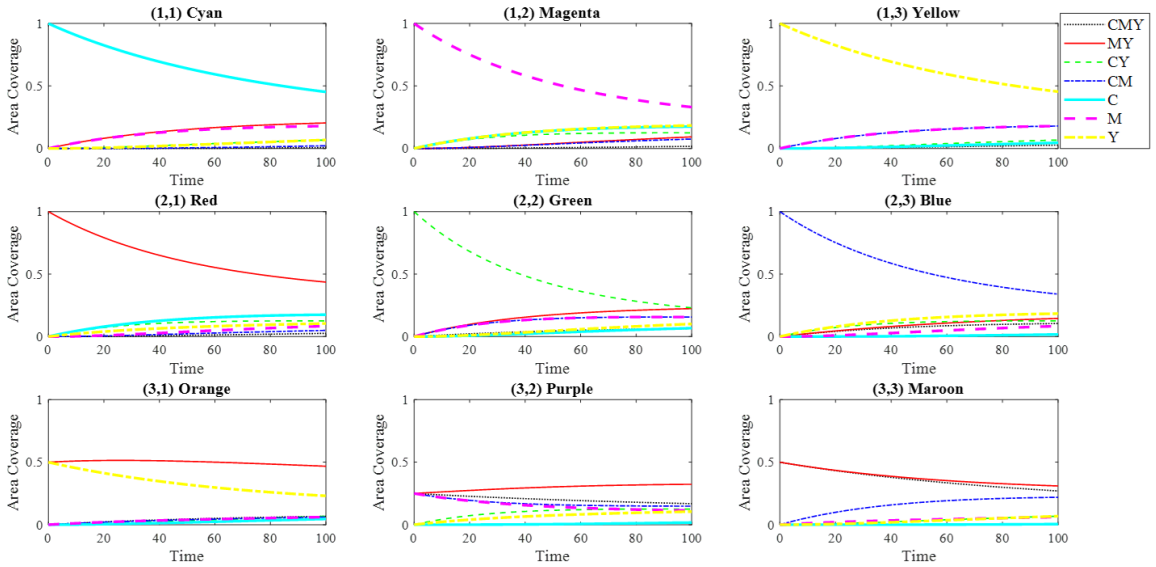

Figure 3.9 Predicted area coverages of states using physics-based ink diffusion model

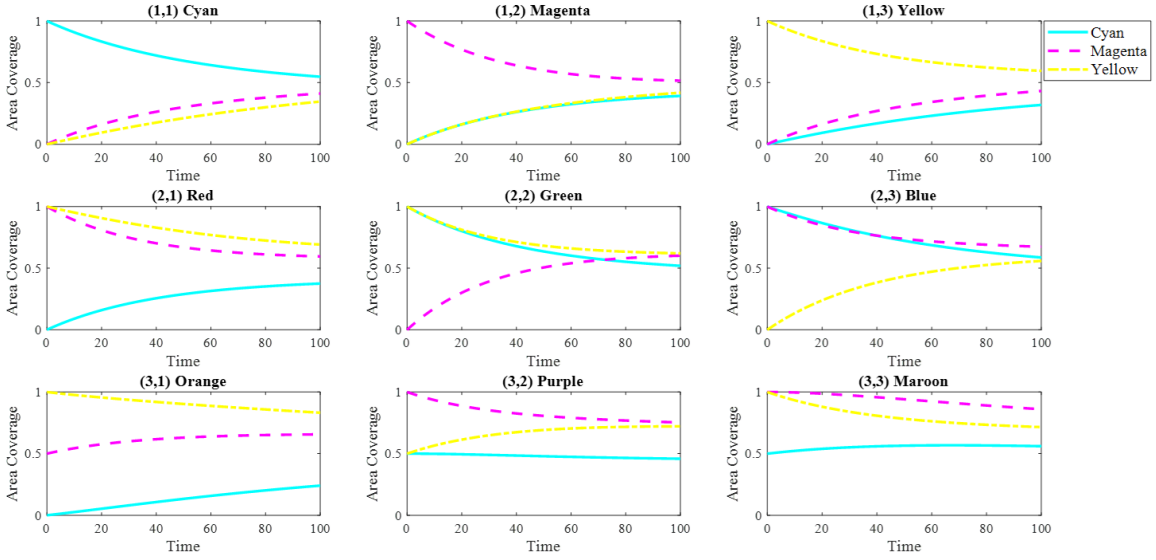

Figure 3.10 Predicted area coverages of inks using physics-based ink diffusion model

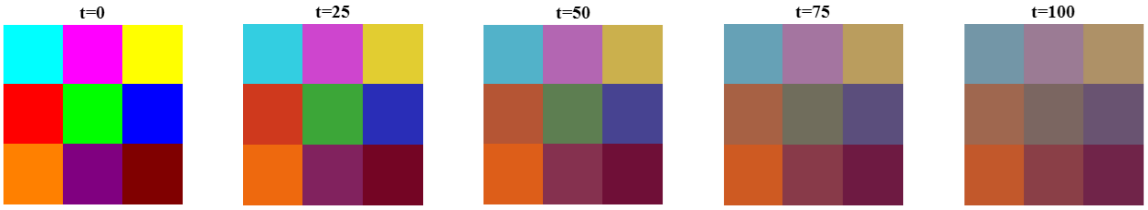

Figure 3.11 Color degradation using physics-based ink diffusion model

An image degradation simulation using diffusion rates δ_i = 0.05 for all the states is shown in Figure 3.12. The ink diffusion results in a blurry effect to the image.

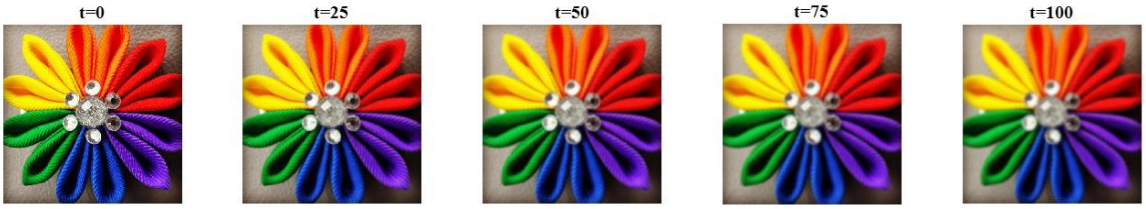

Figure 3.12 Image degradation using physics-based ink diffusion model

3.4 Degradation Model of Ink Fading and Ink Diffusion

Integrating the ink fading model and the ink diffusion model yields the degradation model of ink fading and ink diffusion for state *i* in Eq. (3.15),

$$\frac{\partial a_{i;s}(t)}{\partial t} = \sum_j k_{j,i} a_{j;s}(t) - \kappa_i a_{i;s}(t) + \delta_i \left(\frac{\partial^2 a_{i;s}(t)}{\partial x^2} + \frac{\partial^2 a_{i;s}(t)}{\partial y^2} \right) \tag{3.15}$$

where $a_{i;s}(t)$ is the area coverage of state *i* at pixel *s* at time *t*. Applying finite difference method to Eq. (3.15) results in Eq. (3.16),

$$\begin{aligned} a_{i;s}(t+\Delta t) = & \left(1 - \kappa_i \Delta t - n_s \frac{\delta_i}{(\Delta s)^2} \Delta t \right) a_{i;s}(t) + \\ & \frac{\delta_i}{(\Delta s)^2} \Delta t \sum_{d(s,s')=\Delta s} a_{i;s'}(t) + \Delta t \sum_j k_{j,i} a_{j;s}(t) \end{aligned} \tag{3.16}$$

where n_s is the number of inside-image adjacent pixels of pixel s, $d(s,s')$ is the Euclidean distance between pixels s and s'. The vector autoregressive degradation model of ink fading and ink diffusion is given in Eq. (3.17),

$$\boldsymbol{a}(t+\Delta t) = \boldsymbol{\Pi}\boldsymbol{a}(t) \tag{3.17}$$

where $\boldsymbol{a}(t)$ is the column vector of the area coverage of all the states at time t, and $\boldsymbol{\Pi}$ is the overall fading-diffusion transition matrix as shown in Appendix.

Assuming a multiplicative lognormal error for state i since the area coverage is nonnegative, the random area coverage is given in Eq. (3.18),

$$\tilde{a}_{i;s}(t) = \varepsilon_i a_{i;s}(t) \tag{3.18}$$

where $\tilde{a}_{i;s}(t)$ is the random area coverage of state i at pixel s at time t, and $\varepsilon_i \sim LN\left(-\frac{\sigma_i^2}{2}, \sigma_i^2\right)$ is a spatially and temporally independent lognormal error. The random area coverage then follows a lognormal distribution $\tilde{a}_{i;s}(t) \sim LN\left(\ln a_{i;s}(t) - \frac{\sigma_i^2}{2}, \sigma_i^2\right)$ with expectation $E\left(\tilde{a}_{i;s}(t)\right) = a_{i;s}(t)$ and variance $Var\left(\tilde{a}_{i;s}(t)\right) = a_{i;s}^2(t)\left(e^{\sigma_i^2} - 1\right)$.

3.4.1 *Parameters Estimation*

The fading and diffusion rates of the states can be estimated separately. For example, patches of cyan ink can be printed to estimate the fading rate of state C, the diffusion rate of state C can then be estimated by printing appropriate samples for ink diffusion tests and

considering the fading rate of state C as known value. The fading and diffusion rates of the two-ink state CM can be estimated separately after the fading and diffusion rates of one-ink states C and M are estimated. Similarly, the fading and diffusion rates of the three-ink and four-ink states can be estimated.

Once the fading rates are estimated, the diffusion rates are then estimated sequentially by printing each state as the top state over the space. Assuming that there are *S* pixels in the image and *M*+1 area coverage measurements at time t_m, $m = 0,1,...,M$, $t_0 = 0$, the likelihood function of the area coverage of state *i* is

$$\mathcal{L} = \sum_{s=1}^{S} \sum_{m=1}^{M} \frac{1}{\sqrt{2\pi\sigma_i^2}} \exp\left(-\frac{1}{2\sigma_i^2} \left(\ln x_{i;s}(t_m) - \ln a_{i;s}(t_m) + \frac{\sigma_i^2}{2} \right)^2 \right) \qquad (3.19)$$

where $x_{i;s}(t_m)$ and $a_{i;s}(t_m)$ are the measured and predicted area coverages of state *i* at pixel *s* at time t_m, respectively. The diffusion rate of state *i* is obtained by maximizing the likelihood function given in Eq. (3.19).

3.4.2 *Numerical Examples*

In this section, we provide numerical simulations using the physics-based degradation model of ink fading and ink diffusion. The three models developed in this chapter are compared in Figure 3.13. The fading and diffusion rates used in the ink dot degradation simulation are $k = 0.03$ and $\delta = 0.05$, respectively.

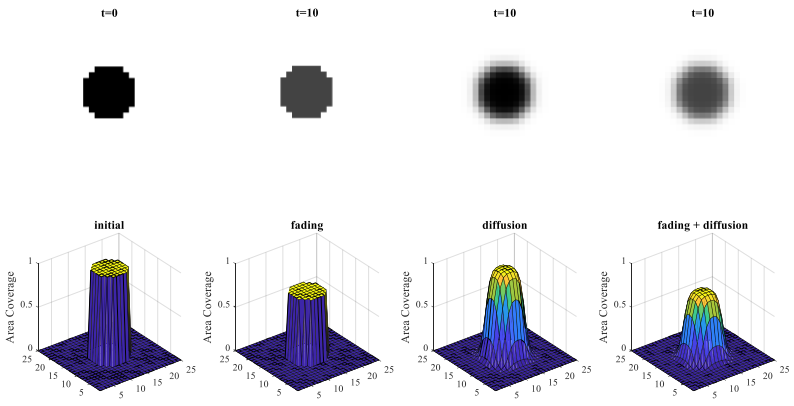

Figure 3.13 Ink dot degradation using physics-based ink fading, ink diffusion, and ink fading and diffusion models

The proposed model is applied to the 3 × 3 color pixels given in Table 3.1. The fading rates are shown in Table 3.3 and the diffusion rates are $\delta_i = 0.005$ for all the states. The predicted area coverages of the states and the CMY inks are plotted in Figure 3.14 and Figure 3.15, respectively. The color degradation is shown in Figure 3.16.

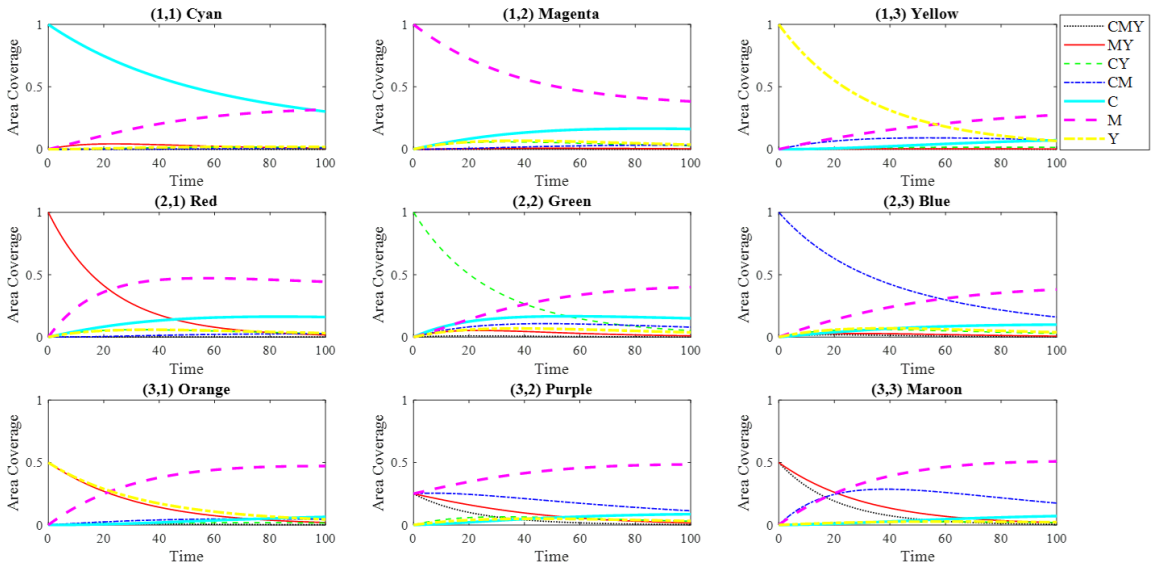

Figure 3.14 Predicted area coverages of states using physics-based degradation model of ink fading and ink diffusion

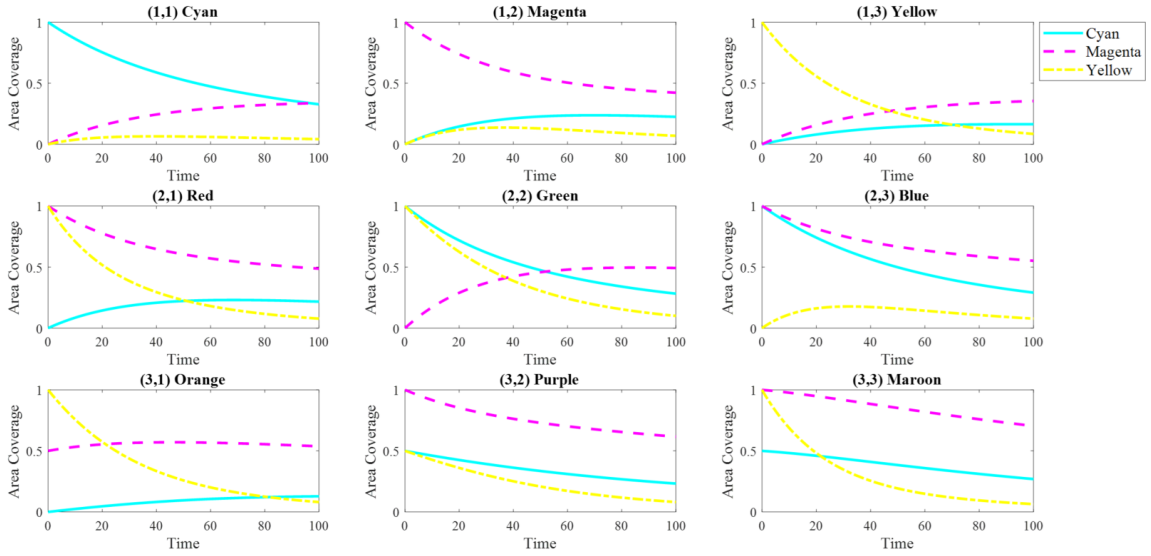

Figure 3.15 Predicted area coverages of inks using physics-based degradation model of ink fading and ink diffusion

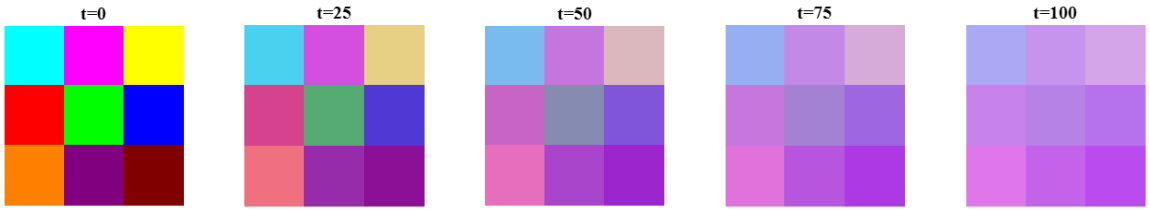

Figure 3.16 Color degradation using physics-based degradation model of ink fading and ink diffusion

The image degradation simulation using the fading rates shown in Table 3.3 and diffusion rates $\delta_i = 0.05$ for all the states is shown in Figure 3.17. The simulation results in the figures show a combined effect of both fading and diffusion.

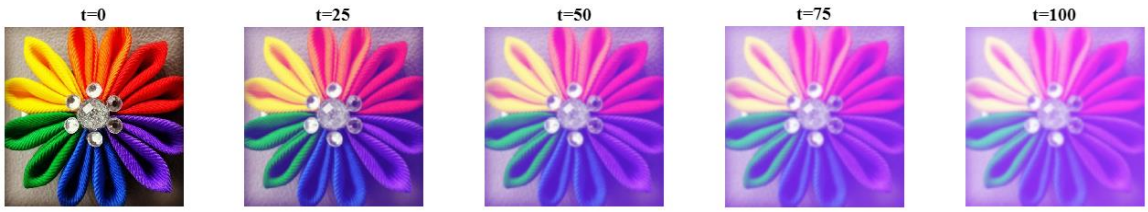

Figure 3.17 Image degradation using physics-based degradation model of ink fading and ink diffusion

3.5 Summary and Conclusions

In this chapter, we first investigate the halftone printing technique used by modern color printers and discuss the performance indicator we use in the degradation modeling of printed images. In consideration of catalytic fading, we propose a multi-layered state transition diagram for the ink fading of printed images. Assuming the ink fading as a first-order reaction, a physics-based ink fading model is derived from differential equations. In addition, ink diffusion of printed images is modeled using the two-dimensional diffusion equation. Discretizing the diffusion equation in both space and time using finite difference method results in a vector autoregressive ink diffusion model. The ink fading model and the ink diffusion model are further integrated into an autoregressive degradation model of ink fading and ink diffusion.

CHAPTER 4

PHYSICS-BASED DEGRADATION MODEL OF PRINTED IMAGES WITH TIME-VARYING FADING AND DIFFUSION RATES

In the previous chapter, it is assumed that inks have constant fading and diffusion rates. Such an assumption constrains the applicability of the degradation model. In this chapter, we relax this assumption and investigate the degradation modeling of printed images with time-varying fading and diffusion rates.

4.1 Hazard Rate and Image Degradation

The degradation model in the previous chapter is developed from the differential equations that describe the physics of ink fading and diffusion. The ink area coverage is used as the performance indicator, and the area coverage loss rate is the degradation rate. Considering no area coverage transition from other states or pixels, the instantaneous area coverage loss rate of a state by ink fading or diffusion is calculated as the product of its fading or diffusion rate and its area coverage.

To relax the assumption of constant fading and diffusion rates, we examine the developed degradation model. For ink fading, we assume that in an infinitesimal area any ink in any state fades completely at the same time, the assumption of constant fading rate then implies an exponential degradation time distribution of the inks. If there is no area coverage transition from other states into a state and its initial area coverage $a_i(0)$ is considered as

a population, the remaining area coverage percentage $\frac{a_i(t)}{a_i(0)}$ is its "reliability" $R_i(t)$.

Discretizing the ink fading model in Eq. (3.1) for a state having no area coverage transition into it and rearranging the terms result in

$$\kappa_i = \lim_{\Delta t \to 0} \frac{\frac{a_i(t)}{a_i(0)} - \frac{a_i(t+\Delta t)}{a_i(0)}}{\Delta t \frac{a_i(t)}{a_i(0)}} = \lim_{\Delta t \to 0} \frac{R_i(t) - R_i(t+\Delta t)}{\Delta t R_i(t)}$$

This is the definition of hazard function. If we only consider the ink diffusion from one pixel to one of its adjacent pixels in the discretized ink diffusion model in Eq. (3.12) and let $\Delta s = 1$, we derive a similar result as

$$\delta_i = \lim_{\Delta t \to 0} \frac{\frac{a_{i;s}(t)}{a_{i;s}(0)} - \frac{a_{i;s}(t+\Delta t)}{a_{i;s}(0)}}{\Delta t \frac{a_{i;s}(t)}{a_{i;s}(0)}} = \lim_{\Delta t \to 0} \frac{R_{i;s}(t) - R_{i;s}(t+\Delta t)}{\Delta t R_{i;s}(t)}$$

Hence, the fading or diffusion rate is equivalent to the hazard rate of the remaining area coverage percentage.

Therefore, ink fading and diffusion can be modeled as a Markov process. For the inks in each infinitesimal area, the degradation process starts from its initial state with probability one. The inks in an infinitesimal area starting from state *i* at pixel *s* are in state *j* at pixel *s′* at time *t* have a state transition probability $\phi_{i,j;s,s'}(t)$. The total area coverage of state *j* at pixel *s′* at time *t* is the sum of the product of the initial area coverage of every state in every pixel and their state transition probability $\phi_{i,j;s,s'}(t)$. The matrix form is expressed in Eq. (4.1),

$$\boldsymbol{a}(t) = \boldsymbol{a}(0)\boldsymbol{\phi}(t) \tag{4.1}$$

where $\boldsymbol{a}(t)$ is a row vector of the area coverage of all the states in all pixels at time *t*, and $\boldsymbol{\phi}(t)$ is the state transition probability matrix satisfying $\sum_{s'}\sum_{j}\phi_{i,j;s,s'}(t) = 1$.

As described above, a Markov process with exponential transition time distribution is equivalent to the developed degradation model in Chapter 3. A degradation model with time-varying fading and diffusion rates is obtained by replacing the exponential distribution with other distributions. By doing so, the Markov model becomes a semi-Markov model. We present the latter model in this chapter.

4.2 Degradation Model of Ink Fading

Hereafter, we refer to the degradation model with constant fading and diffusion rates as the Markov model, and the degradation model with time-varying fading and diffusion rates as the semi-Markov model. The general formulation of the semi-Markov model is given in (Howard 1964, Howard 1971). The developed semi-Markov ink fading model is presented below. Denote the *pdf* and CDF of the transition time that the inks in an infinitesimal area fade from state *i* to one of its one-step transition states *u* as $f_{i,u}(t)$ and $F_{i,u}(t)$, respectively. The one-step state transition probability density that the inks fade from state *i* to state *u* at time *t* is given in Eq. (4.2),

$$q_{i,u}(t) = f_{i,u}(t)\prod_{v\in\Omega_i, v\neq u}\left(1 - F_{i,v}(t)\right) \tag{4.2}$$

where $q_{i,u}(t)$ is the one-step state transition probability density that the inks fade from state *i* to state *u* at time *t*, and Ω_i is the set of the one-step transition states from state *i*. If state *u* is the only one-step transition state from state *i*, $q_{i,u}(t) = f_{i,u}(t)$. Assuming that the inks in an infinitesimal area start from state *i*, the probability that the inks are still in state *i* at time *t* is given in Eq. (4.3),

$$\phi_{i,i}(t) = 1 - \int_0^t \sum_{v \in \Omega_i} q_{i,v}(\tau) d\tau \tag{4.3}$$

where $\phi_{i,i}(t)$ is the probability that the inks are still in state *i* at time *t*. The probability that the inks fade to any other state *j* at time *t* is given in Eq. (4.4),

$$\phi_{i,j}(t) = \sum_{v \in \Omega_i} \int_0^t q_{i,v}(\tau) \phi_{v,j}(t-\tau) d\tau \tag{4.4}$$

where $\phi_{i,j}(t)$ is the probability that the inks fade to any other state *j* at time *t*.

The matrix form of the state transition probability is given in Eq. (4.5),

$$\boldsymbol{\phi}(t) = diag(\boldsymbol{\phi}(t)) + \int_0^t \mathbf{q}(\tau) \boldsymbol{\phi}(t-\tau) d\tau \tag{4.5}$$

where $diag(\boldsymbol{\phi}(t))$ is the diagonal matrix of $\phi_{i,i}(t)$, and $\mathbf{q}(t)$ is the one-step state transition probability density matrix. With initial condition $\boldsymbol{\phi}(0) = \mathbf{I}$, Eq. (4.5) is solved recursively using trapezoidal rule (Nunn and Desiderio 1977) as shown in Eq. (4.6),

$$\boldsymbol{\phi}(t_M) = \left[\mathbf{I} - \frac{\Delta t}{2}\mathbf{q}(0)\right]^{-1} \left[diag(\boldsymbol{\phi}(t_M)) + \Delta t \sum_{m=1}^{M} \mathbf{q}(t_m)\boldsymbol{\phi}(t_M - t_m) - \frac{\Delta t}{2}\mathbf{q}(t_M)\boldsymbol{\phi}(0)\right] \tag{4.6}$$

We discuss the case of the Weibull state transition time distribution. The fading rate then becomes a function of time $k_{i,u}(t)=\frac{\gamma_{i,u}t^{\gamma_{i,u}-1}}{\theta_{i,u}^{\gamma_{i,u}}}$ with shape parameter $\gamma_{i,u}$ and scale parameter $\theta_{i,u}$. When $\gamma_{i,u}>1$, the fading rate is a monotonically increasing function. When $\gamma_{i,u}=1$, Weibull distribution becomes exponential distribution, and the fading rate becomes constant. When $\gamma_{i,u}<1$, the fading rate decreases with time. The one-step state transition probability density and the state transition probability $\phi_{i,i}(t)$ are

$$q_{i,u}(t)=\frac{\gamma_{i,u}t^{\gamma_{i,u}-1}}{\theta_{i,u}^{\gamma_{i,u}}}\exp\left(-\sum_{v\in\Omega_i}\left(\frac{t}{\theta_{i,v}}\right)^{\gamma_{i,v}}\right)$$

$$\phi_{i,i}(t)=\exp\left(-\sum_{v\in\Omega_i}\left(\frac{t}{\theta_{i,v}}\right)^{\gamma_{i,v}}\right)$$

4.2.1 *Parameters Estimation*

We first estimate the fading parameters of the one-ink states. The predicted area coverage of a one-ink state *i* (*i* = 12 C, 13 M, 14 Y, 15 K) is

$$a_i(t)=a_i(0)\phi_{i,i}(t)=a_i(0)\exp\left(-\left(\frac{t}{\theta_{i,16}}\right)^{\gamma_{i,16}}\right)$$

It is linearized as

$$\ln\left(-\ln\frac{a_i(t)}{a_i(0)}\right)=\gamma_{i,16}\ln t-\gamma_{i,16}\ln\theta_{i,16}$$

Assuming that there are N samples and M+1 area coverage measurements at time $t_m,\ m=0,1,...,M,\ t_0=0$. Let $x_{i;n}(t_m)$ be the measured area coverage of state i of the n^{th} sample at time t_m. Denote $\boldsymbol{Y}$ as the column vector of $\ln\left[-\ln\frac{x_{i;n}(t_m)}{x_{i;n}(t_0)}\right]$, $\boldsymbol{X}$ as the column vector of $\begin{bmatrix}\ln t_m & 1\end{bmatrix}$, and $\boldsymbol{b}=\begin{bmatrix}\gamma_{i,16}\\ -\gamma_{i,16}\ln\theta_{i,16}\end{bmatrix}$, the solution using least squares method is

$$\hat{\boldsymbol{b}}=\left(\boldsymbol{X}^{\mathrm{T}}\boldsymbol{X}\right)^{-1}\boldsymbol{X}^{\mathrm{T}}\boldsymbol{Y}$$

The fading parameters of the two-ink states are obtained using the estimated parameters of the one-ink states. Let state i be a two-ink state (i = 6 MY, 7 CY, 8 CM, 9 CK, 10 MK, 11 YK), and u and v are the two transition states from state i. The predicted area coverages of the three states are

$$a_i(t)=a_i(0)\phi_{i,i}(t)$$

$$a_u(t)=a_i(0)\phi_{i,u}(t)+a_u(0)\phi_{u,u}(t)$$

$$a_v(t)=a_i(0)\phi_{i,v}(t)+a_v(0)\phi_{v,v}(t)$$

The estimated fading parameters of states u and v are considered as known values, then $\phi_{u,u}(t)$ and $\phi_{v,v}(t)$ can be predicted. $\phi_{i,i}(t)$ can also be approximated using the measured area coverages of state i. The state transition probabilities $\phi_{i,u}(t)$ and $\phi_{i,v}(t)$ are

$$\phi_{i,u}(t)=\int_0^t k_{i,u}(\tau)\phi_{i,i}(\tau)\phi_{u,u}(t-\tau)\,d\tau=\int_0^t \phi_{i,i}(\tau)\phi_{u,u}(t-\tau)\,d\left(\frac{\tau}{\theta_{i,u}}\right)^{\gamma_{i,u}}$$

$$\phi_{i,v}(t)=\int_0^t k_{i,v}(\tau)\phi_{i,i}(\tau)\phi_{v,v}(t-\tau)\,d\tau=\int_0^t \phi_{i,i}(\tau)\phi_{v,v}(t-\tau)\,d\left(\frac{\tau}{\theta_{i,v}}\right)^{\gamma_{i,v}}$$

where $k_{i,u}(t) = \frac{\gamma_{i,u} t^{\gamma_{i,u}-1}}{\theta_{i,u}^{\gamma_{i,u}}}$ and $k_{i,v}(t) = \frac{\gamma_{i,v} t^{\gamma_{i,v}-1}}{\theta_{i,v}^{\gamma_{i,v}}}$ are the fading rates from state *i* to states *u* and *v*, respectively. The fading parameters of the transition from state *i* to state *u* (or state *v*) are obtained numerically by minimizing the sum of squared errors between the measured and predicted area coverages of state *u*,

$$\min \sum_{n=1}^{N} \sum_{m=1}^{M} \left(x_{u;n}(t_m) - a_{u;n}(t_m) \right)^2$$

where $x_{u;n}(t_m)$ and $a_{u;n}(t_m)$ are the measured and predicted area coverages of state *u* of the n^{th} sample at time t_m, respectively. The same parameters estimation procedure is applied to the three-ink and four-ink states.

4.2.2 *Numerical Examples*

In this section, we provide numerical simulations using the semi-Markov ink fading model. The proposed model is applied to the 3 × 3 color pixels given in Table 3.1. The scale parameters of the fading rates $\theta_{i,j}$ are chosen as the reciprocal of the fading rates in Table 3.3. The shape parameters of all the fading rates are $\gamma_{i,j} = 2$. A shape parameter larger than one means an accelerating fading rate.

The predicted area coverages of the states and the CMY inks are plotted in Figure 4.1 and Figure 4.2, respectively. As shown in the figures, the inks exhibit increasing fading rates as the result of the selected shape parameters. Compared with the Markov ink fading model, this simulation represents the case that inks are more durable initially and significant fading has a time delay.

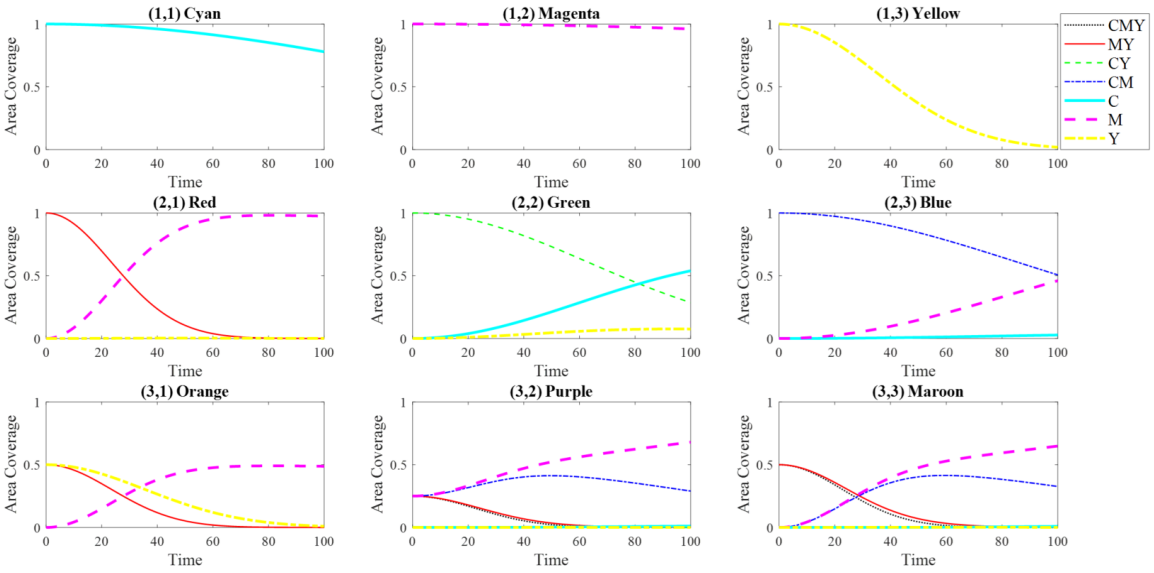

Figure 4.1 Predicted area coverages of states using semi-Markov ink fading model

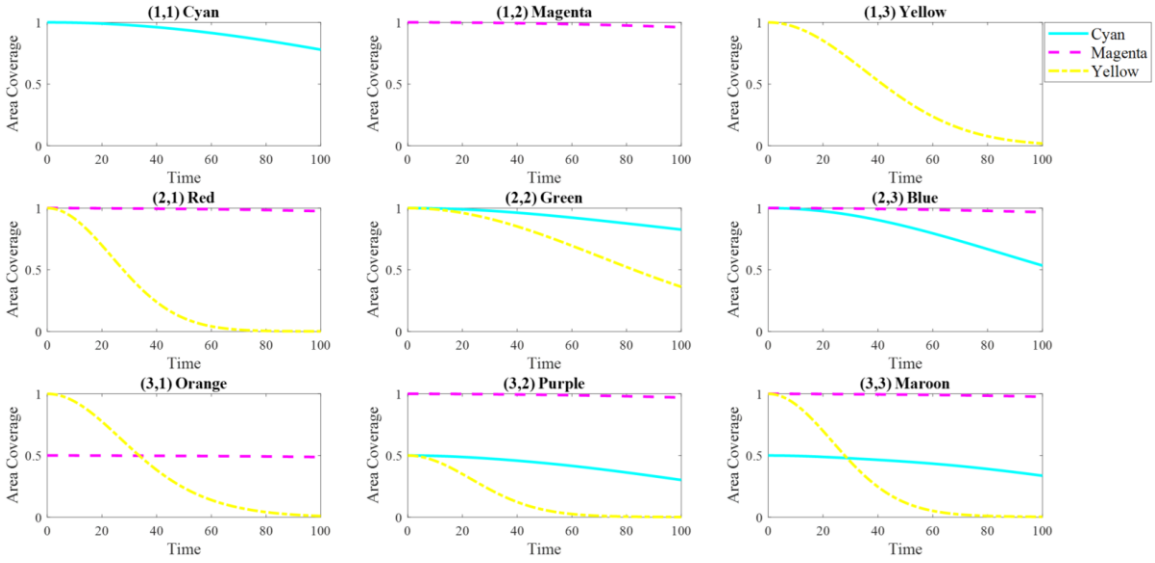

Figure 4.2 Predicted area coverages of inks using semi-Markov ink fading model

A real-life case study is used to demonstrate the application of the proposed model. Yellow ink is printed and tested at an elevated temperature, humidity, and illumination condition in our laboratory. Its microscopic photos are taken every week and shown in Figure 4.3.

The area coverages of the yellow ink in these photos are estimated and fitted by the proposed model, as shown in Figure 4.4. In the figure, the estimated area coverages of the yellow ink are plotted as dots, and the prediction using the semi-Markov ink fading model is plotted as a solid line. The estimated shape and scale parameters of the yellow ink fading are 3.38 and 5.26, respectively. The degradation in this real-life case study shows a clear trend of acceleration and can only be well fitted with a time-varying fading rate.

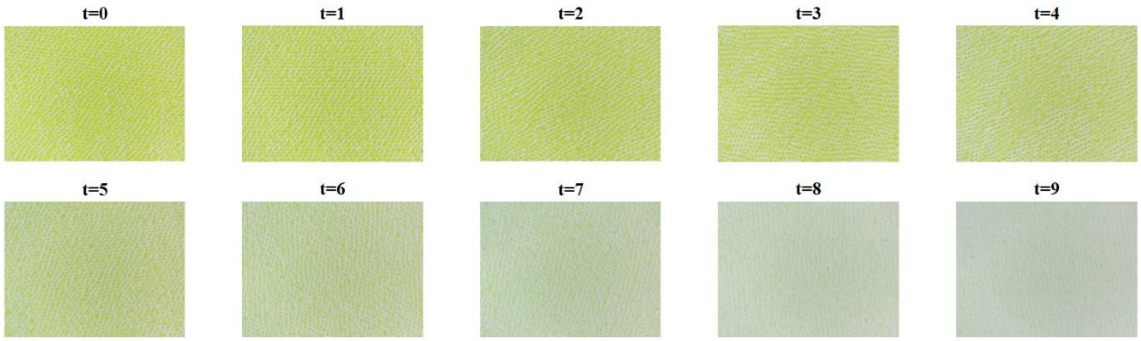

Figure 4.3 Microscopic photos of yellow ink under accelerated degradation test

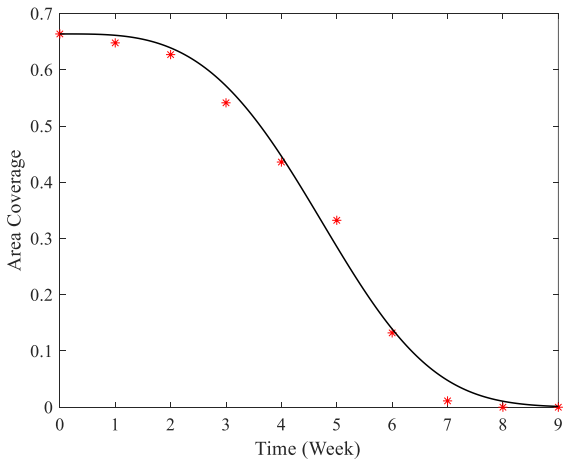

Figure 4.4 Degradation prediction of yellow ink

The microscopic photos of a red color tested under the same environmental condition are shown in Figure 4.5. The red color is printed with the magenta and yellow inks. Magenta ink is also tested in this experiment. The estimated shape and scale parameters of the magenta ink fading are 2.01 and 33.03, respectively. The presence of the yellow ink in state MY is found to have no influence on the degradation characteristics of the magenta ink. The estimated shape and scale parameters of the yellow ink fading in state MY are 1.63 and 10.08, respectively. The estimated area coverages of the states (MY, M and Y) and the degradation prediction using the semi-Markov ink fading model are shown in Figure 4.6. The estimated parameters for the yellow and magenta inks are used in the parameters estimation and degradation prediction of the red color. The degradation prediction of the red color validates the model performance.

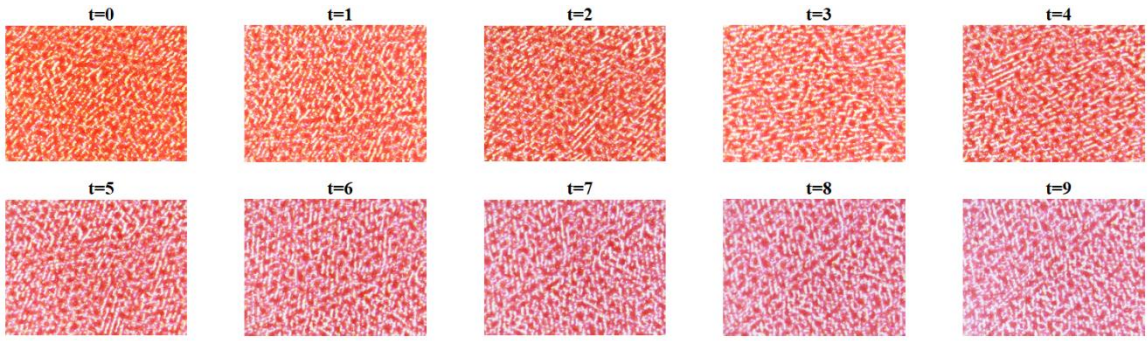

Figure 4.5 Microscopic photos of the red color under accelerated degradation test

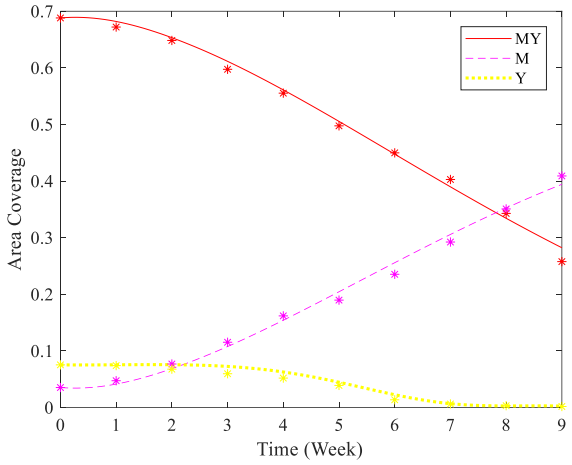

Figure 4.6 Degradation prediction of the red color

4.3 Degradation Model of Ink Diffusion

Denote the *pdf* and CDF of the transition time that the inks in an infinitesimal area diffuse from pixel s to one of its adjacent pixels s' as $f_{s,s'}(t)$ and $F_{s,s'}(t)$, respectively. The one-step state transition probability density that the inks diffuse from pixel s to pixel s' at time t is given in Eq. (4.7),

$$q_{s,s'}(t) = f_{s,s'}(t) \prod_{s'' \in \Omega_s, s'' \neq s'} \left(1 - F_{s,s''}(t)\right) \tag{4.7}$$

where $q_{s,s'}(t)$ is the one-step state transition probability density that the inks diffuse from pixel s to pixel s' at time t, and Ω_s is the set of adjacent pixels of pixel s. Assuming that the inks in an infinitesimal area start from pixel s, the probability that the inks are still at pixel s at time t is given in Eq. (4.8),

$$\phi_{s,s}(t) = 1 - \int_0^t \sum_{s'' \in \Omega_s} q_{s,s''}(\tau) d\tau \tag{4.8}$$

where $\phi_{s,s}(t)$ is the probability that the inks are still at pixel *s* at time *t*. The probability that the inks diffuse to any other pixel *s'''* at time *t* is given in Eq. (4.9),

$$\phi_{s,s'''}(t) = \sum_{s''\in\Omega_s} \int_0^t q_{s,s''}(\tau)\phi_{s'',s'''}(t-\tau)\,d\tau \tag{4.9}$$

where $\phi_{s,s'''}(t)$ is the probability that the inks diffuse to any other pixel *s'''* at time *t*. The matrix form of the state transition probability is given in Eq. (4.5) and solved using trapezoidal rule as shown in Eq. (4.6).

For the case of Weibull state transition time distribution, The diffusion rate is a function of time $\delta_i(t) = \frac{\gamma_i t^{\gamma_i - 1}}{\theta_i^{\gamma_i}}$ with shape parameter γ_i and scale parameter θ_i. Decreasing diffusion rates with shape parameters smaller than one may be more appropriate than constant diffusion rates for the ink diffusion of printed images. The one-step state transition probability density and the state transition probability $\phi_{s,s}(t)$ are

$$q_{s,s'}(t) = \frac{\gamma_i t^{\gamma_i - 1}}{\theta_i^{\gamma_i}} \exp\left(-n_s \left(\frac{t}{\theta_i} \right)^{\gamma_i} \right)$$

$$\phi_{s,s}(t) = \exp\left(-n_s \left(\frac{t}{\theta_i} \right)^{\gamma_i} \right)$$

where n_s is the number of inside-image adjacent pixels of pixel *s*.

4.3.1 *Numerical Examples*

In this section, we provide numerical simulations using the semi-Markov ink diffusion model. The proposed model is applied to the 3 × 3 color pixels given in Table 3.1. The shape and scale parameters of all the diffusion rates are $\gamma_i = 0.5$ and $\theta_i = 1000$. The predicted area coverages of the states and the CMY inks are plotted in Figure 4.7 and Figure 4.8, respectively. As shown in the figures, the inks exhibit obvious decreasing diffusion rates.

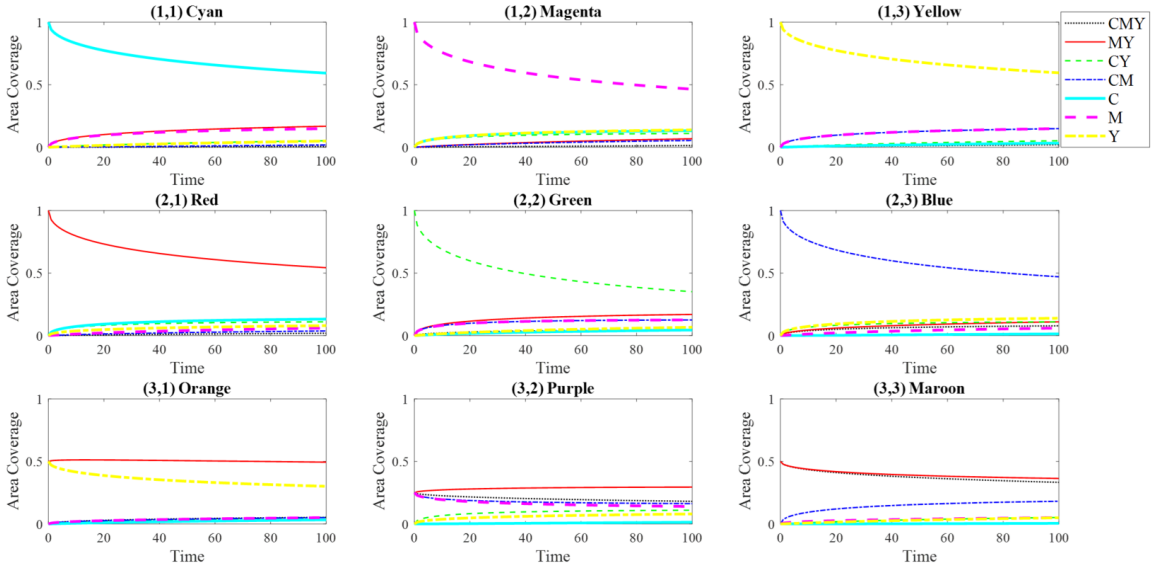

Figure 4.7 Predicted area coverages of states using semi-Markov ink diffusion model

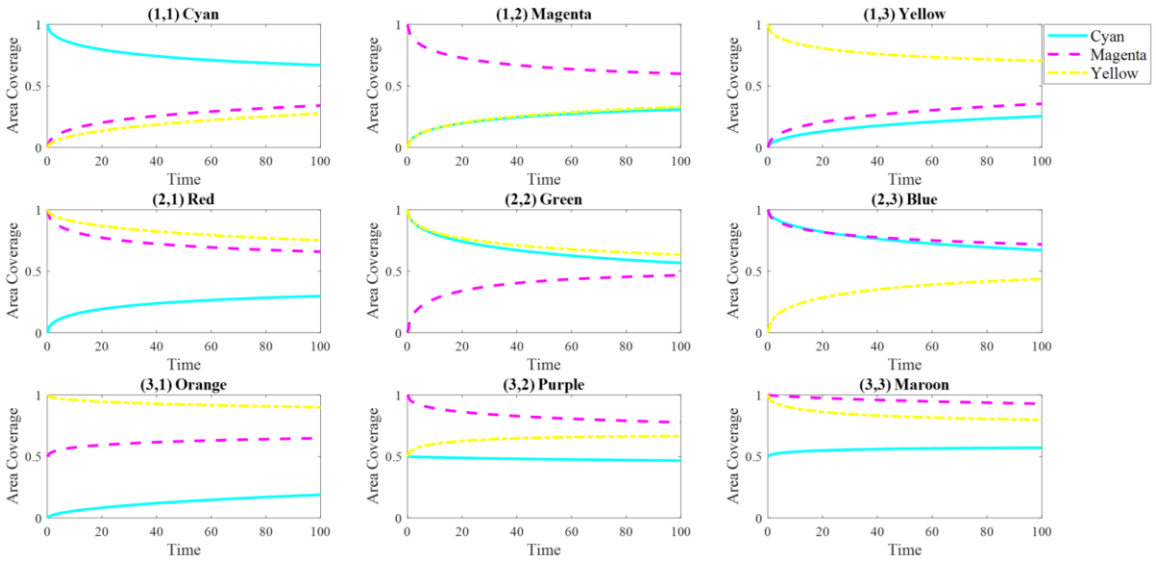

Figure 4.8 Predicted area coverages of inks using semi-Markov ink diffusion model

4.4 Degradation Model of Ink Fading and Ink Diffusion

Denote the *pdf* and CDF of the transition time that the inks in an infinitesimal area fade from state *i* to one of its one-step transition states *u* within pixel *s* as $f_{i,u;s,s}(t)$ and $F_{i,u;s,s}(t)$, respectively, and the *pdf* and CDF of the transition time that the inks in an infinitesimal area diffuse from pixel *s* to one of its adjacent pixels *s′* without fading as $f_{i,i;s,s'}(t)$ and $F_{i,i;s,s'}(t)$, respectively. The one-step state transition probability density that the inks fade from state *i* to state *u* within pixel *s* at time *t* is given in Eq. (4.10),

$$q_{i,u;s,s}(t) = f_{i,u;s,s}(t) \prod_{v\in\Omega_i, v\neq u} \left(1-F_{i,v;s,s}(t)\right) \prod_{s''\in\Omega_s} \left(1-F_{i,i;s,s''}(t)\right) \tag{4.10}$$

where $q_{i,u;s,s}(t)$ is the one-step state transition probability density that the inks fade from state *i* to state *u* within pixel *s* at time *t*. The one-step state transition probability density that the inks diffuse from pixel *s* to pixel *s′* without fading at time *t* is given in Eq. (4.11),

$$q_{i,i;s,s'}(t) = f_{i,i;s,s'}(t) \prod_{s''\in\Omega_s, s''\neq s'} \left(1 - F_{i,i;s,s''}(t)\right) \prod_{v\in\Omega_i} \left(1 - F_{i,v;s,s}(t)\right) \tag{4.11}$$

where $q_{i,i;s,s'}(t)$ is the one-step state transition probability density that the inks diffuse from pixel *s* to pixel *s′* without fading at time *t*. Assuming that the inks in an infinitesimal area start from state *i* at pixel *s*, the probability that the inks are still in state *i* at pixel *s* at time *t* is given in Eq. (4.12),

$$\phi_{i,i;s,s}(t) = 1 - \int_0^t \left(\sum_{v\in\Omega_i} q_{i,v;s,s}(\tau) + \sum_{s''\in\Omega_s} q_{i,i;s,s''}(\tau) \right) d\tau \tag{4.12}$$

where $\phi_{i,i;s,s}(t)$ is the probability that the inks are still in state *i* at pixel *s* at time *t*. The probability that the inks fade to any other state *j* and diffuse to any other pixel *s‴* at time *t* is given in Eq. (4.13),

$$\begin{aligned} \phi_{i,j;s,s'''}(t) = & \sum_{v\in\Omega_i} \int_0^t q_{i,v;s,s}(\tau) \phi_{v,j;s,s'''}(t-\tau) d\tau + \\ & \sum_{s''\in\Omega_s} \int_0^t q_{i,i;s,s''}(\tau) \phi_{i,j;s'',s'''}(t-\tau) d\tau \end{aligned} \tag{4.13}$$

where $\phi_{i,j;s,s'''}(t)$ is the probability that the inks fade to any other state *j* and diffuse to any other pixel *s‴* at time *t*. The matrix form of the state transition probability is given in Eq. (4.5) and solved using trapezoidal rule as shown in Eq. (4.6).

For the case of Weibull state transition time distribution, the one-step state transition probability density and the state transition probability $\phi_{i,i;s,s}(t)$ are

$$q_{i,u;s,s}(t) = \frac{\gamma_{i,u} t^{\gamma_{i,u}-1}}{\theta_{i,u}^{\gamma_{i,u}}} \exp\left(-\sum_{v\in\Omega_i} \left(\frac{t}{\theta_{i,v}} \right)^{\gamma_{i,v}} \right) \exp\left(-n_s \left(\frac{t}{\theta_i} \right)^{\gamma_i} \right)$$

$$q_{i,i;s,s'}(t) = \frac{\gamma_i t^{\gamma_i - 1}}{\theta_i^{\gamma_i}} \exp\left(-\sum_{v \in \Omega_i} \left(\frac{t}{\theta_{i,v}} \right)^{\gamma_{i,v}} \right) \exp\left(-n_s \left(\frac{t}{\theta_i} \right)^{\gamma_i} \right)$$

$$\phi_{i,i;s,s}(t) = \exp\left(-\sum_{v \in \Omega_i} \left(\frac{t}{\theta_{i,v}} \right)^{\gamma_{i,v}} \right) \exp\left(-n_s \left(\frac{t}{\theta_i} \right)^{\gamma_i} \right)$$

4.4.1 *Parameters Estimation*

Once the parameters of the fading rate are estimated, the parameters of the diffusion rate are estimated by sequentially printing each state as the top state over the space. The predicted area coverage of the top state *i* at pixel *s* at time *t* is

$$a_{i;s}(t) = a_{i;s}(0)\phi_{i,i;s,s}(t) + \sum_{s'} a_{i;s'}(0)\phi_{i,i;s',s}(t)$$

where $\phi_{i,i;s,s}(t)$ is given in Eq. (4.12), and $\phi_{i,i;s',s}(t) = \sum_{s'' \in \Omega_{s'}} \int_0^t q_{i,i;s',s''}(\tau)\phi_{i,i;s'',s}(t-\tau)d\tau$.

Assuming that there are *S* pixels in the image and *M*+1 area coverage measurements at time t_m, $m = 0,1,...,M$, $t_0 = 0$, the diffusion parameters of state *i* are obtained numerically by minimizing the sum of squared errors between the measured and predicted area coverages of state *i*,

$$\min \sum_{s=1}^{S} \sum_{m=1}^{M} \left(x_{i;s}(t_m) - a_{i;s}(t_m) \right)^2$$

where $x_{i;s}(t_m)$ and $a_{i;s}(t_m)$ are the measured and predicted area coverages of state *i* at pixel *s* at time t_m, respectively.

4.4.2 *Numerical Examples*

In this section, we provide numerical simulations using the semi-Markov degradation model of ink fading and ink diffusion. The proposed model is applied to the 3 × 3 color pixels given in Table 3.1. The scale parameters of the fading rates $\theta_{i,j}$ are chosen as the reciprocal of the fading rates in Table 3.3. The shape parameters of all the fading rates are $\gamma_{i,j} = 2$. The shape and scale parameters of all the diffusion rates are $\gamma_i = 0.5$ and $\theta_i = 1000$. The predicted area coverages of the states and the CMY inks using the semi-Markov degradation model of ink fading and ink diffusion are plotted in Figure 4.9 and Figure 4.10, respectively. The degradation shows a combined effect of both fading and diffusion. Because of the different fading rates, diffusion of cyan and magenta inks is more dominating, whereas fading of the yellow ink is more significant.

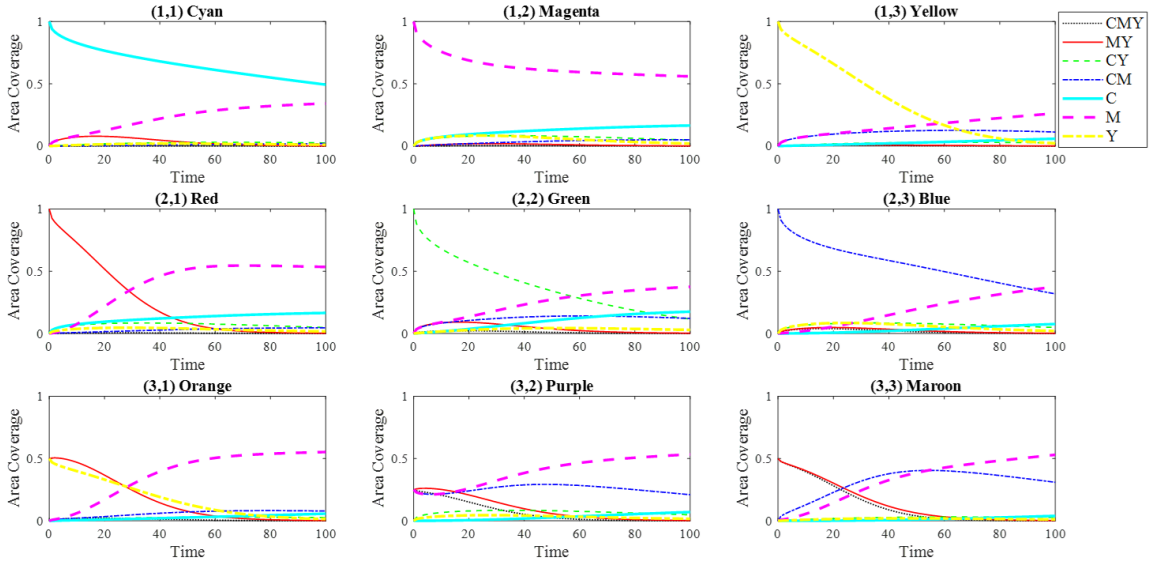

Figure 4.9 Predicted area coverages of states using semi-Markov degradation model of ink fading and ink diffusion

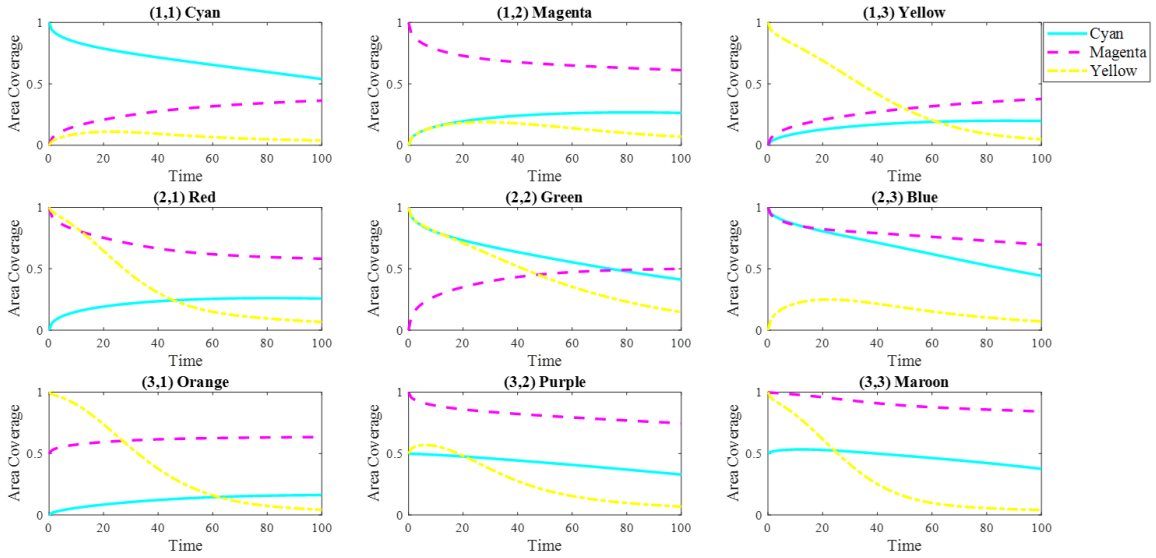

Figure 4.10 Predicted area coverages of inks using semi-Markov degradation model of ink fading and ink diffusion

4.5 Summary and Conclusions

In this chapter, we examine the degradation model developed in Chapter 3 and demonstrate that both the fading and the diffusion rates can be interpreted as hazard rate, and the developed model with constant fading and diffusion rates is equivalent to a Markov process model with exponential transition time distribution. A general model with time-varying fading and diffusion rates is obtained by replacing the exponential distribution with other distributions. By doing so, the Markov model becomes a semi-Markov model. Specifically, we investigate the case of Weibull state transition time distribution, which offers increasing, decreasing, as well as constant fading or diffusion rates by varying the shape parameter. The semi-Markov model provides more realistic predictions than the Markov model.

CHAPTER 5

STATISTICS-BASED DEGRADATION MODEL OF PRINTED IMAGES

In this chapter, we investigate the statistics-based degradation model of printed images. The two aspects of image degradation, i.e. ink fading and ink diffusion, are revisited in this chapter. We first propose a Hull-White/Vasicek (HWV) stochastic process model for ink fading and derive the distribution of time to reach unacceptable degradation. We then present a continuous-space convolution-based ink diffusion model, and integrate the ink fading model and the ink diffusion model into a spatio-temporal stochastic process model for the degradation of printed images.

5.1 Degradation Model of Ink Fading

The stochastic property of the ink fading process is not considered in the physics-based ink fading model. By adding a stochastic process term, we change the deterministic differential equation in Eq. (3.1) into a stochastic differential equation. The developed stochastic model is a Hull-White/Vasicek (HWV) model, which is a type of the Ornstein-Uhlenbeck process. The stochastic differential equation for state *i* is expressed in Eq. (5.1),

$$d\tilde{a}_i(t) = \left(\sum_j k_{j,i} a_j(t) - \kappa_i \tilde{a}_i(t) \right) dt + \sigma_i(t)\, dB_i(t) \tag{5.1}$$

where $a_i(t)$ and $\tilde{a}_i(t)$ are the deterministic and stochastic area coverages of state *i* at time *t*, respectively, $\kappa_i = \sum_j k_{i,j}$ is the overall fading rate of state *i* to other states, and $\sigma_i(t)$ and $B_i(t)$ are the volatility function and the standard Brownian motion process for state *i* at

time *t*, respectively. The randomness in the area coverage transition into state *i* due to ink fading is ignored.

Changing *t* to τ in Eq. (5.1) and multiplying both sides by $e^{\kappa_i t}$ result in

$$d\left(e^{\kappa_i t}\tilde{a}_i(t)\right) = e^{\kappa_i t}\left(r_i(t)dt + \sigma_i(t)dB_i(t)\right)$$

where $r_i(t) = \sum_j k_{j,i} a_j(t)$. Integrating the above equation from 0 to *t* and rearranging the terms, the stochastic ink fading model is obtained as expressed in Eq. (5.2),

$$\begin{aligned}\tilde{a}_i(t) &= a_i(0)e^{-\kappa_i t} + \int_0^t r_i(\tau)e^{-\kappa_i(t-\tau)}d\tau + \int_0^t \sigma_i(t)e^{-\kappa_i(t-\tau)}dB_i(\tau) \\ &= a_i(t) + \int_0^t \sigma_i(t)e^{-\kappa_i(t-\tau)}dB_i(\tau)\end{aligned} \tag{5.2}$$

The expectation of the stochastic area coverage equals the deterministic area coverage $E\left[\tilde{a}_i(t)\right] = a_i(t)$. The variance of the stochastic area coverage is denoted as $\upsilon_i(t)$ and calculated as

$$\begin{aligned}\upsilon_i(t) &= E\left[\left(\tilde{a}_i(t) - E\left[\tilde{a}_i(t)\right]\right)^2\right] \\ &= E\left[\left(\int_0^t \sigma_i(t)e^{-\kappa_i(t-\tau)}dB_i(\tau)\right)^2\right] \\ &= \int_0^t \sigma_i^2(t)e^{-2\kappa_i(t-\tau)}d\tau\end{aligned}$$

According to the property of the HWV model, the stochastic area coverage follows a normal distribution $\tilde{a}_i(t) \sim N\left(a_i(t), \upsilon_i(t)\right)$.

We assume the volatility function is proportional to the area coverage of the state. This is a realistic assumption that guarantees small fluctuation when ink amount is low on paper. Let $\sigma_i(t) = \eta_i \sqrt{a_i(\tau)}$, then the variance of the stochastic area coverage is

$$\upsilon_i(t) = \sum_{j=1}^{i} \frac{\eta_i^2 c_{i,j}}{2\kappa_i - \kappa_j}\left(e^{-\kappa_j t} - e^{-2\kappa_i t}\right)$$

where η_i is the volatility parameter, and $c_{i,j}$ is given in Appendix.

The area coverage of a specific ink $\tilde{a}_{ink}(t) = \sum_{i \in \Omega_{ink}} \tilde{a}_i(t)$ follows a normal distribution with expectation $a_{ink}(t) = \sum_{i \in \Omega_{ink}} a_i(t)$ and variance $\upsilon_{ink}(t) = \sum_{i \in \Omega_{ink}} \upsilon_i(t)$. We assume that a color exhibits unacceptable fading when the area coverage of any of the four inks falls below a predetermined threshold D_{ink}. Given $\tilde{a}_{ink}(t) \geq 0$, the truncated CDF and *pdf* of time for an ink to reach its threshold are

$$F_{ink}(t) = \frac{\Pr\left\{0 \leq \tilde{a}_{ink}(t) < D_{ink}\right\}}{\Pr\left\{\tilde{a}_{ink}(t) \geq 0\right\}} = \frac{\Phi_1 - \Phi_2}{1 - \Phi_2}$$

$$f_{ink}(t) = \frac{(\varphi_1 - \varphi_2)(1 - \Phi_2) - (\Phi_1 - \Phi_2)\varphi_2}{(1 - \Phi_2)^2}$$

where

$$\Phi_1 = \Phi\left(\frac{D_{ink} - a_{ink}(t)}{\sqrt{\upsilon_{ink}(t)}}\right),\ \Phi_2 = \Phi\left(\frac{-a_{ink}(t)}{\sqrt{\upsilon_{ink}(t)}}\right),$$

$$\varphi_1 = \frac{-a'_{ink}(t)\sqrt{\upsilon_{ink}(t)} + \left(D_{ink} - a_{ink}(t)\right)\left(\sqrt{\upsilon_{ink}(t)}\right)'}{\upsilon_{ink}(t)} \times \varphi\left(\frac{D_{ink} - a_{ink}(t)}{\sqrt{\upsilon_{ink}(t)}}\right),$$

$\varphi_2 = -\dfrac{a'_{ink}(t)\sqrt{\upsilon_{ink}(t)} + a_{ink}(t)\left(\sqrt{\upsilon_{ink}(t)}\right)'}{\upsilon_{ink}(t)} \times \varphi\left(\dfrac{-a_{ink}(t)}{\sqrt{\upsilon_{ink}(t)}}\right)$, and $\Phi(\cdot)$ and $\varphi(\cdot)$ are the CDF and *pdf* of the standard normal distribution, respectively.

Assuming that the area coverages of the four inks are independent, then the CDF and *pdf* of time for an ink color to reach unacceptable fading are

$$\begin{aligned} F_{color}(t) &= 1 - \prod_{ink \in \Omega} \Pr\left\{\tilde{a}_{ink}(t) > D_{ink}\right\} \\ &= 1 - \prod_{ink \in \Omega} \left[1 - F_{ink}(t)\right] \\ &= 1 - \prod_{ink \in \Omega} \bar{F}_{ink}(t) \end{aligned}$$

$$f_{color}(t) = \frac{\partial F_{color}(t)}{\partial t} = \sum_{ink \in \Omega} \left\{ f_{ink}(t) \prod_{INK \in \Omega, INK \neq ink} \bar{F}_{INK}(t) \right\}$$

where **Ω** is the set of inks used in printing this color (The color may not be printed with all four inks).

5.1.1 *Parameters Estimation*

The parameters of the fading rate are estimated sequentially by printing each state as the top state over the space. Assuming that there are N samples and M+1 area coverage measurements at time t_m, $m = 0,1,...,M$, $t_0 = 0$, the log-likelihood function of the area coverage of state i is

$$\ln \mathcal{L} = \sum_{n=1}^{N} \sum_{m=1}^{M} \ln \frac{1}{\sqrt{2\pi \upsilon_{i;n}(t_m)}} - \sum_{n=1}^{N} \sum_{m=1}^{M} \frac{\left[x_{i;n}(t_m) - a_{i;n}(t_m)\right]^2}{2\upsilon_{i;n}(t_m)} \qquad (5.3)$$

where $x_{i;n}(t_m)$ and $a_{i;n}(t_m)$ are the measured and predicted area coverages of state *i* of the n^{th} sample at time t_m, respectively, and $\upsilon_{i;n}(t_m)$ is the predicted variance of the area coverage of state *i* of the n^{th} sample at time t_m. The parameters are estimated numerically by maximizing the log-likelihood function given in Eq. (5.3).

5.1.2 *Numerical Examples*

In this section, we provide numerical simulations using the HWV ink fading model. In the simulation, we assume colors are printed using the CMY inks and randomly generate the initial ink area coverages as $a_{cyan}(0) = 0.22$, $a_{magenta}(0) = 0.95$, and $a_{yellow}(0) = 0.46$. The area coverages of the states are approximated using the Demichel equations given in Eq. (3.8). The fading rates in this simulation are also randomly generated and shown in Table 5.1. The volatility parameters are chosen as $\eta_i = 0.002$ for all the states.

Table 5.1 Random fading rates

$k_{cyan}^{(CMY)}$	0.0127	$k_{cyan}^{(CY)}$	0.0394	$k_{cyan}^{(CM)}$	0.0168	$k_{cyan}^{(C)}$	0.0280
$k_{magenta}^{(CMY)}$	0.0381	$k_{magenta}^{(MY)}$	0.0373	$k_{magenta}^{(CM)}$	0.0111	$k_{magenta}^{(M)}$	0.0096
$k_{yellow}^{(CMY)}$	0.0211	$k_{yellow}^{(MY)}$	0.0265	$k_{yellow}^{(CY)}$	0.0043	$k_{yellow}^{(Y)}$	0.0194

The predicted variances of the area coverages of the states using the HWV ink fading model are plotted in Figure 5.1. The expected area coverages of the states and their 95% prediction intervals are plotted in Figure 5.2. The variances first increase due to the stochastic fading and then decrease as the area coverages reduce. The change of the variances is the result of the mean-reverting property of the HWV model. The expected area coverages of the

CMY inks and their 95% prediction intervals are shown in Figure 5.3. The variance of each ink also increases at the beginning and then decreases.

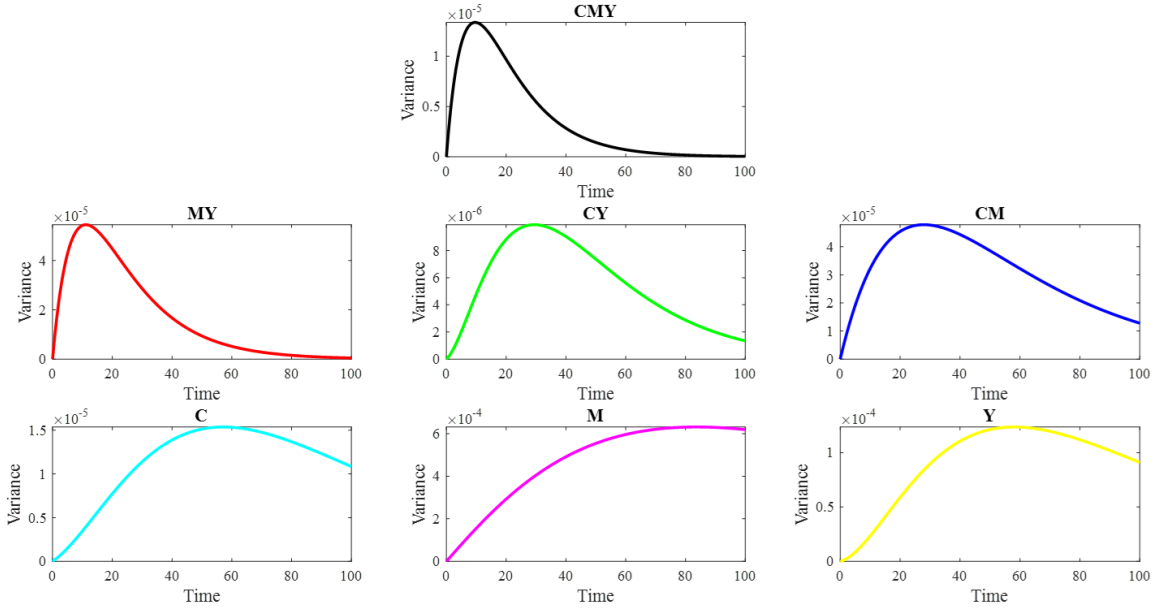

Figure 5.1 Predicted variances of area coverages of states using statistics-based ink fading model with constant fading rates

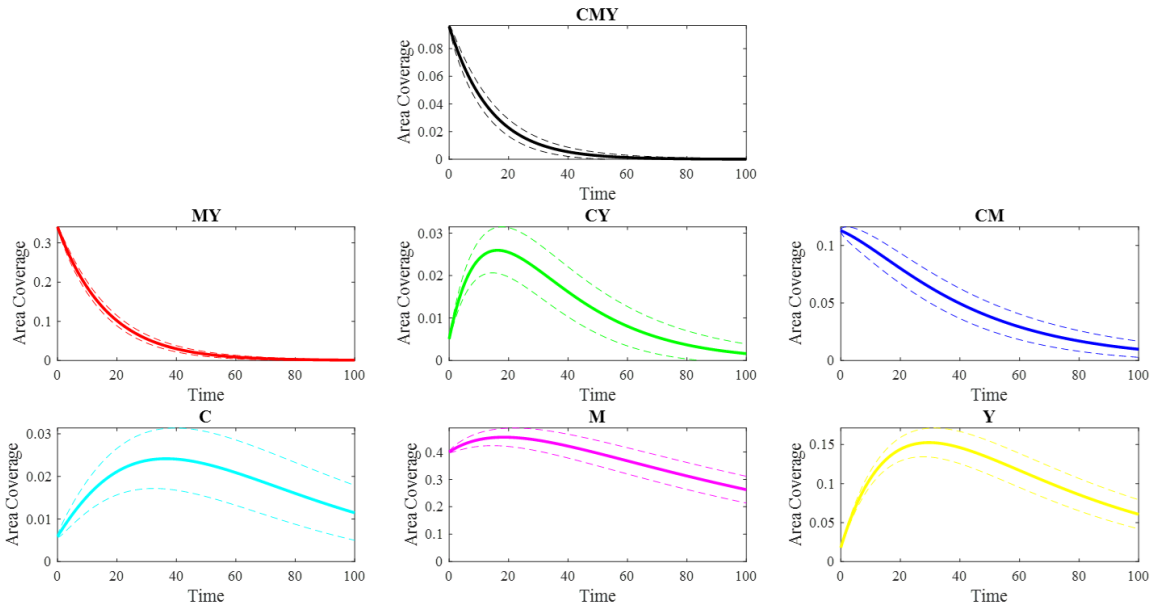

Figure 5.2 95% prediction intervals of area coverages of states using statistics-based ink fading model with constant fading rates

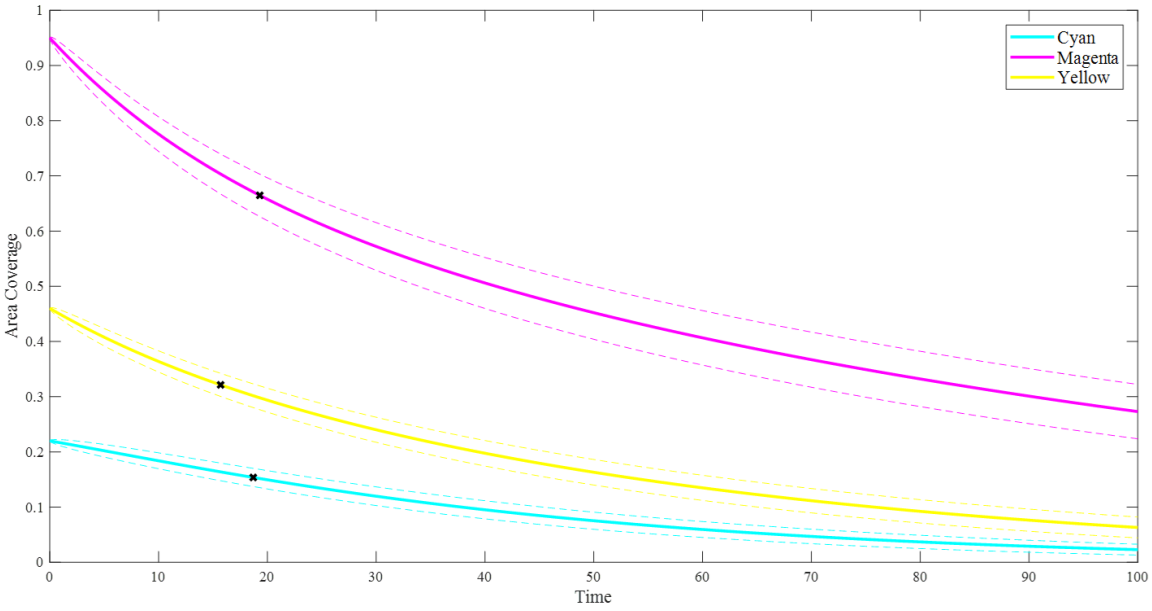

Figure 5.3 95% prediction intervals of area coverages of inks using statistics-based ink fading model with constant fading rates

The criterion for unacceptable color fading is chosen as 30% loss of the initial area coverage of any ink. The times that the expected area coverages of the inks reach their thresholds are marked in Figure 5.3. The distributions of time to unacceptable ink and color fading predicted using the HWV ink fading model are plotted in Figure 5.4. The distribution of time to unacceptable color fading is a joint result of the distributions of time to unacceptable ink fading.

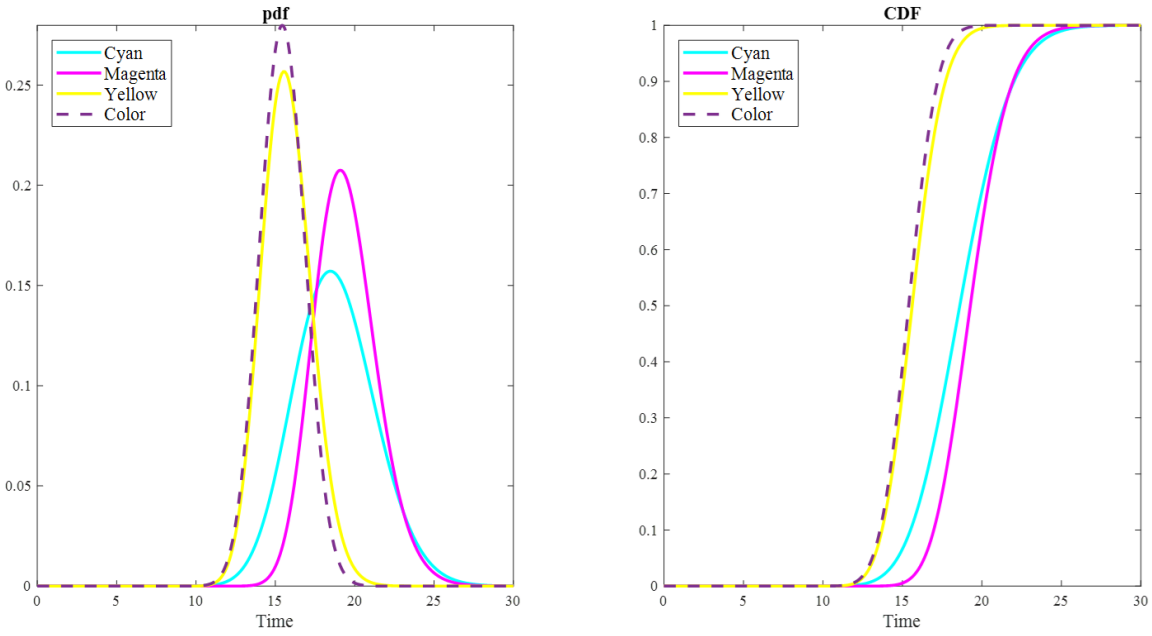

Figure 5.4 Predicted *pdf* and CDF of time to unacceptable ink and color fading using statistics-based ink fading model with constant fading rates

5.2 Degradation Model of Ink Diffusion

In this section, we investigate a continuous-space convolution-based ink diffusion model. The autoregressive ink diffusion model in Chapter 3 is equivalent to applying a convolution

to the image with a 3 × 3 kernel of $\begin{bmatrix} 0 & h_i & 0 \\ h_i & 1-4h_i & h_i \\ 0 & h_i & 0 \end{bmatrix}$, where $h_i = \frac{\delta_i \Delta t}{(\Delta s)^2}$ and δ_i is the diffusion rate of state *i*. The kernel derived from the finite difference method ignores the diagonal ink diffusion. Brown *et al.* (2000) study the blurring functions and conclude that the Gaussian function is the only one that behaves sensibly as $\Delta t \to 0$, that is, the tails of the blurring function must shrink rapidly as the time spacing becomes small. By substituting a bivariate Gaussian density function for the kernel, the ink diffusion is modeled as a spatial convolution as given in Eq. (5.4),

$$a_{i;\boldsymbol{s}}(t+\Delta t) = \int_{\mathbb{R}^2} \varphi(\Delta \boldsymbol{s}; \boldsymbol{\mu}, \boldsymbol{\Sigma}_i)\, a_{i;\boldsymbol{s}'}(t)\, d(\Delta \boldsymbol{s}) \tag{5.4}$$

where $a_{i;\boldsymbol{s}}(t)$ is the deterministic area coverage of state *i* at pixel $\boldsymbol{s} = [x \quad y]^{\mathrm{T}}$ at time *t*, $\mathbb{R}^2$ denotes two-dimensional space, $\Delta \boldsymbol{s} = \boldsymbol{s}' - \boldsymbol{s}$, $\varphi(\Delta \boldsymbol{s}; \boldsymbol{\mu}, \boldsymbol{\Sigma}_i)$ is a bivariate Gaussian density function with $\boldsymbol{\mu} = \begin{bmatrix} 0 \\ 0 \end{bmatrix}$ and $\boldsymbol{\Sigma}_i = \begin{bmatrix} \rho_i \Delta t & 0 \\ 0 & \rho_i \Delta t \end{bmatrix}$, and ρ_i is a constant.

It can be demonstrated that Eq. (5.4) is strongly connected with the diffusion equation model given in Eq. (3.10). After Taylor expansion at $a_{i;\boldsymbol{s}}(t)$, Eq. (5.4) becomes

$$a_{i;\boldsymbol{s}}(t+\Delta t) \approx \int_{\mathbb{R}^2} \varphi(\Delta \boldsymbol{s}; \boldsymbol{\mu}, \boldsymbol{\Sigma}_i) \left\{ a_{i;\boldsymbol{s}}(t) + \frac{\partial a_{i;\boldsymbol{s}}(t)}{\partial \boldsymbol{s}^{\mathrm{T}}} \Delta \boldsymbol{s} + \frac{1}{2} (\Delta \boldsymbol{s})^{\mathrm{T}} \frac{\partial^2 a_{i;\boldsymbol{s}}(t)}{\partial \boldsymbol{s} \partial \boldsymbol{s}^{\mathrm{T}}} \Delta \boldsymbol{s} \right\} d(\Delta \boldsymbol{s})$$

where $\frac{\partial}{\partial \boldsymbol{s}^{\mathrm{T}}} a_{i;\boldsymbol{s}}(t) = \begin{bmatrix} \frac{\partial a_{i;\boldsymbol{s}}(t)}{\partial x} & \frac{\partial a_{i;\boldsymbol{s}}(t)}{\partial y} \end{bmatrix}$ and $\frac{\partial^2 a_{i;\boldsymbol{s}}(t)}{\partial \boldsymbol{s} \partial \boldsymbol{s}^{\mathrm{T}}} = \begin{bmatrix} \frac{\partial^2 a_{i;\boldsymbol{s}}(t)}{\partial x^2} & \frac{\partial^2 a_{i;\boldsymbol{s}}(t)}{\partial x \partial y} \\ \frac{\partial^2 a_{i;\boldsymbol{s}}(t)}{\partial y \partial x} & \frac{\partial^2 a_{i;\boldsymbol{s}}(t)}{\partial y^2} \end{bmatrix}$.

Separately integrating the three terms results in

$$a_{i;\boldsymbol{s}}(t+\Delta t) \approx a_{i;\boldsymbol{s}}(t)\int_{\mathbb{R}^2}\varphi(\Delta\boldsymbol{s};\boldsymbol{\mu},\boldsymbol{\Sigma}_i)\,d(\Delta\boldsymbol{s}) + \int_{\mathbb{R}^2}\varphi(\Delta\boldsymbol{s};\boldsymbol{\mu},\boldsymbol{\Sigma}_i)\left(\frac{\partial a_{i;\boldsymbol{s}}(t)}{\partial x}\Delta x + \frac{\partial a_{i;\boldsymbol{s}}(t)}{\partial y}\Delta y\right)d(\Delta\boldsymbol{s}) + \frac{1}{2}\int_{\mathbb{R}^2}\varphi(\Delta\boldsymbol{s};\boldsymbol{\mu},\boldsymbol{\Sigma}_i)\begin{pmatrix}\frac{\partial^2 a_{i;\boldsymbol{s}}(t)}{\partial x^2}(\Delta x)^2 + \\ \left(\frac{\partial^2 a_{i;\boldsymbol{s}}(t)}{\partial x\partial y} + \frac{\partial^2 a_{i;\boldsymbol{s}}(t)}{\partial y\partial x}\right)\Delta x\Delta y + \\ \frac{\partial^2 a_{i;\boldsymbol{s}}(t)}{\partial y^2}(\Delta y)^2\end{pmatrix}d(\Delta\boldsymbol{s})$$

Deleting the terms that integrate to zero, we have

$$a_{i;\boldsymbol{s}}(t+\Delta t) \approx a_{i;\boldsymbol{s}}(t) + \frac{1}{2}\int_{\mathbb{R}^2}\varphi(\Delta\boldsymbol{s};\boldsymbol{\mu},\boldsymbol{\Sigma}_i)\left(\frac{\partial^2 a_{i;\boldsymbol{s}}(t)}{\partial x^2}(\Delta x)^2 + \frac{\partial^2 a_{i;\boldsymbol{s}}(t)}{\partial y^2}(\Delta y)^2\right)d(\Delta\boldsymbol{s})$$

Using the definition of variance, the solution of the integration is obtained as

$$a_{i;\boldsymbol{s}}(t+\Delta t) \approx a_{i;\boldsymbol{s}}(t) + \frac{\rho_i\Delta t}{2}\left(\frac{\partial^2 a_{i;\boldsymbol{s}}(t)}{\partial x^2} + \frac{\partial^2 a_{i;\boldsymbol{s}}(t)}{\partial y^2}\right)$$

Rearranging the terms and taking $\lim_{\Delta t\to 0}$ of both sides, we have

$$\frac{\partial a_{i;\boldsymbol{s}}(t)}{\partial t} \approx \frac{\rho_i}{2}\left(\frac{\partial^2 a_{i;\boldsymbol{s}}(t)}{\partial x^2} + \frac{\partial^2 a_{i;\boldsymbol{s}}(t)}{\partial y^2}\right)$$

The relationship between the Gaussian density parameter ρ in the convolution-based ink diffusion model and the diffusion rate δ in the diffusion equation model is $\rho = 2\delta$.

Since the convolution of two Gaussian functions is still Gaussian, with its variance being the sum of the variances of the two Gaussian functions, the continuous-time continuous space convolution-based ink diffusion model is derived as given in Eq. (5.5),

$$a_{i;\boldsymbol{s}}(t) = \int_{\mathbb{R}^2}\varphi\left(\Delta\boldsymbol{s};\boldsymbol{\mu},{}_0^t\boldsymbol{\Sigma}_i\right)a_{i;\boldsymbol{s}'}(0)\,d(\Delta\boldsymbol{s}) \tag{5.5}$$

where $\varphi\left(\Delta \boldsymbol{s}; \boldsymbol{\mu}, {}_0^t\boldsymbol{\Sigma}_i\right)$ is a bivariate Gaussian density function with $\boldsymbol{\mu} = \begin{bmatrix} 0 \\ 0 \end{bmatrix}$ and ${}_0^t\boldsymbol{\Sigma}_i = \begin{bmatrix} 2\delta_i t & 0 \\ 0 & 2\delta_i t \end{bmatrix}$.

To apply the continuous-space convolution-based ink diffusion model on image pixels, we create the $h_s \times h_s$ (h_s is a positive odd integer and the side length of the kernel) discrete Gaussian kernel *h* as given in Eq. (5.6),

$$h_g\left(\Delta x, \Delta y\right) = \exp\left(-\frac{1}{2}\begin{pmatrix}\Delta x \\ \Delta y\end{pmatrix}^{\mathrm{T}} \boldsymbol{\Sigma}^{-1}\begin{pmatrix}\Delta x \\ \Delta y\end{pmatrix}\right)$$
$$h\left(\Delta x, \Delta y\right) = \frac{h_g\left(\Delta x, \Delta y\right)}{\sum_{\Delta x}\sum_{\Delta y} h_g\left(\Delta x, \Delta y\right)} \tag{5.6}$$

where Δx and Δy are integers between $-\frac{h_s - 1}{2}$ and $\frac{h_s - 1}{2}$.

5.3 Degradation Model of Ink Fading and Ink Diffusion

Integrating the stochastic ink fading model in Eq. (5.2) and the convolution-based ink diffusion model in Eq. (5.5) results in the spatio-temporal stochastic degradation model as given in Eq. (5.7),

$$
\begin{aligned}
\tilde{a}_{i;\boldsymbol{s}}(t) &= e^{-\kappa_i t}\int_{\mathbb{R}^2}\varphi\left(\Delta\boldsymbol{s};\boldsymbol{\mu},{}_0^t\boldsymbol{\Sigma}_i\right)a_{i;\boldsymbol{s}'}(0)\,d(\Delta\boldsymbol{s}) + \\
&\int_0^t\left[e^{-\kappa_i(t-\tau)}\int_{\mathbb{R}^2}\varphi\left(\Delta\boldsymbol{s};\boldsymbol{\mu},{}_0^{t-\tau}\boldsymbol{\Sigma}_i\right)r_{i;\boldsymbol{s}'}(\tau)\,d(\Delta\boldsymbol{s})\right]d\tau + \\
&\int_0^t\left[e^{-\kappa_i(t-\tau)}\int_{\mathbb{R}^2}\varphi\left(\Delta\boldsymbol{s};\boldsymbol{\mu},{}_0^{t-\tau}\boldsymbol{\Sigma}_i\right)\sigma_{i;\boldsymbol{s}'}(\tau)\,d(\Delta\boldsymbol{s})\right]dB_{i;\boldsymbol{s}}(\tau) \\
&= a_{i;\boldsymbol{s}}(t) + \int_0^t\left[e^{-\kappa_i(t-\tau)}\int_{\mathbb{R}^2}\varphi\left(\Delta\boldsymbol{s};\boldsymbol{\mu},{}_0^{t-\tau}\boldsymbol{\Sigma}_i\right)\sigma_{i;\boldsymbol{s}'}(\tau)\,d(\Delta\boldsymbol{s})\right]dB_{i;\boldsymbol{s}}(\tau)
\end{aligned}
\tag{5.7}
$$

where $a_{i;\boldsymbol{s}}(t)$ and $\tilde{a}_{i;\boldsymbol{s}}(t)$ are the deterministic and stochastic area coverages of state *i* at pixel $\boldsymbol{s}=\begin{bmatrix}x & y\end{bmatrix}^{\mathrm{T}}$ at time *t*, respectively, $\kappa_i=\sum_j k_{i,j}$ is the overall fading rate of state *i* to other states, $\mathbb{R}^2$ denotes two-dimensional space, $\Delta\boldsymbol{s}=\boldsymbol{s}'-\boldsymbol{s}$, $\varphi\left(\Delta\boldsymbol{s};\boldsymbol{\mu},{}_0^t\boldsymbol{\Sigma}_i\right)$ is a bivariate Gaussian density function with $\boldsymbol{\mu}=\begin{bmatrix}0 & 0\end{bmatrix}^{\mathrm{T}}$ and ${}_0^t\boldsymbol{\Sigma}_i=\begin{bmatrix}2\delta_i t & 0\\ 0 & 2\delta_i t\end{bmatrix}$, δ_i is the diffusion rate of state *i*, $r_{i;\boldsymbol{s}}(t)=\sum_j k_{j,i}a_{j;\boldsymbol{s}}(t)$ is the deterministic area coverage transition rate into state *i* due to ink fading at pixel $\boldsymbol{s}$ at time *t*, and $\sigma_{i;\boldsymbol{s}}(t)$ and $B_{i;\boldsymbol{s}}(t)$ are the spatially independent volatility function and the standard Brownian motion process for state *i* at pixel $\boldsymbol{s}$ at time *t*, respectively. The randomness in the area coverage transition into state *i* due to ink fading is ignored. The bivariate Gaussian density captures the probability that the inks in an infinitesimal area at pixel $\boldsymbol{s}'$ diffuse to pixel $\boldsymbol{s}$ within a time interval.

The spatio-temporal stochastic degradation model with constant fading and diffusion rates as given in Eq. (5.7) is extended to the case of time-varying fading and diffusion rates as shown in Eq. (5.8),

$$\begin{aligned}\tilde{a}_{i;\boldsymbol{s}}(t) &= \exp\left(-\int_0^t \kappa_i(\xi)\,d\xi\right)\int_{\mathbb{R}^2}\varphi\left(\Delta\boldsymbol{s};\boldsymbol{\mu},{}_0^t\boldsymbol{\Sigma}_i\right)a_{i;\boldsymbol{s}'}(0)\,d(\Delta\boldsymbol{s}) + \\ &\int_0^t\left[\exp\left(-\int_0^{t-\tau}\kappa_i(\xi)\,d\xi\right)\int_{\mathbb{R}^2}\varphi\left(\Delta\boldsymbol{s};\boldsymbol{\mu},{}_0^{t-\tau}\boldsymbol{\Sigma}_i\right)r_{i;\boldsymbol{s}'}(\tau)\,d(\Delta\boldsymbol{s})\right]d\tau + \\ &\int_0^t\left[\exp\left(-\int_0^{t-\tau}\kappa_i(\xi)\,d\xi\right)\int_{\mathbb{R}^2}\varphi\left(\Delta\boldsymbol{s};\boldsymbol{\mu},{}_0^{t-\tau}\boldsymbol{\Sigma}_i\right)\sigma_{i;\boldsymbol{s}'}(\tau)\,d(\Delta\boldsymbol{s})\right]dB_{i;\boldsymbol{s}}(\tau) \\ &= a_{i;\boldsymbol{s}}(t) + \int_0^t\left[\exp\left(-\int_0^{t-\tau}\kappa_i(\xi)\,d\xi\right)\int_{\mathbb{R}^2}\varphi\left(\Delta\boldsymbol{s};\boldsymbol{\mu},{}_0^{t-\tau}\boldsymbol{\Sigma}_i\right)\sigma_{i;\boldsymbol{s}'}(\tau)\,d(\Delta\boldsymbol{s})\right]dB_{i;\boldsymbol{s}}(\tau)\end{aligned} \tag{5.8}$$

where ${}_a^b\boldsymbol{\Sigma}_i = \begin{bmatrix} 2\int_a^b \delta_i(\xi)\,d\xi & 0 \\ 0 & 2\int_a^b \delta_i(\xi)\,d\xi \end{bmatrix}$. The exponential fading term and the covariance of the bivariate Gaussian density captures the recurrent property of the fading and diffusion rates when state transition happens in the semi-Markov model. There is no simple expression for $r_{i;\boldsymbol{s}}(t)$.

Define an operator and its operations as given in Eq. (5.9),

$$\begin{aligned}{}_a^b\mathrm{Z}_i &= \exp\left(-\int_a^b \kappa_i(\xi)\,d\xi\right)\varphi\left(\boldsymbol{x};\boldsymbol{\mu},{}_a^b\boldsymbol{\Sigma}_i\right) \\ &= \frac{1}{2\pi\sqrt{\left|{}_a^b\boldsymbol{\Sigma}_i\right|}}\exp\left(-\frac{1}{2}(\boldsymbol{x}-\boldsymbol{\mu})^{\mathrm{T}}\,{}_a^b\boldsymbol{\Sigma}_i^{-1}(\boldsymbol{x}-\boldsymbol{\mu}) - \int_a^b \kappa_i(\xi)\,d\xi\right) \\ {}_a^b\mathrm{Z}_i * \mathrm{X}_{i;\boldsymbol{s}} &= \exp\left(-\int_a^b \kappa_i(\xi)\,d\xi\right)\int_{\mathbb{R}^2}\varphi\left(\Delta\boldsymbol{s};\boldsymbol{\mu},{}_a^b\boldsymbol{\Sigma}_i\right)\mathrm{X}_{i;\boldsymbol{s}'}d(\Delta\boldsymbol{s}) \\ {}_a^b\mathrm{Z}_i^n &= \exp\left(-n\int_a^b \kappa_i(\xi)\,d\xi\right)\varphi\left(\boldsymbol{\mu},n\,{}_a^b\boldsymbol{\Sigma}_i\right)\end{aligned} \tag{5.9}$$

where * denotes the spatial convolution. Eq. (5.8) is rewritten as Eq. (5.10),

$$\begin{aligned}\tilde{a}_{i;\boldsymbol{s}}(t) &= \underbrace{{}_0^t\mathrm{Z}_i * a_{i;\boldsymbol{s}}(0)}_{\mathrm{A}} + \underbrace{\int_0^t {}_0^{t-\tau}\mathrm{Z}_i * r_{i;\boldsymbol{s}}(\tau)\,d\tau}_{\mathrm{B}} + \underbrace{\int_0^t {}_0^{t-\tau}\mathrm{Z}_i * \sigma_{i;\boldsymbol{s}}(\tau)\,dB_{i;\boldsymbol{s}}(\tau)}_{\mathrm{C}} \\ &= a_{i;\boldsymbol{s}}(t) + \int_0^t {}_0^{t-\tau}\mathrm{Z}_i * \sigma_{i;\boldsymbol{s}}(\tau)\,dB_{i;\boldsymbol{s}}(\tau)\end{aligned} \tag{5.10}$$

where the terms A, B, and C are explained as the fading and diffusion of the initial ink amount, the ink amount obtained from state transition, and the volatility of state *i* at pixel ***s***, respectively. The expectation of the stochastic area coverage equals the deterministic area coverage $E\left[\tilde{a}_{i;\boldsymbol{s}}(t)\right] = a_{i;\boldsymbol{s}}(t)$. The variance of the stochastic area coverage is denoted as $\upsilon_{i;\boldsymbol{s}}(t)$ and calculated as

$$\begin{aligned}\upsilon_{i;\boldsymbol{s}}(t) &= E\left[\left(\tilde{a}_{i;\boldsymbol{s}}(t) - E\left[\tilde{a}_{i;\boldsymbol{s}}(t)\right]\right)^2\right] \\ &= E\left[\left(\int_0^t {}_0^{t-\tau}\mathrm{Z}_i * \sigma_{i;\boldsymbol{s}}(\tau)\,dB_{i;\boldsymbol{s}}(\tau)\right)^2\right] \\ &= \int_0^t {}_0^{t-\tau}\mathrm{Z}_i^2 * \sigma_{i;\boldsymbol{s}}^2(\tau)\,d\tau\end{aligned}$$

The stochastic area coverage follows a normal distribution $\tilde{a}_{i;\boldsymbol{s}}(t) \sim N\left(a_{i;\boldsymbol{s}}(t), \upsilon_{i;\boldsymbol{s}}(t)\right)$.

5.3.1 *Parameters Estimation*

Once the parameters of the fading rate are estimated, the parameters of the diffusion rate are estimated sequentially by printing each state as the top state over the space. Assuming that there are $M+1$ area coverage measurements at pixel ***s*** at time $t_m,\ m = 0,1,...,M,\ t_0 = 0$, the log-likelihood function of the area coverage of state *i* is

$$\ln \mathcal{L} = \sum_{\boldsymbol{s}}\sum_{m=1}^{M} \ln \frac{1}{\sqrt{2\pi\upsilon_{i;\boldsymbol{s}}(t_m)}} - \sum_{\boldsymbol{s}}\sum_{m=1}^{M} \frac{\left[x_{i;\boldsymbol{s}}(t_m) - a_{i;\boldsymbol{s}}(t_m)\right]^2}{2\upsilon_{i;\boldsymbol{s}}(t_m)} \tag{5.11}$$

where $x_{i;\boldsymbol{s}}(t_m)$ and $a_{i;\boldsymbol{s}}(t_m)$ are the measured and predicted area coverages of state *i* at pixel ***s*** at time t_m, respectively, and $\upsilon_{i;\boldsymbol{s}}(t_m)$ is the predicted variance of the area coverage of state *i* at pixel ***s*** at time t_m. The parameters are estimated numerically by maximizing the log-likelihood function given in Eq. (5.11).

5.3.2 *Numerical Examples*

In this section, we provide numerical simulations using the statistics-based degradation model of ink fading and ink diffusion. The simulations show the 95% prediction intervals of area coverages of states and CMY inks in (3,2) Purple in the 3 × 3 color pixels given in Table 3.1. The volatility function is chosen as $\sigma_{i;\boldsymbol{s}}(t) = \eta_i \sqrt{a_{i;\boldsymbol{s}}(t)}$, where $a_{i;\boldsymbol{s}}(t)$ is the deterministic area coverage predicted using the degradation model, and η_i is the volatility parameter. We use $\eta_i = 0.005$ for all the states. The variance of the stochastic area coverage is calculated using trapezoidal rule.

The 95% prediction intervals of the area coverages of the states and the CMY inks in (3,2) Purple with constant fading and diffusion rates are plotted in Figure 5.5. The fading rates used in the simulation are shown in Table 3.3 and the diffusion rates are δ_i = 0.005 for all the states.

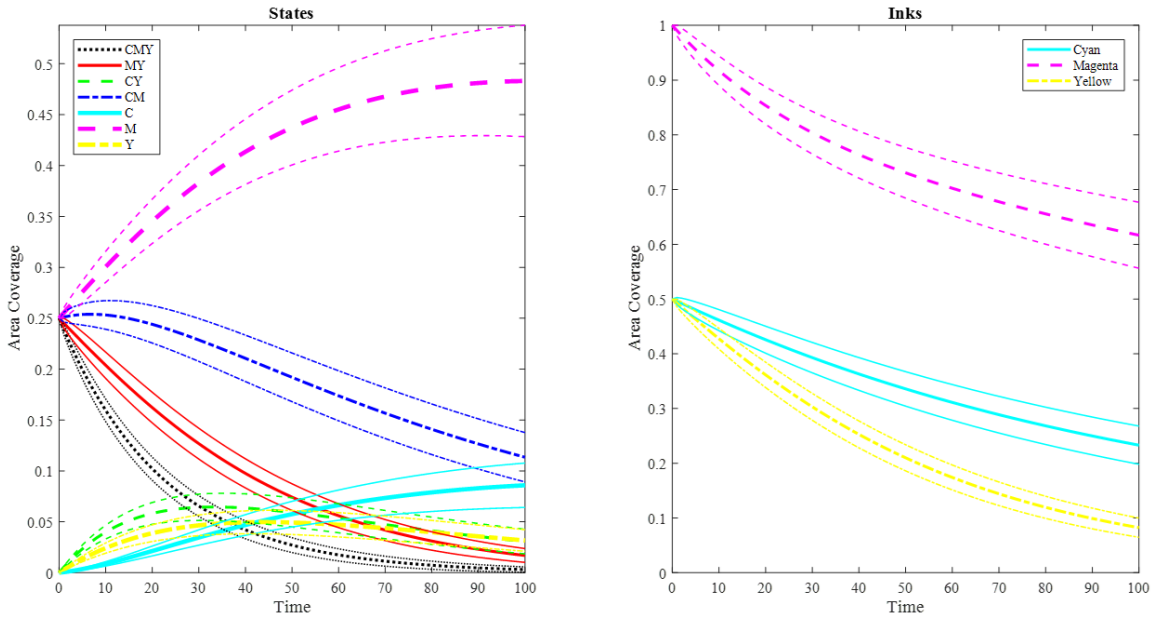

Figure 5.5 95% prediction intervals of area coverages of states and inks in (3,2) Purple with constant fading and diffusion rates

The 95% prediction intervals of the area coverages of the states and the CMY inks in (3,2) Purple with recurrent time-varying fading and diffusion rates are plotted in Figure 5.6. The fading and diffusion rates used in the simulation are $k_{i,j}(t) = \theta_{i,j}\gamma_{i,j}t^{\gamma_{i,j}-1}$ and $\delta_i(t) = \theta_i\gamma_i t^{\gamma_i-1}$, respectively. The values of the parameters are $\gamma_{i,j} = 2$, $\theta_{i,j}$ as 1% of the fading rates in Table 3.3, $\gamma_i = 0.5$, and $\theta_i = 0.01$.

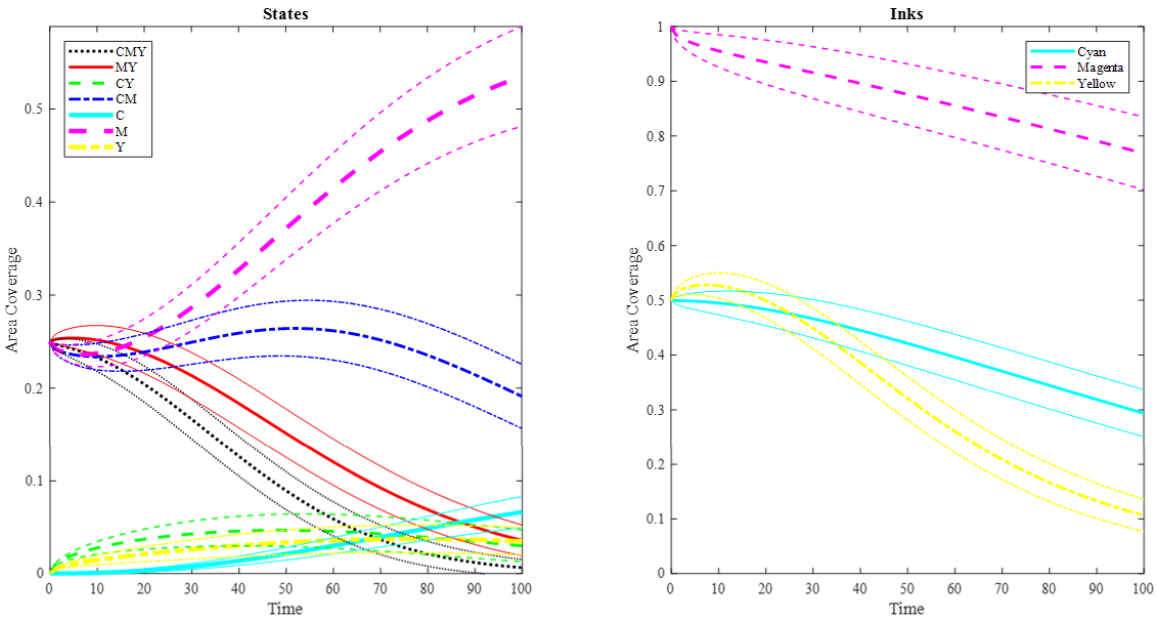

Figure 5.6 95% prediction intervals of area coverages of states and inks in (3,2) Purple with recurrent time-varying fading and diffusion rates

5.4 Summary and Conclusions

In this chapter, we investigate the statistics-based degradation modeling of printed images. We first propose a Hull-White/Vasicek stochastic degradation model for ink fading, then present a convolution-based degradation model for ink diffusion. The connection between the convolution-based and the physics-based ink diffusion models is investigated. Compared with the physics-based ink diffusion model, the convolution-based ink diffusion model considers the diagonal ink diffusion. The two models are integrated into a spatio-temporal stochastic degradation model with constant fading and diffusion rates, which is further extended to a model with recurrent time-varying fading and diffusion rates. The expectation of the stochastic area coverage equals the deterministic area coverage predicted

using the degradation models presented in previous chapters, and the variance of the stochastic area coverage can be calculated.

CHAPTER 6

DEGRADATION MODEL OF INK-PAPER INTERACTIONS

In previous chapters, we develop deterministic and stochastic degradation models with both constant and recurrent time-varying fading and diffusion rates. However, the recurrent time-varying diffusion rates is not a valid assumption. In this chapter, we develop the stochastic degradation models with non-recurrent time-varying fading and diffusion rates and investigate the degradation modeling of the ink-paper interactions of printed images. Two aspects of the ink-paper interactions are considered, i.e., the effect of paper aging such as depolymerization and yellowing, and the fiber orientation of the paper, on the ink fading and diffusion rates. Paper aging effect is modeled as the acceleration of the fading and diffusion rates, and the fiber orientation affects the ink diffusion direction.

6.1 Degradation Model of Ink Fading

We first develop the degradation model of ink fading with non-recurrent time-varying fading rates. The ink fading is modeled as given in Eq. (6.1),

$$d\tilde{a}_i(t) = \left(\sum_j k_{j,i}(t) a_j(t) - \kappa_i(t) \tilde{a}_i(t) \right) dt + \sigma_i(t) dB_i(t) \tag{6.1}$$

where $a_i(t)$ and $\tilde{a}_i(t)$ are the deterministic and stochastic area coverages of state *i* at time *t*, respectively, $\kappa_i(t) = \sum_j k_{i,j}(t)$ is the overall fading rate of state *i* to other states at time *t*, and $\sigma_i(t)$ and $B_i(t)$ are the volatility function and the standard Brownian motion

process of state *i* at time *t*, respectively. The randomness in the area coverage transition into state *i* due to ink fading is ignored.

According to Leibniz integral rule, $\frac{d}{dt}\int_0^{\tau}\kappa_i(\xi)d\xi=\kappa_i(\tau)$. Therefore, changing *t* to τ in Eq. (6.1) and multiplying both sides by $\exp\left(\int_0^{\tau}\kappa_i(\xi)d\xi\right)$ result in

$$d\left(\exp\left(\int_0^{\tau}\kappa_i(\xi)d\xi\right)\tilde{a}_i(\tau)\right)=\exp\left(\int_0^{\tau}\kappa_i(\xi)d\xi\right)\left(r_i(\tau)d\tau+\sigma_i(\tau)dB_i(\tau)\right)$$

where $r_i(t)=\sum_j k_{j,i}(t)a_j(t)$ is the deterministic area coverage transition rate into state *i* due to ink fading. Integrating the above equation from 0 to *t* and rearranging the terms, the degradation model of ink fading with non-recurrent time-varying fading rates is obtained as shown in Eq. (6.2),

$$\begin{aligned}\tilde{a}_i(t)&=a_i(0)\exp\left(-\int_0^t\kappa_i(\xi)d\xi\right)+\int_0^t r_i(\tau)\exp\left(-\int_{\tau}^t\kappa_i(\xi)d\xi\right)d\tau+\\&\int_0^t\sigma_i(\tau)\exp\left(-\int_{\tau}^t\kappa_i(\xi)d\xi\right)dB_i(\tau)\\&=a_i(t)+\int_0^t\sigma_i(\tau)\exp\left(-\int_{\tau}^t\kappa_i(\xi)d\xi\right)dB_i(\tau)\end{aligned}\qquad(6.2)$$

The expectation of the stochastic area coverage equals the deterministic area coverage, and the variance of the stochastic area coverage is calculated as

$$\upsilon_i(t) = E\left[\left(\tilde{a}_i(t) - E\left[\tilde{a}_i(t)\right]\right)^2\right]$$
$$= E\left[\left(\int_0^t \sigma_i(\tau)\exp\left(-\int_\tau^t \kappa_i(\xi)\,d\xi\right)dB_i(\tau)\right)^2\right]$$
$$= \int_0^t \sigma_i^2(\tau)\exp\left(-2\int_\tau^t \kappa_i(\xi)\,d\xi\right)d\tau$$

The stochastic area coverage $\tilde{a}_i(t)$ follows a normal distribution $\tilde{a}_i(t) \sim N\left(a_i(t), \upsilon_i(t)\right)$.

For a time-varying fading rate with no paper aging effect $k_{i,j}(t) = \theta_{i,j}\gamma_{i,j}t^{\gamma_{i,j}-1}$, the area coverage transition from state *i* to state *j* until time *t* is $a_i(0)\exp\left(-\int_0^t k_{i,j}(\tau)\,d\tau\right) = a_i(0)\exp\left(-\theta_{i,j}t^{\gamma_{i,j}}\right)$, where $\gamma_{i,j}$ and $\theta_{i,j}$ are constant parameters associated with the time-varying fading rate. The paper ageing effect is assumed to increase the fading rate. The area coverage transition from state *i* to state *j* under the paper aging effect is then modeled as $a_i(0)\exp\left(-\theta_{i,j}e^{\lambda_{i,j}t}t^{\gamma_{i,j}}\right)$, where $\lambda_{i,j}$ is a constant parameter for the paper aging effect. The fading rate with paper aging effect is rewritten as shown in Eq. (6.3),

$$k_{i,j}(t) = \frac{d}{dt}\left(\theta_{i,j}e^{\lambda_{i,j}t}t^{\gamma_{i,j}}\right) = \theta_{i,j}e^{\lambda_{i,j}t}\left(\lambda_{i,j}t^{\gamma_{i,j}} + \gamma_{i,j}t^{\gamma_{i,j}-1}\right) \tag{6.3}$$

6.1.1 *Parameters Estimation*

The parameters of the fading rate are estimated sequentially by printing each state as the top state over the space. Assuming that there are *N* samples and *M*+1 area coverage

measurements at time t_m, $m = 0,1,...,M$, $t_0 = 0$, the log-likelihood function of the area coverage of state *i* is

$$\ln \mathcal{L} = \sum_{n=1}^{N}\sum_{m=1}^{M} \ln \frac{1}{\sqrt{2\pi \upsilon_{i;n}\left(t_m\right)}} - \sum_{n=1}^{N}\sum_{m=1}^{M} \frac{\left[x_{i;n}\left(t_m\right) - a_{i;n}\left(t_m\right)\right]^2}{2\upsilon_{i;n}\left(t_m\right)} \tag{6.4}$$

where $x_{i;n}\left(t_m\right)$ and $a_{i;n}\left(t_m\right)$ are the measured and predicted area coverages of state *i* of the n^{th} sample at time t_m, respectively, and $\upsilon_{i;n}\left(t_m\right)$ is the predicted variance of the area coverage of state *i* of the n^{th} sample at time t_m. The parameters are estimated numerically by maximizing the log-likelihood function given in Eq. (6.4).

The least squares estimation is an alternative parameters' estimation method. For example, we first estimate the fading parameters of the one-ink states. The predicted area coverage of a one-ink state *i* (*i* = 12 C, 13 M, 14 Y, 15 K) is

$$a_i\left(t\right) = a_i\left(0\right)\exp\left(-\theta_{i,16}e^{\lambda_{i,16}t}t^{\gamma_{i,16}}\right)$$

It is linearized as

$$\ln\left(-\ln\frac{a_i\left(t\right)}{a_i\left(0\right)}\right) = \gamma_{i,16}\ln t + \ln\theta_{i,16} + \lambda_{i,16}t$$

Let $x_i\left(n,t_m\right)$ be the measured area coverage of state *i* of the n^{th} sample at time t_m. Denote $\boldsymbol{Y}$ as the column vector of $\ln\left[-\ln\frac{x_{i;n}\left(t_m\right)}{x_{i;n}\left(t_0\right)}\right]$, $\boldsymbol{X}$ as the column vector of $\begin{bmatrix}\ln t_m & 1 & t_m\end{bmatrix}$, and $\boldsymbol{b} = \begin{bmatrix}\gamma_{i,16} & \ln\theta_{i,16} & \lambda_{i,16}\end{bmatrix}^{\mathrm{T}}$, the solution using least squares method is

$$\widehat{\boldsymbol{b}} = \left(\boldsymbol{X}^{\mathrm{T}}\boldsymbol{X}\right)^{-1}\boldsymbol{X}^{\mathrm{T}}\boldsymbol{Y}$$

The fading parameters of the two-ink states are obtained using the estimated parameters of the one-ink states. Let state *i* be a two-ink state (*i* = 6 MY, 7 CY, 8 CM, 9 CK, 10 MK, 11 YK), and *u* and *v* are the two transition states from state *i*. The predicted area coverages of the three states are

$$a_i(t) = a_i(0)\exp\left(-\theta_{i,u}e^{\lambda_{i,u}t}t^{\gamma_{i,u}} - \theta_{i,v}e^{\lambda_{i,v}t}t^{\gamma_{i,v}}\right)$$

$$a_u(t) = a_i(0)\exp\left(-\theta_{i,u}e^{\lambda_{i,u}t}t^{\gamma_{i,u}}\right) + a_u(0)\exp\left(-\widehat{\theta}_{u,16}e^{\widehat{\lambda}_{u,16}t}t^{\widehat{\gamma}_{u,16}}\right)$$

$$a_v(t) = a_i(0)\exp\left(-\theta_{i,v}e^{\lambda_{i,v}t}t^{\gamma_{i,v}}\right) + a_v(0)\exp\left(-\widehat{\theta}_{v,16}e^{\widehat{\lambda}_{v,16}t}t^{\widehat{\gamma}_{v,16}}\right)$$

where the estimated fading parameters of states *u* and *v*, $\left\{\widehat{\gamma}_{u,16}, \widehat{\theta}_{u,16}, \widehat{\lambda}_{u,16}, \widehat{\gamma}_{v,16}, \widehat{\theta}_{v,16}, \widehat{\lambda}_{v,16}\right\}$, are considered as known values. The fading parameters of state *i* can then be estimated in the same way as the parameters estimation of the one-ink states. The same parameters estimation procedure is applied to the three-ink and four-ink states.

6.1.2 *Simulation and Validation*

In this section, we provide numerical simulations using the degradation model of ink fading with non-recurrent time-varying fading rates and demonstrate the ink-paper interactions using simulation results. Three sets of degradation images with different ink-paper combinations (Wilhelm 2007, Wilhelm *et al.* 2007) are cropped, registered, and resized to align the pixels across the images. The observed degradation images as well as the fitted degradation images (ink-paper interactions not considered yet) are shown in Figures 6.1 – 6.3. The time above the image is the equivalent year of exposure under certain environmental condition. The images are in RGB format and converted to CMY values

using Eq. (3.9). The parameters shown in Table 6.1 are adjusted iteratively using a gradient descent method to minimize the difference between the observed and the predicted area coverages of CMY inks until no significant improvement can be made. The histograms of the prediction errors of the CMY inks for the fitted degradation images are shown in Figures 6.4 – 6.6. The skewness of the prediction errors in the histograms is a result of the rough approximation of the ink area coverage using RGB values and the fact that the image pixels share a number of similar colors. Nevertheless, the color of the fitted degradation images matching the color of the observed degradation images demonstrates the flexibility and capability of the proposed degradation model.

Figure 6.1 Fitted degradation images (#1) w/o ink-paper interactions

Figure 6.2 Fitted degradation images (#2) w/o ink-paper interactions

Figure 6.3 Fitted degradation images (#3) w/o ink-paper interactions

Table 6.1 Estimated parameters for degradation images w/o ink-paper interactions

	#1		#2		#3	
i, j	$\gamma_{i,j}$	$\theta_{i,j}$	$\gamma_{i,j}$	$\theta_{i,j}$	$\gamma_{i,j}$	$\theta_{i,j}$
2, 6	1.3769	0.0000	2.3936	0.0048	0.4541	0.7619
2, 7	0.2165	0.1359	0.8035	0.2612	1.0425	0.0497
2, 8	0.7003	0.0145	2.3863	0.0205	1.6500	0.0166
6, 13	1.8174	0.0000	2.6999	0.0143	1.4951	0.0030
6, 14	0.9943	0.0533	2.0280	0.1222	0.5646	0.2441
7, 12	2.3752	0.2418	0.6822	0.0008	1.3312	0.0002
7, 14	1.0697	0.0000	0.9099	0.0004	1.1768	1.3729
8, 12	1.1193	0.0216	1.6928	0.0002	1.5961	0.3792
8, 13	1.2966	0.0000	0.5399	0.0001	1.7835	0.0562
12, 16	1.5061	0.0000	1.6553	0.0011	0.4149	0.3091
13, 16	0.5822	0.4172	0.2285	0.5458	0.6934	0.0645
14, 16	1.1192	1.1810	0.3750	0.1314	1.2176	0.0042

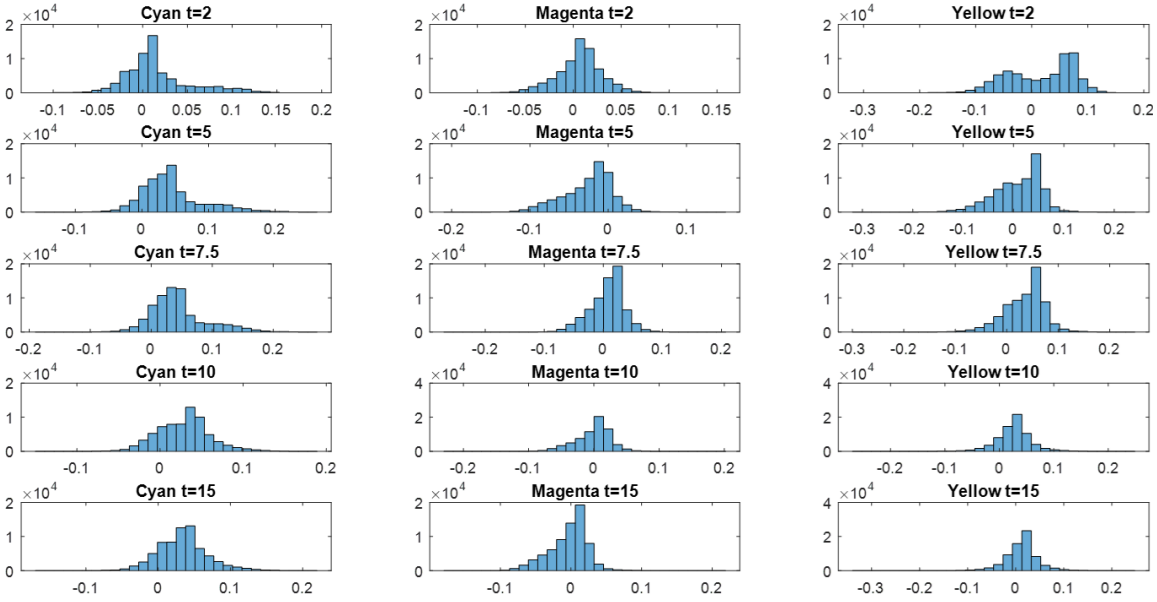

Figure 6.4 Histograms of prediction errors of fitted degradation images (#1) w/o ink-paper interactions

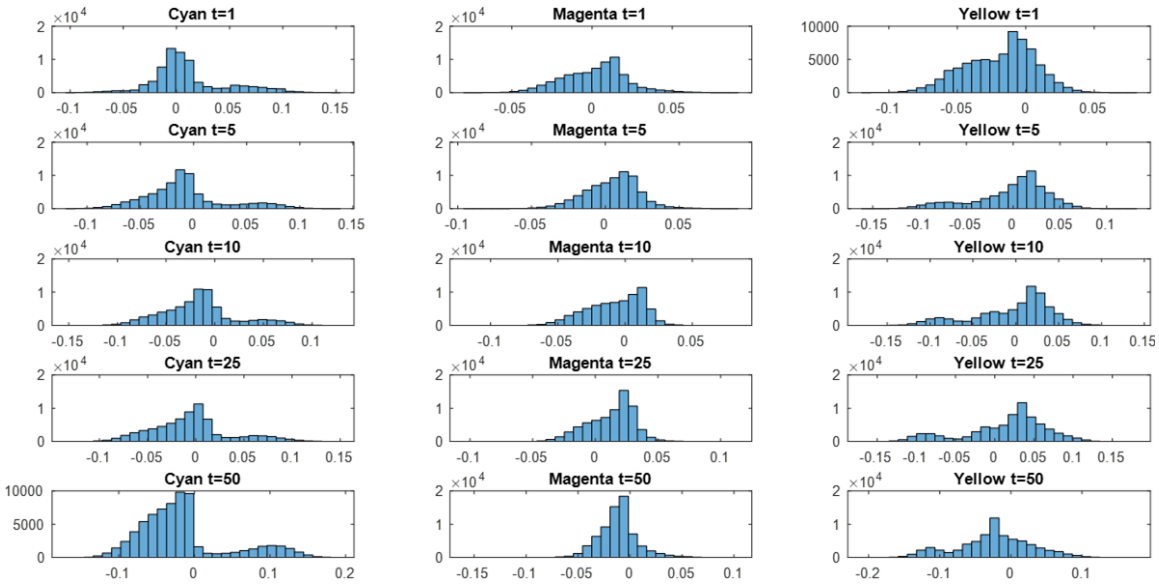

Figure 6.5 Histograms of prediction errors of fitted degradation images (#2) w/o ink-paper interactions

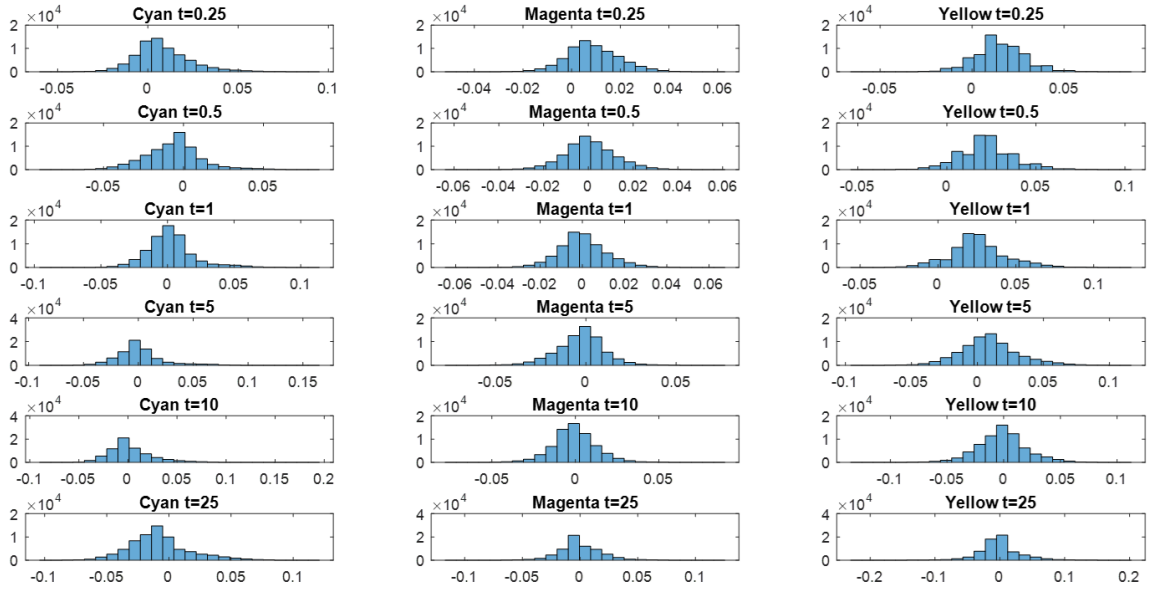

Figure 6.6 Histograms of prediction errors of fitted degradation images (#3) w/o ink-paper interactions

We then fit the observed degradation images again and consider the ink-paper interactions. The overall sum of squared errors between the observed and the predicted area coverages of the three inks in the 325 $\times$ 215 pixels of the five degradation images (#2) improves from 1605.5 (average deviation per ink per pixel: $\frac{1605.5}{325\times215\times3\times5}=0.00153$) to 1450.1 (average deviation per ink per pixel: 0.00138). The observed degradation images, the fitted degradation images without paper aging effect, and the fitted degradation images with paper aging effect are shown in the first, second, and third row in Figure 6.7, respectively. The color improvement is visually noticeable. The result shows that the ink-paper interactions have a major impact on the color degradation of printed images.

Figure 6.7 Fitted degradation images (#2) w/ ink-paper interactions

6.2 Degradation Model of Ink Fading and Ink Diffusion

We first develop the degradation model of ink fading and ink diffusion with non-recurrent fading and diffusion rates. By reviewing the degradation model of ink fading with non-recurrent time-varying fading rates in Eq. (6.2) and the degradation model of ink fading and ink diffusion with recurrent time-varying fading and diffusion rates in Eq. (5.8), the degradation model of ink fading and ink diffusion with non-recurrent time-varying fading and diffusion rates is given in Eq. (6.5),

$$\begin{aligned}\tilde{a}_{i;\boldsymbol{s}}(t) &= \exp\left(-\int_0^t \kappa_i(\xi)\,d\xi\right)\int_{\mathbb{R}^2}\varphi\left(\Delta\boldsymbol{s};\boldsymbol{\mu},{}_0^t\boldsymbol{\Sigma}_i\right)a_{i;\boldsymbol{s}'}(0)\,d(\Delta\boldsymbol{s}) + \\ &\int_0^t\left[\exp\left(-\int_\tau^t \kappa_i(\xi)\,d\xi\right)\int_{\mathbb{R}^2}\varphi\left(\Delta\boldsymbol{s};\boldsymbol{\mu},{}_\tau^t\boldsymbol{\Sigma}_i\right)r_{i;\boldsymbol{s}'}(\tau)\,d(\Delta\boldsymbol{s})\right]d\tau + \\ &\int_0^t\left[\exp\left(-\int_\tau^t \kappa_i(\xi)\,d\xi\right)\int_{\mathbb{R}^2}\varphi\left(\Delta\boldsymbol{s};\boldsymbol{\mu},{}_\tau^t\boldsymbol{\Sigma}_i\right)\sigma_{i;\boldsymbol{s}'}(\tau)\,d(\Delta\boldsymbol{s})\right]dB_{i;\boldsymbol{s}}(\tau) \\ &= a_{i;\boldsymbol{s}}(t) + \int_0^t\left[\exp\left(-\int_\tau^t \kappa_i(\xi)\,d\xi\right)\int_{\mathbb{R}^2}\varphi\left(\Delta\boldsymbol{s};\boldsymbol{\mu},{}_\tau^t\boldsymbol{\Sigma}_i\right)\sigma_{i;\boldsymbol{s}'}(\tau)\,d(\Delta\boldsymbol{s})\right]dB_{i;\boldsymbol{s}}(\tau)\end{aligned} \tag{6.5}$$

where $a_{i;\boldsymbol{s}}(t)$ and $\tilde{a}_{i;\boldsymbol{s}}(t)$ are the deterministic and stochastic area coverages of state i at pixel $\boldsymbol{s}=[x \quad y]^{\mathrm{T}}$ at time t, respectively, $\kappa_i(t)=\sum_j k_{i,j}(t)$ is the overall fading rate of state i to other states at time t, $\mathbb{R}^2$ denotes two-dimensional space, $\Delta\boldsymbol{s}=\boldsymbol{s}'-\boldsymbol{s}$, $\varphi\left(\Delta\boldsymbol{s};\boldsymbol{\mu},{}_\tau^t\boldsymbol{\Sigma}_i\right)$ is a bivariate Gaussian density function with $\boldsymbol{\mu}=[0 \quad 0]^{\mathrm{T}}$ and ${}_\tau^t\boldsymbol{\Sigma}_i=\begin{bmatrix}2\int_\tau^t\delta_i(\xi)\,d\xi & 0\\ 0 & 2\int_\tau^t\delta_i(\xi)\,d\xi\end{bmatrix}$, $\delta_i(t)$ is the diffusion rate of state i at time t, $r_{i;\boldsymbol{s}}(t)=\sum_j k_{j,i}(t)a_{j;\boldsymbol{s}}(t)$ is the deterministic area coverage transition rate into state i due

to ink fading at pixel $\boldsymbol{s}$ at time t, and $\sigma_{i;\boldsymbol{s}}(t)$ and $B_{i;\boldsymbol{s}}(t)$ are the spatially independent volatility function and the standard Brownian motion process for state i at pixel $\boldsymbol{s}$ at time t, respectively. The randomness in the area coverage transition into state i due to ink fading is ignored.

Eq. (6.5) is rewritten as Eq. (6.6) using the operator defined in Eq. (5.9),

$$\begin{aligned}\tilde{a}_{i;\boldsymbol{s}}(t) &= {}_0^t Z_i * a_{i;\boldsymbol{s}}(0) + \int_0^t {}_\tau^t Z_i * \left\{ r_{i;\boldsymbol{s}}(\tau)\, d\tau + \sigma_{i;\boldsymbol{s}}(\tau)\, dB_{i;\boldsymbol{s}}(\tau) \right\} \\ &= a_{i;\boldsymbol{s}}(t) + \int_0^t {}_\tau^t Z_i * \sigma_{i;\boldsymbol{s}}(\tau)\, dB_{i;\boldsymbol{s}}(\tau)\end{aligned} \tag{6.6}$$

The expectation of the stochastic area coverage equals the deterministic area coverage, and the variance of the stochastic area coverage is calculated as

$$\begin{aligned}\upsilon_{i;\boldsymbol{s}}(t) &= E\left[\left(\tilde{a}_{i;\boldsymbol{s}}(t) - E\left[\tilde{a}_{i;\boldsymbol{s}}(t) \right] \right)^2 \right] \\ &= E\left[\left(\int_0^t {}_\tau^t Z_i * \sigma_{i;\boldsymbol{s}}(\tau)\, dB_{i;\boldsymbol{s}}(\tau) \right)^2 \right] \\ &= \int_0^t {}_\tau^t Z_i^2 * \sigma_{i;\boldsymbol{s}}^2(\tau)\, d\tau\end{aligned}$$

The stochastic area coverage follows a normal distribution $\tilde{a}_{i;\boldsymbol{s}}(t) \sim N\left(a_{i;\boldsymbol{s}}(t), \upsilon_{i;\boldsymbol{s}}(t) \right)$.

Define a variant of the operator in Eq. (5.9) as given in Eq. (6.7),

$${}_{a;c}^{b;d} Z_i = \exp\left(-\int_a^b \kappa_i(\xi)\, d\xi \right) \varphi\left(\boldsymbol{\mu}, {}_c^d \boldsymbol{\Sigma}_i \right) \tag{6.7}$$

We obtain two variations of the spatio-temporal stochastic degradation models as shown in Eq. (6.8) and Eq. (6.9) that either the fading or diffusion has recurrent property but the other does not,

$$\tilde{a}_{i;\boldsymbol{s}}(t) = {}_{0}^{t}\mathrm{Z}_i * a_{i;\boldsymbol{s}}(0) + \int_0^t {}_{0;\tau}^{t-\tau;t}\mathrm{Z}_i * r_{i;\boldsymbol{s}}(\tau)\,d\tau + \int_0^t {}_{0;\tau}^{t-\tau;t}\mathrm{Z}_i * \sigma_{i;\boldsymbol{s}}(\tau)\,dB_{i;\boldsymbol{s}}(\tau) \quad (6.8)$$

$$\tilde{a}_{i;\boldsymbol{s}}(t) = {}_{0}^{t}\mathrm{Z}_i * a_{i;\boldsymbol{s}}(0) + \int_0^t {}_{\tau;0}^{t;t-\tau}\mathrm{Z}_i * r_{i;\boldsymbol{s}}(\tau)\,d\tau + \int_0^t {}_{\tau;0}^{t;t-\tau}\mathrm{Z}_i * \sigma_{i;\boldsymbol{s}}(\tau)\,dB_{i;\boldsymbol{s}}(\tau) \quad (6.9)$$

The covariance of the Gaussian density function in the previous degradation models represents the case of isotropic ink diffusion. For the case of anisotropic ink diffusion where the ink diffusion rates at different directions over the space are different due to the fiber orientation of paper, we rewrite the covariance as

$${}_{\tau}^{t}\boldsymbol{\Sigma}_i = R_{\vartheta}\begin{bmatrix} 2\int_{\tau}^{t}\delta_i^{\parallel}(\xi)\,d\xi & 0 \\ 0 & 2\int_{\tau}^{t}\delta_i^{\perp}(\xi)\,d\xi \end{bmatrix} R_{\vartheta}^{\mathrm{T}}$$

where $\delta_i^{\parallel}$ and $\delta_i^{\perp}$ are the orthogonal largest and smallest diffusion rates over the space, respectively, $R_{\vartheta} = \begin{bmatrix} \cos\vartheta & -\sin\vartheta \\ \sin\vartheta & \cos\vartheta \end{bmatrix}$ is the rotation matrix, and ϑ ($0 \le \vartheta < \pi$) is the counterclockwise angle of the largest diffusion rate $\delta_i^{\parallel}$ from the horizontal axis.

Denote the density function of the fiber orientation distribution as $f(\vartheta)$ and $\int_0^{\pi} f(\vartheta)\,d\vartheta = 1$. For a paper with uniformly oriented fibers, $f(\vartheta) = \frac{1}{\pi}$ (Yang *et al.* 1987).

We redefine δ_i as the diffusion rate of state *i* along the fiber orientation for a paper with perfectly oriented fibers and assume ink diffusion is negligible in the perpendicular direction to the fiber orientation. The covariance of the Gaussian density function in the degradation model for a paper with perfectly oriented fibers at angle ϑ is then calculated as

$$ {}_{\tau}^{t}\boldsymbol{\Sigma}_i^{(\vartheta)} = R_{\vartheta} \begin{bmatrix} 2\int_{\tau}^{t} \delta_i(\xi)\, d\xi & 0 \\ 0 & \epsilon \end{bmatrix} R_{\vartheta}^{\mathrm{T}} $$

where ${}_{\tau}^{t}\boldsymbol{\Sigma}_i^{(\vartheta)}$ is the covariance of the Gaussian density function for state *i* on a paper with perfectly oriented fibers at angle ϑ, and ϵ is a minimal positive value representing the negligible diffusion rate in the perpendicular direction to the fiber orientation. The covariance of the Gaussian density function in the degradation model for a paper with a general fiber orientation distribution is derived as

$$ {}_{\tau}^{t}\boldsymbol{\Sigma}_i = \int_0^{\pi} f^2(\vartheta)\, {}_{\tau}^{t}\boldsymbol{\Sigma}_i^{(\vartheta)} d\vartheta $$

Similarly, for a general time-varying diffusion rate $\delta_i(t) = \theta_i \gamma_i t^{\gamma_i - 1}$, the diffusion rate under the paper aging effect is given in Eq. (6.10),

$$ \delta_i(t) = \theta_i e^{\lambda_i t}\left(\lambda_i t^{\gamma_i} + \gamma_i t^{\gamma_i - 1}\right) \tag{6.10} $$

where γ_i, θ_i, and λ_i are constants.

6.2.1 *Parameters Estimation*

Once the parameters of the fading rate are estimated, the parameters of the diffusion rate are estimated sequentially by printing each state as the top state over the space. Assuming that there are $M+1$ area coverage measurements at pixel $\boldsymbol{s}$ at time $t_m,\ m=0,1,...,M,\ t_0=0$, the log-likelihood function of the area coverage of state i is

$$\ln \mathcal{L} = \sum_{\boldsymbol{s}} \sum_{m=1}^{M} \ln \frac{1}{\sqrt{2\pi \upsilon_{i;\boldsymbol{s}}(t_m)}} - \sum_{\boldsymbol{s}} \sum_{m=1}^{M} \frac{\left[x_{i;\boldsymbol{s}}(t_m) - a_{i;\boldsymbol{s}}(t_m) \right]^2}{2\upsilon_{i;\boldsymbol{s}}(t_m)} \tag{6.11}$$

where $x_{i;\boldsymbol{s}}(t_m)$ and $a_{i;\boldsymbol{s}}(t_m)$ are the measured and predicted area coverages of state i at pixel $\boldsymbol{s}$ at time t_m, respectively, and $\upsilon_{i;\boldsymbol{s}}(t_m)$ is the predicted variance of the area coverage of state i at pixel $\boldsymbol{s}$ at time t_m. The parameters are estimated numerically by maximizing the log-likelihood function given in Eq. (6.11).

6.2.2 *Simulation and Validation*

In this section, we first compare the difference between the models with recurrent and non-recurrent fading and diffusion rates. The prediction intervals of the area coverages of the states and the CMY inks in (3,2) Purple with non-recurrent time-varying fading and diffusion rates are plotted in Figure 6.8. The parameters in the simulation are the same as in Section 5.3.2. The paper aging effect is not considered in this simulation. Compared with the result of recurrent time-varying fading and diffusion rates shown in Figure 5.6, the expected area coverages decrease more rapidly and the prediction intervals narrow faster due to the non-recurrent monotonically increasing fading rates.

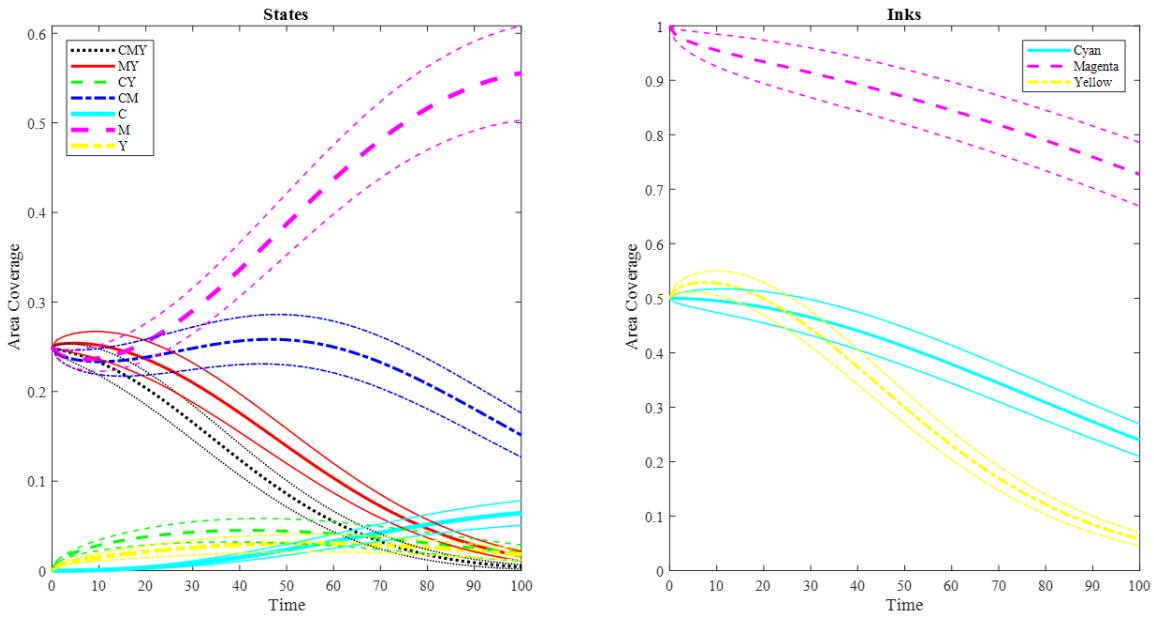

Figure 6.8 95% prediction intervals of area coverages of states and inks in (3,2) Purple with non-recurrent time-varying fading and diffusion rates

We then illustrate how fiber orientation affects the ink diffusion. We compare three cases of ink diffusion: isotropic, anisotropic, and anisotropic with rotation. In the isotropic case, ink diffuses at the same speed in every direction. In the anisotropic case, ink diffuses faster in the horizontal direction than in the vertical direction. In the anisotropic with rotation case, the faster horizontal direction in the anisotropic case is rotated 45° counterclockwise from the horizontal axis. The diffusion rates of the three cases are constant and shown in Table 6.2, where $\delta_{\parallel}$ and $\delta_{\perp}$ are the largest and smallest diffusion rates over the space, respectively, and ϑ is the counterclockwise angle of the largest diffusion rate $\delta_{\parallel}$ from the horizontal axis. An illustration of the diffusion rates in the three cases is shown in Figure 6.9.

Table 6.2 Diffusion rates and fiber orientation

	$\delta_{\parallel}$	$\delta_{\perp}$	ϑ
Isotropic	0.125	0.125	
Anisotropic	0.5	0.045	0°
Anisotropic with rotation	0.5	0.045	45°

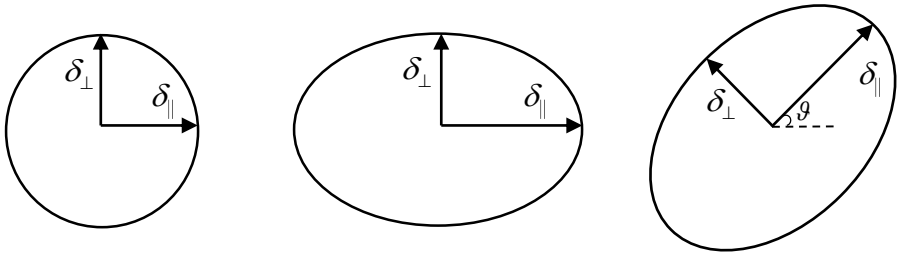

Figure 6.9 Illustration of isotropic, anisotropic, and anisotropic with rotation diffusion rates

To apply the model on image pixels, 3 × 3 discrete Gaussian kernels of the three cases are created using Eq. (5.6) as $h_1 = \begin{bmatrix} 0.0113 & 0.0838 & 0.0113 \\ 0.0838 & 0.6193 & 0.0838 \\ 0.0113 & 0.0838 & 0.0113 \end{bmatrix}$, $h_2 = \begin{bmatrix} 0.0011 & 0.0017 & 0.0011 \\ 0.2720 & 0.4484 & 0.2720 \\ 0.0011 & 0.0017 & 0.0011 \end{bmatrix}$, $h_3 = \begin{bmatrix} 0.0000 & 0.0251 & 0.1907 \\ 0.0251 & 0.5183 & 0.0251 \\ 0.1907 & 0.0251 & 0.0000 \end{bmatrix}$. The three Gaussian kernels are applied in an ink dot degradation simulation shown in Figure 6.10 and an image degradation simulation shown in Figure 6.11.

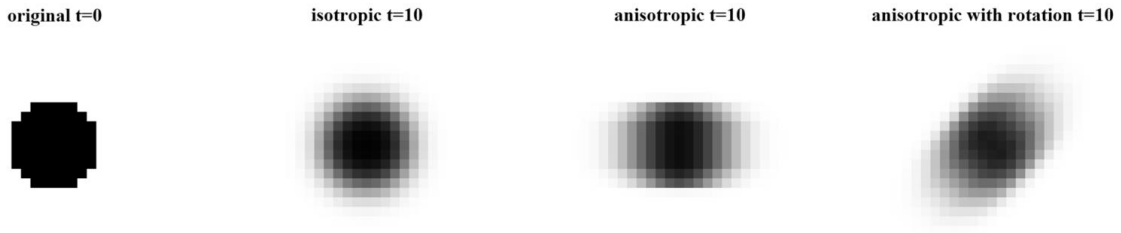

Figure 6.10 Ink dot degradation by ink diffusion considering fiber orientation

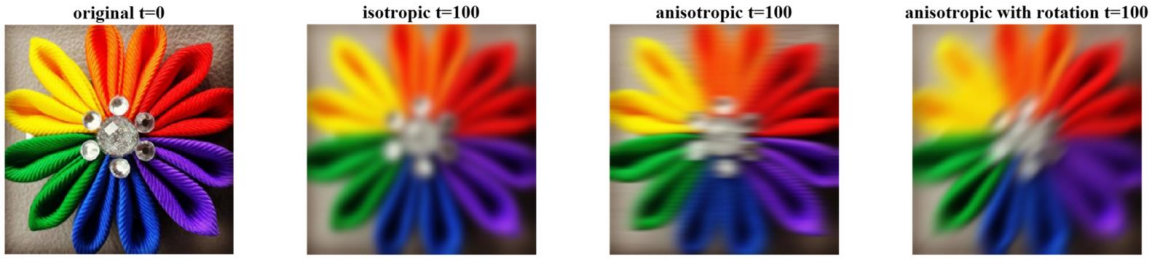

Figure 6.11 Image degradation by ink diffusion considering fiber orientation

6.3 Summary and Conclusions

In this chapter, we propose the degradation modeling of ink fading and ink diffusion with non-recurrent ink fading and diffusion rates and investigate the ink-paper interactions. Two aspects of the ink-paper interactions are considered, i.e., the effect of paper aging such as depolymerization and yellowing, and the fiber orientation of the paper, on the ink fading and diffusion rates. Paper aging effect is modeled as the acceleration of the ink fading and diffusion rates, and the fiber orientation of paper affects the ink diffusion direction. Simulation results demonstrate the validity of the proposed degradation model and the effect of ink-paper interactions.

CHAPTER 7

ACCELERATED DEGRADATION OF PRINTED IMAGES

In this chapter, we investigate accelerated degradation modeling and optimal design of accelerated degradation testing (ADT) plans of ink fading and ink diffusion. We propose an accelerated degradation model by establishing the link between different environmental stress levels and the ink fading and diffusion of printed images and validate the model through experiments. We then design optimal ADT plans for the proposed accelerated degradation model.

7.1 Accelerated Degradation Model of Ink Fading and Ink Diffusion

By reviewing the degradation models presented in previous chapters, it is observed that the area coverage prediction is only related to three factors: fading rate, diffusion rate, and a volatility parameter. It is intuitive to model the fading and diffusion rates as stress-dependent functions, while we keep the volatility parameter constant for all stress levels. The degradation model of ink fading and ink diffusion with recurrent time-varying fading and diffusion rates under environmental stress condition z is given in Eq. (7.1),

$$
\begin{aligned}
&\tilde{a}_{i;\boldsymbol{s}}(t;z) \\
&= \exp\left(-\int_0^t \kappa_i(\xi;z)\,d\xi\right)\int_{\mathbb{R}^2}\varphi\left(\Delta\boldsymbol{s};\boldsymbol{\mu},{}_0^t\boldsymbol{\Sigma}_i(z)\right)a_{i;\boldsymbol{s}'}(0;z)\,d(\Delta\boldsymbol{s}) + \\
&\int_0^t\left[\exp\left(-\int_\tau^t \kappa_i(\xi;z)\,d\xi\right)\int_{\mathbb{R}^2}\varphi\left(\Delta\boldsymbol{s};\boldsymbol{\mu},{}_\tau^t\boldsymbol{\Sigma}_i(z)\right)r_{i;\boldsymbol{s}'}(\tau;z)\,d(\Delta\boldsymbol{s})\right]d\tau + \\
&\int_0^t\left[\exp\left(-\int_\tau^t \kappa_i(\xi;z)\,d\xi\right)\int_{\mathbb{R}^2}\varphi\left(\Delta\boldsymbol{s};\boldsymbol{\mu},{}_\tau^t\boldsymbol{\Sigma}_i(z)\right)\sigma_{i;\boldsymbol{s}'}(\tau;z)\,d(\Delta\boldsymbol{s})\right]dB_{i;\boldsymbol{s}}(\tau) \\
&= a_{i;\boldsymbol{s}}(t;z) + \int_0^t\left[\exp\left(-\int_\tau^t \kappa_i(\xi;z)\,d\xi\right)\int_{\mathbb{R}^2}\varphi\left(\Delta\boldsymbol{s};\boldsymbol{\mu},{}_\tau^t\boldsymbol{\Sigma}_i(z)\right)\sigma_{i;\boldsymbol{s}'}(\tau;z)\,d(\Delta\boldsymbol{s})\right]dB_{i;\boldsymbol{s}}(\tau)
\end{aligned}
\tag{7.1}
$$

where z is the environmental stress condition (stresses include temperature, humidity, and illumination intensity), $a_{i;\boldsymbol{s}}(t;z)$ and $\tilde{a}_{i;\boldsymbol{s}}(t;z)$ are the deterministic and stochastic area coverages of state i at pixel $\boldsymbol{s}=\begin{bmatrix}x & y\end{bmatrix}^{\mathrm{T}}$ at time t under environmental stress condition z, respectively, $\kappa_i(t;z)=\sum_j k_{i,j}(t;z)$ is the overall fading rate of state i to other states at time t under environmental stress condition z, $\mathbb{R}^2$ denotes two-dimensional space, $\Delta\boldsymbol{s}=\boldsymbol{s}'-\boldsymbol{s}$, $\varphi\left(\Delta\boldsymbol{s};\boldsymbol{\mu},{}_\tau^t\boldsymbol{\Sigma}_i(z)\right)$ is a bivariate Gaussian density function with $\boldsymbol{\mu}=\begin{bmatrix}0 & 0\end{bmatrix}^{\mathrm{T}}$ and ${}_\tau^t\boldsymbol{\Sigma}_i(z)=\begin{bmatrix}2\int_\tau^t \delta_i(\xi;z)\,d\xi & 0\\ 0 & 2\int_\tau^t \delta_i(\xi;z)\,d\xi\end{bmatrix}$, $\delta_i(t;z)$ is the diffusion rate of state i at time t under environmental stress condition z, $r_{i;\boldsymbol{s}}(t;z)=\sum_j k_{j,i}(t;z)\,a_{j;\boldsymbol{s}}(t;z)$ is the deterministic area coverage transition rate into state i due to ink fading at pixel $\boldsymbol{s}$ at time t under environmental stress condition z, and $\sigma_{i;\boldsymbol{s}}(t;z)$ and $B_{i;\boldsymbol{s}}(t)$ are the spatially independent volatility function and the standard Brownian motion process for state i at pixel $\boldsymbol{s}$ at time t

under environmental stress condition *z*, respectively. The volatility function is chosen as $\sigma_{i;s}(t;z)=\eta_i\sqrt{a_{i;s}(t;z)}$, where η_i is the volatility parameter.

Eq. (7.1) is rewritten as Eq. (7.2) using the operator defined in Eq. (5.9),

$$\begin{aligned}\tilde{a}_{i;s}(t;z) &= {}_0^t Z_i * a_{i;s}(0;z)+\int_0^t {}_\tau^t Z_i * \left\{ r_{i;s}(\tau;z)\,d\tau+\sigma_{i;s}(\tau;z)\,dB_{i;s}(\tau)\right\} \\ &= a_{i;s}(t;z)+\int_0^t {}_\tau^t Z_i * \sigma_{i;s}(\tau;z)\,dB_{i;s}(\tau)\end{aligned} \tag{7.2}$$

The expectation of the stochastic area coverage equals the deterministic area coverage, and the variance of the stochastic area coverage is calculated as

$$\begin{aligned}\upsilon_{i;s}(t;z) &= E\left[\left(\tilde{a}_{i;s}(t;z)-E\left[\tilde{a}_{i;s}(t;z)\right]\right)^2\right] \\ &= E\left[\left(\int_0^t {}_\tau^t Z_i * \sigma_{i;s}(\tau;z)\,dB_{i;s}(\tau)\right)^2\right] \\ &= \int_0^t {}_\tau^t Z_i^2 * \sigma_{i;s}^2(\tau;z)\,d\tau\end{aligned}$$

The stochastic area coverage follows a normal distribution $\tilde{a}_{i;s}(t;z)\sim N\left(a_{i;s}(t;z),\upsilon_{i;s}(t;z)\right)$.

Next we model the fading and diffusion rates as stress-dependent functions. Three types of environmental stresses are considered, they are: temperature, humidity, and illumination intensity. The effect of temperature on kinetic reaction rate is commonly modeled by the Arrhenius equation (Gagliardi *et al.* 2017). The effect of humidity on kinetic reaction rate can be modeled by the exponential law or power law (Escobar and Meeker 2006). Baumann and Hofmann (2003) state that changes induced by ink diffusion are generally small at

relative humidity below a certain threshold. Most prints have very little humidity diffusion at or below 60% RH and show a more or less steep increase between 70% RH and 80% RH. In this case, a power law relationship is more appropriate. The effect of illumination intensity is modeled as exponential law (Wilhelm and Brower 1993). Denote stress combination $z = [T, RH, I]$, where *T* is temperature in Kelvin, *RH* is relative humidity %, and *I* is illumination intensity in klux. The stress-dependent time-varying fading rate from state *i* to state *j* and diffusion rate of state *i* are written as shown in Eq. (7.3) and Eq. (7.4),

$$k_{i,j}(t;z) = \theta_{i,j}(z) e^{\lambda_{i,j}(\boldsymbol{z})t} \left(\lambda_{i,j}(z) t^{\gamma_{i,j}} + \gamma_{i,j} t^{\gamma_{i,j}-1} \right) \tag{7.3}$$

$$\delta_i(t;z) = \theta_i(z) e^{\lambda_i(\boldsymbol{z})t} \left(\lambda_i(z) t^{\gamma_i} + \gamma_i t^{\gamma_i - 1} \right) \tag{7.4}$$

where $\gamma_{i,j}$ and γ_i are constants, $\theta_{i,j}(z) = \exp(\boldsymbol{\alpha}_{i,j}\boldsymbol{z})$ and $\theta_i(z) = \exp(\boldsymbol{\alpha}_i \boldsymbol{z})$ are stress-dependent parameters of fading rate and diffusion rate, respectively, $\lambda_{i,j}(z) = \boldsymbol{\beta}_{i,j}\boldsymbol{z}$ and $\lambda_i(z) = \boldsymbol{\beta}_i \boldsymbol{z}$ are stress-dependent parameters of paper-aging effect on fading rate and diffusion rate, respectively, $\boldsymbol{z} = \left[1, \frac{1}{T}, \ln RH, I, \frac{\ln RH}{T}, \frac{I}{T}, I \ln RH, \frac{I \ln RH}{T}\right]^{\mathrm{T}}$ is the stresses and their interaction terms, and $\boldsymbol{\alpha}_{i,j} = [\alpha_{i,j;\iota}]$, $\boldsymbol{\alpha}_i = [\alpha_{i;\iota}]$, $\boldsymbol{\beta}_{i,j} = [\beta_{i,j;\iota}]$, and $\boldsymbol{\beta}_i = [\beta_{i;\iota}]$ for $\iota = 0,1,2,\ldots,7$ are constant coefficients of the ι^{th} element in $\boldsymbol{z}$. The proposed model considers the stress interactions as well as the accelerated degradation of the printed medium (paper) by the environmental stresses.

7.1.1 *Parameters Estimation*

The parameters of the fading rate are estimated sequentially by printing each state as the top state over the space. For a full factorial constant stress accelerated degradation testing plan where temperature, humidity, and illumination intensity having L_1, L_2, and L_3 levels, respectively, there are $G = L_1 L_2 L_3$ experiments or stress combinations (stress combinations are unordered in the multi-stress scenario). An example of the experiments with three levels of each environmental stress is given in Table 7.1.

Table 7.1 Experiments with three levels of each environmental stress

Expr. No.	T	RH	I	Expr. No.	T	RH	I	Expr. No.	T	RH	I
1	1	1	1	10	2	1	1	19	3	1	1
2	1	1	2	11	2	1	2	20	3	1	2
3	1	1	3	12	2	1	3	21	3	1	3
4	1	2	1	13	2	2	1	22	3	2	1
5	1	2	2	14	2	2	2	23	3	2	2
6	1	2	3	15	2	2	3	24	3	2	3
7	1	3	1	16	2	3	1	25	3	3	1
8	1	3	2	17	2	3	2	26	3	3	2
9	1	3	3	18	2	3	3	27	3	3	3

Assuming that there are N_g samples and M_g+1 area coverage measurements at time t_{m_g}, $m_g = 0,1,...,M_g$, $t_0 = 0$, under stress combination z_g, $g = 1,2,\ldots,G$, the log-likelihood function of the area coverage of state *i* is

$$\ln \mathcal{L}_i = \sum_{g=1}^{G} \sum_{n_g=1}^{N_g} \sum_{m_g=1}^{M_g} \ln \frac{1}{\sqrt{2\pi \upsilon_{i;n_g}\left(t_{m_g}; z_g\right)}} - \sum_{g=1}^{G} \sum_{n_g=1}^{N_g} \sum_{m=1}^{M_g} \frac{\left[x_{i;n_g}\left(t_{m_g}; z_g\right) - a_{i;n_g}\left(t_{m_g}; z_g\right)\right]^2}{2\upsilon_{i;n_g}\left(t_{m_g}; z_g\right)} \tag{7.5}$$

where $x_{i;n_g}\left(t_{m_g}; z_g\right)$ and $a_{i;n_g}\left(t_{m_g}; z_g\right)$ are the measured and predicted area coverages of state *i* in the n_g^{th} sample at time t_{m_g} under stress combination z_g, respectively, and

$\upsilon_{i;n_g}\left(t_{m_g};z_g\right)$ is the predicted variance of the area coverage of state *i* in the n_g^{th} sample at time t_{m_g} under stress combination z_g. The parameters are estimated numerically by maximizing the log-likelihood function given in Eq. (7.5).

Once the parameters of the fading rate are estimated, the parameters of the diffusion rate are estimated sequentially by printing each state as the top state over the space. Assuming that there are *G* stress combinations and M_g+1 area coverage measurements at pixel $\boldsymbol{s}$ at time t_{m_g}, $m_g=0,1,...,M_g$, $t_0=0$, the log-likelihood function of the area coverage of state *i* is

$$\ln\mathcal{L}_i=\sum_{g=1}^{G}\sum_{\boldsymbol{s}}\sum_{m_g=1}^{M}\ln\frac{1}{\sqrt{2\pi\upsilon_{i;\boldsymbol{s}}\left(t_{m_g};z_g\right)}}-\sum_{g=1}^{G}\sum_{\boldsymbol{s}}\sum_{m_g=1}^{M}\frac{\left[x_{i;\boldsymbol{s}}\left(t_{m_g};z_g\right)-a_{i;\boldsymbol{s}}\left(t_{m_g};z_g\right)\right]^2}{2\upsilon_{i;\boldsymbol{s}}\left(t_{m_g};z_g\right)} \tag{7.6}$$

where $x_{i;\boldsymbol{s}}\left(t_{m_g};z_g\right)$ and $a_{i;\boldsymbol{s}}\left(t_{m_g};z_g\right)$ are the measured and predicted area coverages of state *i* at pixel $\boldsymbol{s}$ at time t_{m_g} under stress combination z_g, respectively, and $\upsilon_{i;\boldsymbol{s}}\left(t_{m_g};z_g\right)$ is the predicted variance of the area coverage of state *i* at pixel $\boldsymbol{s}$ at time t_{m_g} under stress combination z_g. The parameters are estimated numerically by maximizing the log-likelihood function given in Eq. (7.6).

7.1.2 *Experimental Validation*

In this section, we validate the proposed ink fading model by conducting an accelerated degradation test. Nine color patches of magenta ink (M), yellow ink (Y), and magenta and yellow inks (MY) named as M1, M2, M3, Y1, Y2, Y3, MY1, MY2, MY3 are printed with

different initial ink amounts and subjected to accelerated degradation tests using a full factorial experimental design with stress levels of temperature, humidity, and illumination intensity shown in Table 7.2. Temperature and humidity are controlled by the chamber, and illumination intensity is controlled by changing the number of LED lamps, as shown in Figure 7.1. The tests under different stress combinations z_g, $g = 1, 2, \ldots, 27$ are conducted for two to four weeks depending on the degradation progress. Microscopic photos of the color patches are taken every week and the ink area coverage is estimated. Examples of the microscopic photos of the color patches for a period of four weeks are given in Figures 7.2 – 7.7 and titled as the name of the color patch followed by the measurement time (week).

Table 7.2 Stress levels in accelerated degradation test

	T (°C)	RH (%)	I (klux)
Low	40	60	30
Medium	60	70	35
High	80	80	40

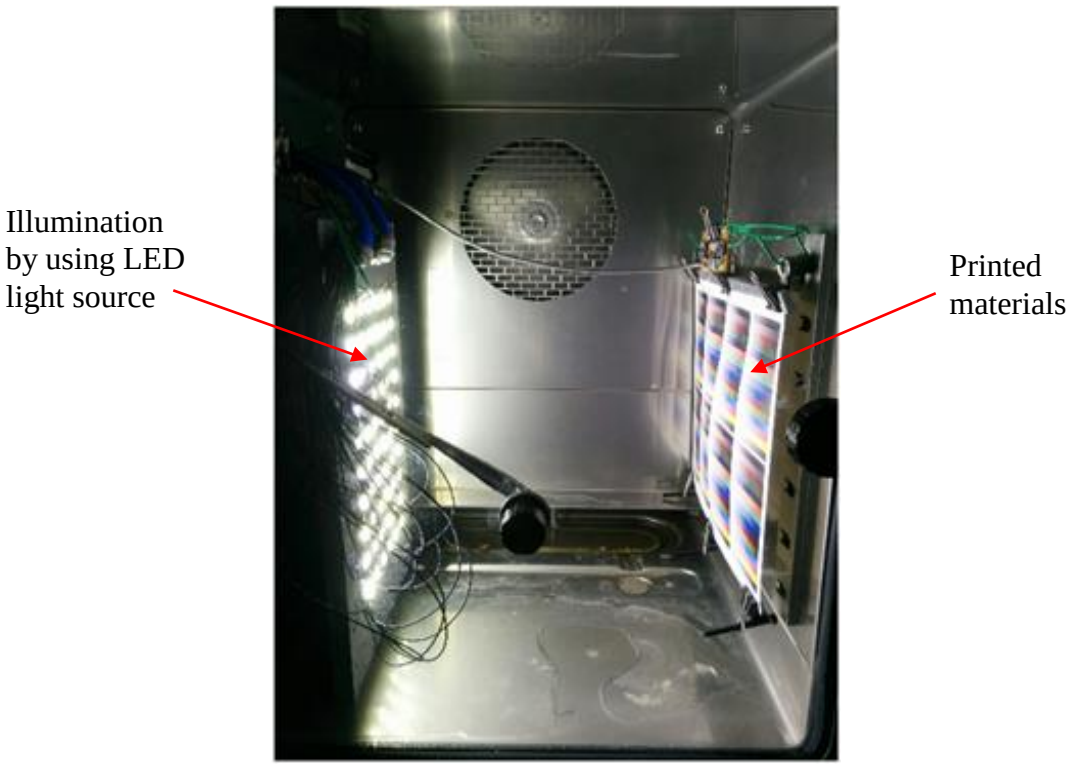

Figure 7.1 Accelerated degradation test experiment in temperature and humidity controlled chamber

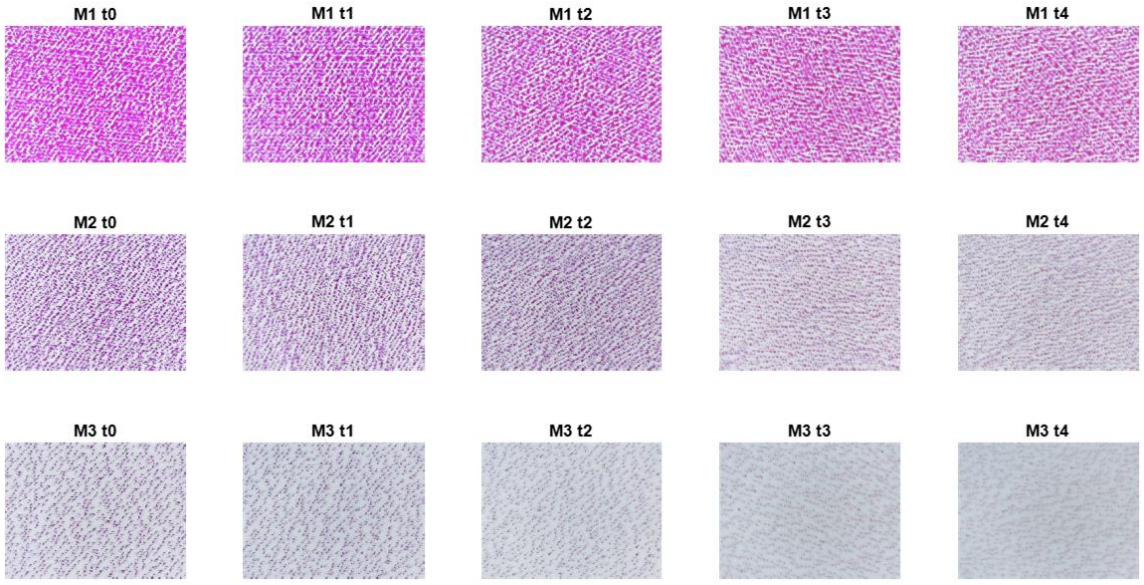

Figure 7.2 Microscopic photos of magenta ink under stress combination T40 RH60 I30

Figure 7.3 Microscopic photos of magenta ink under stress combination T60 RH70 I35

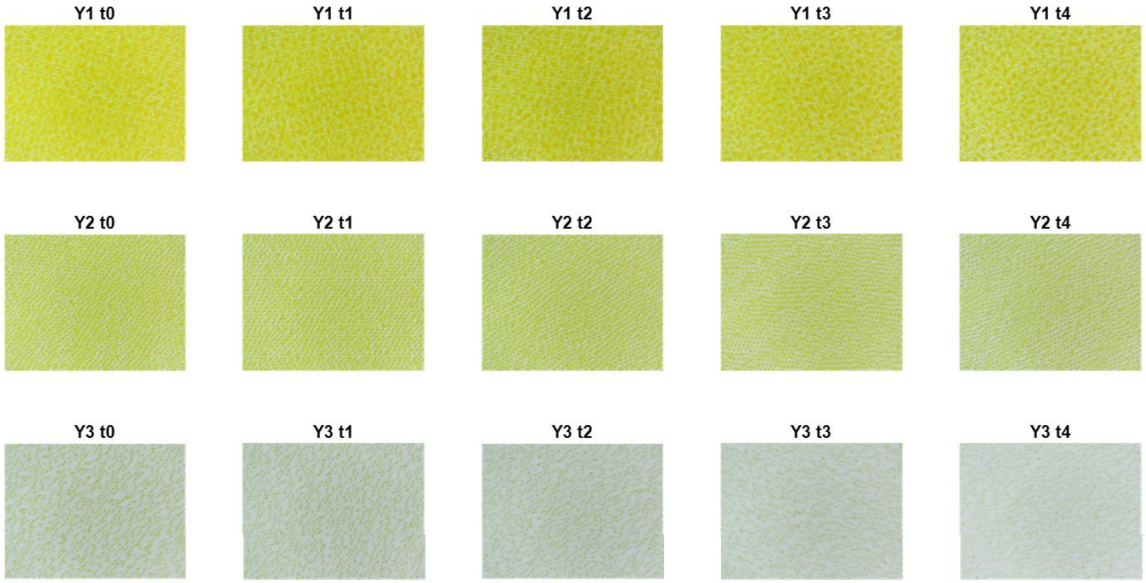

Figure 7.4 Microscopic photos of yellow ink under stress combination T40 RH60 I30

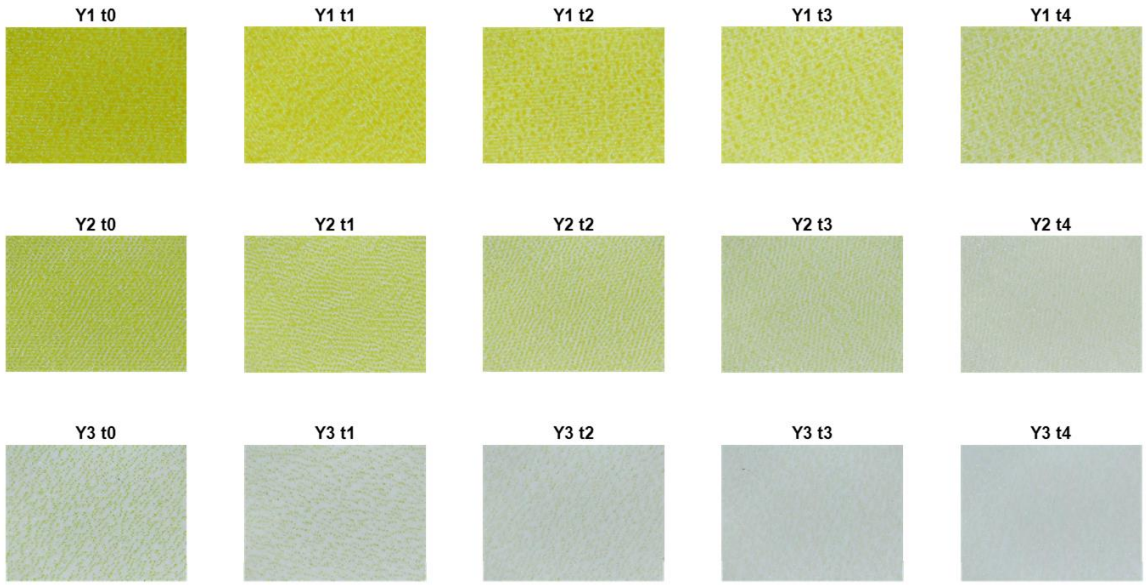

Figure 7.5 Microscopic photos of yellow ink under stress combination T60 RH70 I35

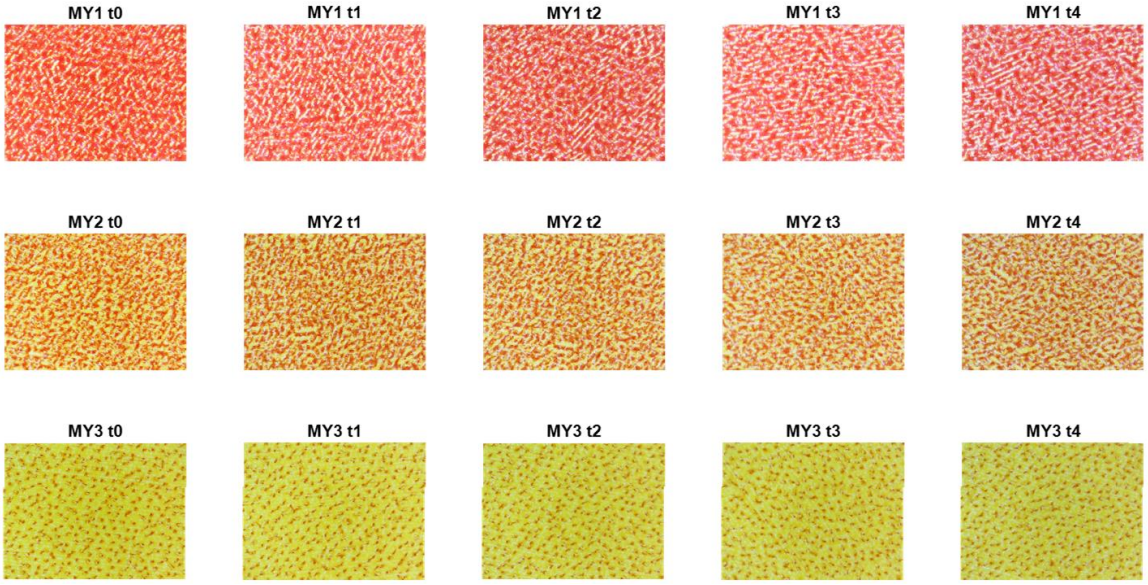

Figure 7.6 Microscopic photos of magenta and yellow inks under stress combination T40 RH60 I30

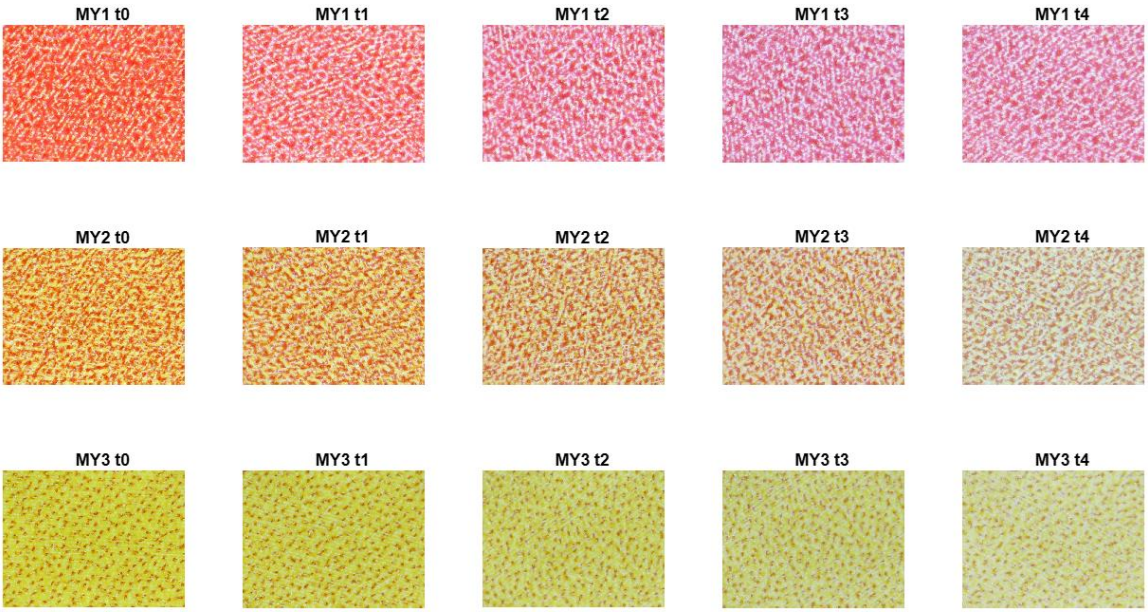

Figure 7.7 Microscopic photos of magenta and yellow inks under stress combination T60 RH70 I35

We simulate the degradation of the microscopic photos using the estimated parameters. Examples of the simulation are shown in Figures 7.8 – 7.10. The first row is the observed degradation process, while the second row is the predicted degradation process. The predicted ink area coverage (in the sequence of the ink state(s) given in the figure caption) is provided above the second row. By visually comparing the observed degraded colors and the predicted degraded colors using estimated parameters, it can be found that the predicted degraded colors match the observed degraded colors. The histograms of the prediction errors of the nine color patches are given in Figure 7.11 and titled as the name of the color patch followed by the ink state in parenthesis. The figure shows that the prediction errors are approximately normal and centered around zero. The result demonstrates that the accelerated degradation model provides accurate prediction at different stress combination levels.

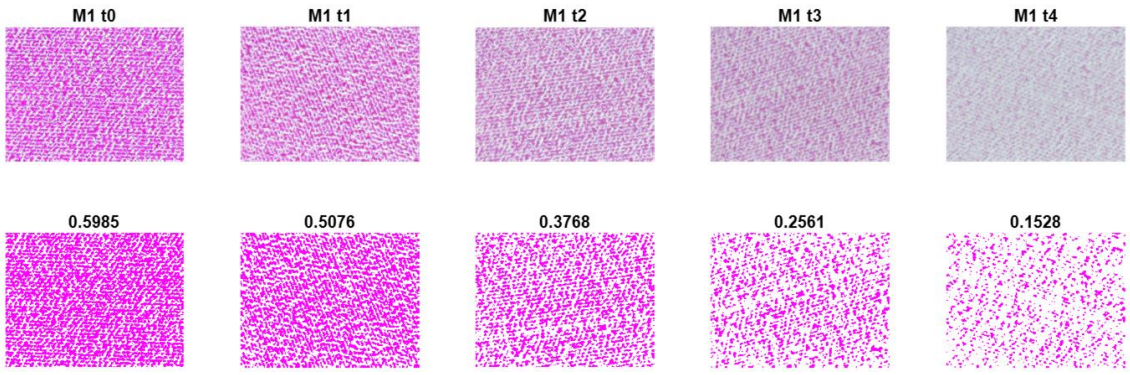

Figure 7.8 Degradation prediction of magenta ink (ink state: M) under stress combination T60 RH70 I35

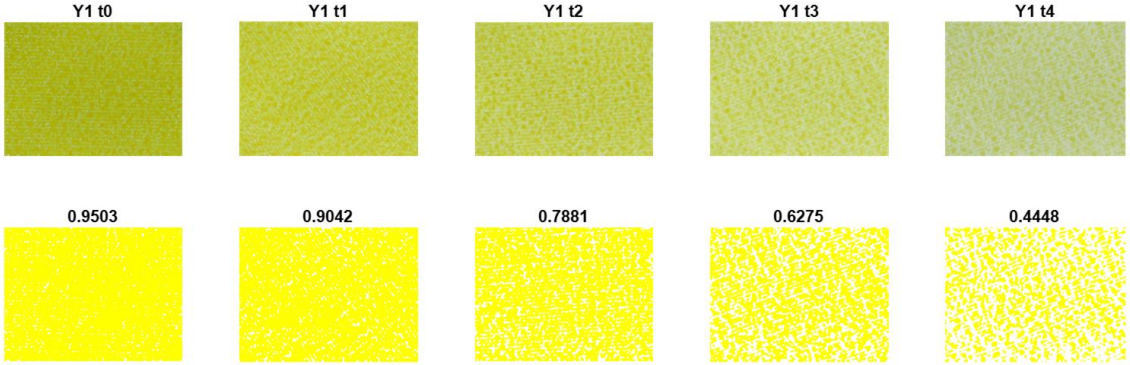

Figure 7.9 Degradation prediction of yellow ink (ink state: Y) under stress combination T60 RH70 I35

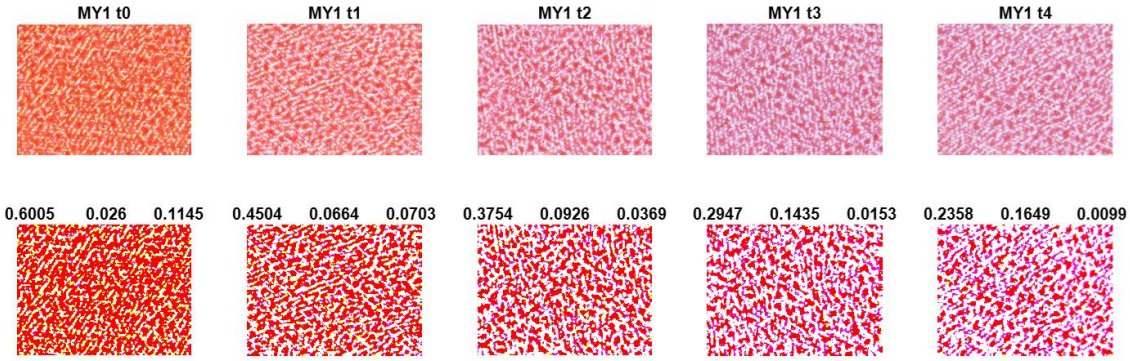

Figure 7.10 Degradation prediction of magenta and yellow inks (ink states: MY, M, Y) under stress combination T60 RH70 I35

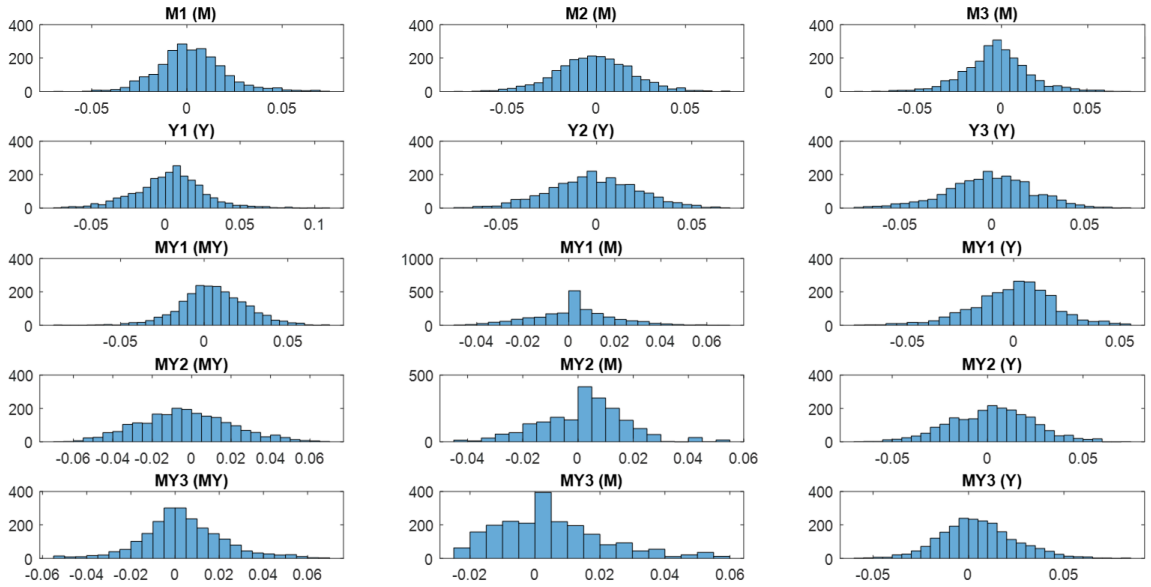

Figure 7.11 Histograms of prediction errors of the color patches

7.2 Optimal Design of ADT Planning

In this section, we provide a general framework of the optimal design of ADT plans for the proposed degradation model. In reliability, a carefully designed accelerated test plan is needed to obtain accurate reliability at normal operating conditions. The objective of the test plan is usually the minimization of a specific criterion, for example, the variance of the reliability prediction, mean time to failure, or a percentile of the failure time, under the constraints of experimental requirements such as the number of failures observed, duration of the experiment, or budget. Other criteria such as A-optimality and D-optimality focus on improving the estimation accuracy of model parameters. The A-optimality obtains the parameter estimates with optimal total variance by minimizing the trace of the asymptotic variance-covariance matrix of the maximum likelihood estimates of the model parameters. The D-optimality achieves the highest joint estimation precision of model parameters by maximizing the determinant of the Fisher information matrix, which is inversely

proportional to the asymptotic variance-covariance matrix of the maximum likelihood estimates of the model parameters. Since there is no concept of reliability or failure in the color degradation of printed images, we choose D-optimality criterion in the proposed ADT plan design to optimize the prediction accuracy of the degradation model.

The constant stress accelerated degradation test plan is chosen. Without loss of generality, the case of single ink fading with no ink-paper interactions and stress interaction terms is used to illustrate the design of the test plan. The stress-dependent time-varying fading rate from state *i* to state *j* is

$$k_{i,j}\left(t;z\right)=\exp\left(\boldsymbol{\alpha}_{i,j}\boldsymbol{z}\right)\gamma_{i,j}t^{\gamma_{i,j}-1}$$

where $\gamma_{i,j}$ is a constant, $\boldsymbol{z}=\left[1,\frac{1}{T},\ln RH,I\right]^{\mathrm{T}}$, and $\boldsymbol{\alpha}_{i,j}=\left[\alpha_{i,j;\iota}\right]$ for $\iota=0,1,2,3$ are constant coefficients of the ι^{th} element in $\boldsymbol{z}$. Assuming that the three environmental stresses: temperature, humidity, and illumination intensity, have L_1, L_2, and L_3 levels, respectively, the accelerated degradation test is conducted on G stress combinations z_g, $g=1,2,\ldots,G$ (for a full factorial experimental design, $G=L_1L_2L_3$, see Table 7.1), each having N_g, $n_g=1,2,\ldots,N_g$ samples and M_g + 1 area coverage measurements at time t_{m_g}, $m_g=0,1,...,M_g$, $t_0=0$, the log-likelihood function of the area coverage of state *i* in the n_g^{th} sample under stress combination z_g is

$$\ln\mathcal{L}_{i;n_g}\left(z_g\right)=-\frac{1}{2}\sum_{m_g=1}^{M_g}\left\{\ln\left(2\pi\upsilon_{i;n_g}\left(t_{m_g};z_g\right)\right)+\frac{\left[x_{i;n_g}\left(t_{m_g};z_g\right)-a_{i;n_g}\left(t_{m_g};z_g\right)\right]^2}{\upsilon_{i;n_g}\left(t_{m_g};z_g\right)}\right\} \tag{7.7}$$

where $a_{i;n_g}\left(t_{m_g};z_g\right)=\exp\left(-\sum_j e^{\boldsymbol{\alpha}_{i,j}\mathbf{z}_g}t_{m_g}^{\gamma_{i,j}}\right)a_{i;n_g}\left(0;z_g\right)$ is the deterministic area coverage of state i in the n_g^{th} sample at time t_{m_g} under stress combination z_g, and $\upsilon_{i;n_g}\left(t_{m_g};z_g\right)=\eta_i^2\exp\left(-2\sum_j e^{\boldsymbol{\alpha}_{i,j}\mathbf{z}_g}t_{m_g}^{\gamma_{i,j}}\right)a_{i;n_g}\left(0;z_g\right)\int_0^{t_{m_g}}\exp\left(\sum_j e^{\boldsymbol{\alpha}_{i,j}\mathbf{z}_g}\tau^{\gamma_{i,j}}\right)d\tau$ is the variance of the area coverage of state i in the n_g^{th} sample at time t_{m_g} under stress combination z_g.

The Fisher information matrix is obtained from the partial derivatives of the log-likelihood with respect to the model parameters. As shown in Eq. (7.7), the log-likelihood $\ln\mathcal{L}_{i;n_g}\left(z_g\right)$ is a function of $a_{i;n_g}\left(t_{m_g};z_g\right)$ and $\upsilon_{i;n_g}\left(t_{m_g};z_g\right)$. We first write the partial derivatives of the log-likelihood as a function of the partial derivatives of $a_{i;n_g}\left(t_{m_g};z_g\right)$ and $\upsilon_{i;n_g}\left(t_{m_g};z_g\right)$. For dummy variables $\omega,\ \varpi\in\Theta_i=\left\{\gamma_{i,j},\alpha_{i,j;0},\alpha_{i,j;1},\alpha_{i,j;2},\alpha_{i,j;3},\eta_i\right\},\ \omega\neq\varpi$, where Θ_i is the set of the model parameters of state i and η_i is the volatility parameter of state i, the first partial derivative of the log-likelihood with respect to one model parameter is

$$\frac{\partial\ln\mathcal{L}_{i;n_g}\left(z_g\right)}{\partial\omega}=-\frac{1}{2}\sum_{m_g=1}^{M_g}\left\{\begin{array}{l}\upsilon_{i;n_g}^{-1}\left(t_{m_g};z_g\right)\dfrac{\partial\upsilon_{i;n_g}\left(t_{m_g};z_g\right)}{\partial\omega}\\ -2\left[x_{i;n_g}\left(t_{m_g};z_g\right)-a_{i;n_g}\left(t_{m_g};z_g\right)\right]\dfrac{\partial a_{i;n_g}\left(t_{m_g};z_g\right)}{\partial\omega}\upsilon_{i;n_g}^{-1}\left(t_{m_g};z_g\right)\\ -\left[x_{i;n_g}\left(t_{m_g};z_g\right)-a_{i;n_g}\left(t_{m_g};z_g\right)\right]^2\upsilon_{i;n_g}^{-2}\left(t_{m_g};z_g\right)\dfrac{\partial\upsilon_{i;n_g}\left(t_{m_g};z_g\right)}{\partial\omega}\end{array}\right\}$$

The second partial derivatives of the log-likelihood with respect to the model parameters are

$$\frac{\partial^2 \ln \mathcal{L}_{i;n_g}\left(z_g\right)}{\partial \omega^2} =$$

$$-\frac{1}{2}\sum_{m_g=1}^{M_g}\left\{\begin{array}{l}
-\upsilon_{i;n_g}^{-2}\left(t_{m_g};z_g\right)\left(\frac{\partial \upsilon_{i;n_g}\left(t_{m_g};z_g\right)}{\partial \omega}\right)^2+\upsilon_{i;n_g}^{-1}\left(t_{m_g};z_g\right)\frac{\partial^2 \upsilon_{i;n_g}\left(t_{m_g};z_g\right)}{\partial \omega^2} \\
+2\left(\frac{\partial a_{i;n_g}\left(t_{m_g};z_g\right)}{\partial \omega}\right)^2\upsilon_{i;n_g}^{-1}\left(t_{m_g};z_g\right) \\
-2\left[x_{i;n_g}\left(t_{m_g};z_g\right)-a_{i;n_g}\left(t_{m_g};z_g\right)\right]\frac{\partial^2 a_{i;n_g}\left(t_{m_g};z_g\right)}{\partial \omega^2}\upsilon_{i;n_g}^{-1}\left(t_{m_g};z_g\right) \\
+4\left[x_{i;n_g}\left(t_{m_g};z_g\right)-a_{i;n_g}\left(t_{m_g};z_g\right)\right]\frac{\partial a_{i;n_g}\left(t_{m_g};z_g\right)}{\partial \omega}\upsilon_{i;n_g}^{-2}\left(t_{m_g};z_g\right)\frac{\partial \upsilon_{i;n_g}\left(t_{m_g};z_g\right)}{\partial \omega} \\
+2\left[x_{i;n_g}\left(t_{m_g};z_g\right)-a_{i;n_g}\left(t_{m_g};z_g\right)\right]^2\upsilon_{i;n_g}^{-3}\left(t_{m_g};z_g\right)\left(\frac{\partial \upsilon_{i;n_g}\left(t_{m_g};z_g\right)}{\partial \omega}\right)^2 \\
-\left[x_{i;n_g}\left(t_{m_g};z_g\right)-a_{i;n_g}\left(t_{m_g};z_g\right)\right]^2\upsilon_{i;n_g}^{-2}\left(t_{m_g};z_g\right)\frac{\partial^2 \upsilon_{i;n_g}\left(t_{m_g};z_g\right)}{\partial \omega^2}
\end{array}\right\}$$

$$\frac{\partial^2 \ln \mathcal{L}_{i;n_g}\left(z_g\right)}{\partial\omega\partial\varpi} =$$

$$-\frac{1}{2}\sum_{m_g=1}^{M_g}\left\{\begin{array}{l}
-\upsilon_{i;n_g}^{-2}\left(t_{m_g};z_g\right)\dfrac{\partial \upsilon_{i;n_g}\left(t_{m_g};z_g\right)}{\partial\omega}\dfrac{\partial \upsilon_{i;n_g}\left(t_{m_g};z_g\right)}{\partial\varpi}+\upsilon_{i;n_g}^{-1}\left(t_{m_g};z_g\right)\dfrac{\partial^2 \upsilon_{i;n_g}\left(t_{m_g};z_g\right)}{\partial\omega\partial\varpi} \\
+2\dfrac{\partial a_{i;n_g}\left(t_{m_g};z_g\right)}{\partial\omega}\dfrac{\partial a_{i;n_g}\left(t_{m_g};z_g\right)}{\partial\varpi}\upsilon_{i;n_g}^{-1}\left(t_{m_g};z_g\right) \\
-2\left[x_{i;n_g}\left(t_{m_g};z_g\right)-a_{i;n_g}\left(t_{m_g};z_g\right)\right]\dfrac{\partial^2 a_{i;n_g}\left(t_{m_g};z_g\right)}{\partial\omega\partial\varpi}\upsilon_{i;n_g}^{-1}\left(t_{m_g};z_g\right) \\
+2\left[x_{i;n_g}\left(t_{m_g};z_g\right)-a_{i;n_g}\left(t_{m_g};z_g\right)\right]\dfrac{\partial a_{i;n_g}\left(t_{m_g};z_g\right)}{\partial\omega}\upsilon_{i;n_g}^{-2}\left(t_{m_g};z_g\right)\dfrac{\partial \upsilon_{i;n_g}\left(t_{m_g};z_g\right)}{\partial\varpi} \\
+2\left[x_{i;n_g}\left(t_{m_g};z_g\right)-a_{i;n_g}\left(t_{m_g};z_g\right)\right]\dfrac{\partial a_{i;n_g}\left(t_{m_g};z_g\right)}{\partial\varpi}\upsilon_{i;n_g}^{-2}\left(t_{m_g};z_g\right)\dfrac{\partial \upsilon_{i;n_g}\left(t_{m_g};z_g\right)}{\partial\omega} \\
+2\left[x_{i;n_g}\left(t_{m_g};z_g\right)-a_{i;n_g}\left(t_{m_g};z_g\right)\right]^2\upsilon_{i;n_g}^{-3}\left(t_{m_g};z_g\right)\dfrac{\partial \upsilon_{i;n_g}\left(t_{m_g};z_g\right)}{\partial\omega}\dfrac{\partial \upsilon_{i;n_g}\left(t_{m_g};z_g\right)}{\partial\varpi} \\
-\left[x_{i;n_g}\left(t_{m_g};z_g\right)-a_{i;n_g}\left(t_{m_g};z_g\right)\right]^2\upsilon_{i;n_g}^{-2}\left(t_{m_g};z_g\right)\dfrac{\partial^2 \upsilon_{i;n_g}\left(t_{m_g};z_g\right)}{\partial\omega\partial\varpi}
\end{array}\right\}$$

The expectations of the negative of the second partial derivatives of the log-likelihood are

$$E\left[-\frac{\partial^2 \ln \mathcal{L}_{i;n_g}\left(z_g\right)}{\partial\omega^2}\right]=\sum_{m_g=1}^{M_g}\left\{\begin{array}{l}
\left(\dfrac{\partial a_{i;n_g}\left(t_{m_g};z_g\right)}{\partial\omega}\right)^2\upsilon_{i;n_g}^{-1}\left(t_{m_g};z_g\right) \\
+\dfrac{1}{2}\upsilon_{i;n_g}^{-2}\left(t_{m_g};z_g\right)\left(\dfrac{\partial \upsilon_{i;n_g}\left(t_{m_g};z_g\right)}{\partial\omega}\right)^2
\end{array}\right\}$$

$$E\left[-\frac{\partial^2 \ln \mathcal{L}_{i;n_g}\left(z_g\right)}{\partial\omega\partial\varpi}\right]=\sum_{m_g=1}^{M_g}\left\{\begin{array}{l}
\dfrac{\partial a_{i;n_g}\left(t_{m_g};z_g\right)}{\partial\omega}\dfrac{\partial a_{i;n_g}\left(t_{m_g};z_g\right)}{\partial\varpi}\upsilon_{i;n_g}^{-1}\left(t_{m_g};z_g\right) \\
+\dfrac{1}{2}\upsilon_{i;n_g}^{-2}\left(t_{m_g};z_g\right)\dfrac{\partial \upsilon_{i;n_g}\left(t_{m_g};z_g\right)}{\partial\omega}\dfrac{\partial \upsilon_{i;n_g}\left(t_{m_g};z_g\right)}{\partial\varpi}
\end{array}\right\}$$

We then derive the partial derivatives of $a_{i;n_g}\left(t_{m_g};z_g\right)$ and $\upsilon_{i;n_g}\left(t_{m_g};z_g\right)$. The first partial derivatives of $a_{i;n_g}\left(t_{m_g};z_g\right)$ and $\upsilon_{i;n_g}\left(t_{m_g};z_g\right)$ with respect to the model parameters are

$$\frac{\partial a_{i;n_g}\left(t_{m_g};z_g\right)}{\partial \gamma_{i,j}}=\left(-\ln t_{m_g}\sum_j e^{\boldsymbol{\alpha}_{i,j}\mathbf{z}_g}t_{m_g}^{\gamma_{i,j}}\right)\exp\left(-\sum_j e^{\boldsymbol{\alpha}_{i,j}\mathbf{z}_g}t_{m_g}^{\gamma_{i,j}}\right)a_{i;n_g}\left(0;z_g\right)$$

$$\frac{\partial a_{i;n_g}\left(t_{m_g};z_g\right)}{\partial \alpha_{i,j;\iota}}=\left(-\mathbf{z}_{g;\iota}\sum_j e^{\boldsymbol{\alpha}_{i,j}\mathbf{z}_g}t_{m_g}^{\gamma_{i,j}}\right)\exp\left(-\sum_j e^{\boldsymbol{\alpha}_{i,j}\mathbf{z}_g}t_{m_g}^{\gamma_{i,j}}\right)a_{i;n_g}\left(0;z_g\right),\ \iota=0,1,2,3$$

$$\frac{\partial a_{i;n_g}\left(t_{m_g};z_g\right)}{\partial \eta_i}=0$$

$$\frac{\partial \upsilon_{i;n_g}\left(t_{m_g};z_g\right)}{\partial \gamma_{i,j}}=\eta_i^2\exp\left(-2\sum_j e^{\boldsymbol{\alpha}_{i,j}\mathbf{z}_g}t_{m_g}^{\gamma_{i,j}}\right)a_{i;n_g}\left(0;z_g\right)\times$$
$$\int_0^{t_{m_g}}\exp\left(\sum_j e^{\boldsymbol{\alpha}_{i,j}\mathbf{z}_g}\tau^{\gamma_{i,j}}\right)\left(\ln\tau\sum_j e^{\boldsymbol{\alpha}_{i,j}\mathbf{z}_g}\tau^{\gamma_{i,j}}-2\ln t_{m_g}\sum_j e^{\boldsymbol{\alpha}_{i,j}\mathbf{z}_g}t_{m_g}^{\gamma_{i,j}}\right)d\tau$$

$$\frac{\partial \upsilon_{i;n_g}\left(t_{m_g};z_g\right)}{\partial \alpha_{i,j;\iota}}=\eta_i^2\exp\left(-2\sum_j e^{\boldsymbol{\alpha}_{i,j}\mathbf{z}_g}t_{m_g}^{\gamma_{i,j}}\right)a_{i;n_g}\left(0;z_g\right)\times$$
$$\int_0^{t_{m_g}}\exp\left(\sum_j e^{\boldsymbol{\alpha}_{i,j}\mathbf{z}_g}\tau^{\gamma_{i,j}}\right)\left(\mathbf{z}_{g;\iota}\sum_j e^{\boldsymbol{\alpha}_{i,j}\mathbf{z}_g}\tau^{\gamma_{i,j}}-2\mathbf{z}_{g;\iota}\sum_j e^{\boldsymbol{\alpha}_{i,j}\mathbf{z}_g}t_{m_g}^{\gamma_{i,j}}\right)d\tau,\ \iota=0,1,2,3$$

$$\frac{\partial \upsilon_{i;n_g}\left(t_{m_g};z_g\right)}{\partial \eta_i}=2\eta_i^{-1}\upsilon_{i;n_g}\left(t_{m_g};z_g\right)$$

where $\mathbf{z}_{g;\iota}$ is the ι^{th} element of $\mathbf{z}$ under stress combination z_g.

The Fisher information matrix of one sample of state i under stress combination z_g is obtained by taking expectation of the negative of the second partial derivatives of the log-likelihood with respect to the model parameters,

$$\boldsymbol{F}_{i;n_g}\left(z_g\right)=-E\begin{bmatrix}\dfrac{\partial^2 \ln \mathcal{L}_{i;n_g}\left(z_g\right)}{\partial \widehat{\gamma}_{i,j}^2} & \dfrac{\partial^2 \ln \mathcal{L}_{i;n_g}\left(z_g\right)}{\partial \widehat{\gamma}_{i,j}\partial \widehat{\alpha}_{i,j;0}} & \cdots & \dfrac{\partial^2 \ln \mathcal{L}_{i;n_g}\left(z_g\right)}{\partial \widehat{\gamma}_{i,j}\partial \widehat{\eta}_i} \\ \dfrac{\partial^2 \ln \mathcal{L}_{i;n_g}\left(z_g\right)}{\partial \widehat{\alpha}_{i,j;0}\partial \widehat{\gamma}_{i,j}} & \dfrac{\partial^2 \ln \mathcal{L}_{i;n_g}\left(z_g\right)}{\partial \widehat{\alpha}_{i,j;0}^2} & \cdots & \dfrac{\partial^2 \ln \mathcal{L}_{i;n_g}\left(z_g\right)}{\partial \widehat{\alpha}_{i,j;0}\partial \widehat{\eta}_i} \\ \vdots & \vdots & \ddots & \vdots \\ \dfrac{\partial^2 \ln \mathcal{L}_{i;n_g}\left(z_g\right)}{\partial \widehat{\eta}_i\partial \widehat{\gamma}_{i,j}} & \dfrac{\partial^2 \ln \mathcal{L}_{i;n_g}\left(z_g\right)}{\partial \widehat{\eta}_{i,j}\partial \widehat{\alpha}_{i,j;0}} & \cdots & \dfrac{\partial^2 \ln \mathcal{L}_{i;n_g}\left(z_g\right)}{\partial \widehat{\eta}_i^2}\end{bmatrix}$$

Suppose that the proportion of samples allocated to stress combination z_g is π_g, $\sum_{g=1}^{G}\pi_g=1$, and the number of samples allocated to stress combination z_g is $N_g=\pi_g N$, where N is the total number of samples used in the accelerated degradation test. The Fisher information matrix of state i for all the stress combinations is

$$\boldsymbol{F}_i=\sum_{g=1}^{G}\sum_{n_g=1}^{N_g}\boldsymbol{F}_{i;n_g}\left(z_g\right)$$

The asymptotic variance-covariance matrix of the maximum likelihood estimates of the model parameters is obtained by taking the inverse of the Fisher information matrix,

$$\boldsymbol{\Sigma}_i=\boldsymbol{F}_i^{-1}=\begin{bmatrix}\mathrm{Var}\left(\widehat{\gamma}_{i,j}\right) & \mathrm{Cov}\left(\widehat{\gamma}_{i,j},\widehat{\alpha}_{i,j;0}\right) & \cdots & \mathrm{Cov}\left(\widehat{\gamma}_{i,j},\widehat{\eta}_i\right) \\ \mathrm{Cov}\left(\widehat{\alpha}_{i,j;0},\widehat{\gamma}_{i,j}\right) & \mathrm{Var}\left(\widehat{\alpha}_{i,j;0}\right) & \cdots & \mathrm{Cov}\left(\widehat{\alpha}_{i,j;0},\widehat{\eta}_i\right) \\ \vdots & \vdots & \ddots & \vdots \\ \mathrm{Cov}\left(\widehat{\eta}_i,\widehat{\gamma}_{i,j}\right) & \mathrm{Cov}\left(\widehat{\eta}_i,\widehat{\alpha}_{i,j;0}\right) & \cdots & \mathrm{Var}\left(\widehat{\eta}_i\right)\end{bmatrix}$$

Assuming that the duration of the experiment at each stress combination z_g is a predetermined value t_{M_g} (either given or until degradation reaches a threshold D_i as the same area coverage percentage loss for all samples), and the total number of samples is given. The objective is to find the optimal stress combinations and the proportion of

samples allocated to each stress combination that maximize the precision of parameters estimation. The optimization is formulated as

$$
\begin{aligned}
&\text{Max} \quad \left|\boldsymbol{F}_i\right| \\
&\text{s.t.} \\
&\quad 0 < \pi_g < 1,\ g = 1,\ldots,G \\
&\quad \sum_{g=1}^{G} \pi_g = 1 \\
&\quad T_0 \le T_1 \le \cdots \le T_{L_1} \le T_{\max} \\
&\quad RH_0 \le RH_1 \le \cdots \le RH_{L_2} \le RH_{\max} \\
&\quad I_0 \le I_1 \le \cdots \le I_{L_3} \le I_{\max} \\
&\quad \frac{a_{i;n_g}\left(t_{M_g}; z_g\right)}{a_{i;n_g}\left(0; z_g\right)} = D_i,\ g = 1,\ldots,G
\end{aligned}
$$

where T_0, RH_0, I_0 and $T_{\max}$, $RH_{\max}$, $I_{\max}$ are the predetermined lowest and highest temperature, humidity, and illumination intensity in the accelerated degradation test, and D_i is the degradation threshold for state i. The optimal decision variables T_1, …, T_{L_1}, RH_1, …, RH_{L_2}, I_1, …, I_{L_3} and π_g, $g = 1,\cdots,G$ (for a full factorial experimental design, $G = L_1 L_2 L_3$, see Table 7.1) are obtained by solving the constrained nonlinear optimization problem.

A full factorial design of experiment for multiple stresses is often time-consuming. The Latin hypercube sampling is frequently used for fractional factorial design. Johnson *et al.* (1990) propose a maximin distance criterion, which maximizes the minimum inter-site distance. Based on this criterion, Morris and Mitchell (1995) further propose a scalar-valued function to find the optimal Latin hypercube design,

$$\phi_p(D) = \left[\sum_{j=1}^{m} J_j d_j^{-p} \right]^{1/p}$$

where p is a positive integer, and J_j and d_j characterize the design D. The optimal design of experiment minimizes $\phi_p(D)$.

7.2.1 *Numerical Examples*

In this section, we provide a numerical simulation for optimal design of accelerated degradation test planning using the degradation model and the optimality criterion proposed in this chapter. The Latin Hypercube Design (LHD) for G experiments (or stress combinations) and n stresses is denoted as LHD (G, n). Suppose due to time constraint only five experiments can be conducted. The optimal LHD (5, 3) found through exhaustive enumeration is shown in Table 7.3.

Table 7.3 Optimal LHD (5, 3): Experiments and corresponding stress levels

Expr. No.	T	RH	I
1	1	1	2
2	2	5	3
3	3	2	5
4	4	3	1
5	5	4	4

In the simulation, the range of temperature is 40 ~ 80 °C, relative humidity is 60 ~ 80%, and illumination intensity is 10 ~ 30 klux. We use the same number of samples at each stress combination due to the ignorable cost of image reproduction, and the experiments at all the stress combinations run a period of four weeks. The optimal stress combinations of the ADT planning are found through numerical search and is shown in Table 7.4.

Table 7.4 Optimal stress combinations in ADT planning using LHD (5, 3)

Expr. No.	T (°C)	RH (%)	I (klux)
1	42	60	18
2	44	80	22
3	72	62	30
4	76	72	14
5	80	76	26

7.3 Summary and Conclusions

In this chapter, modeling of the fading and diffusion rates as functions of three environmental stresses that commonly affect the color degradation of printed images: temperature, humidity, and illumination intensity, is studied. We develop an accelerated degradation model of ink fading and ink diffusion. Experimental results demonstrate the validity of the model. We further propose methodology for optimal design of the accelerated degradation test planning. The D-optimality criterion is chosen to maximize the estimation accuracy of the model parameters, and a Latin hypercube design is adopted to run the experiments. Compared with a full factorial experimental design, an ADT planning using LHD significantly reduces the number of experiments and can be conducted within a reasonable amount of time.

CHAPTER 8

CONCLUSIONS

In this dissertation we investigate the degradation modeling of ink fading and ink diffusion of printed images. We formulate the problem as a spatio-temporal multistate transition system and develop degradation models to predict the color degradation of printed images. The effect of the printed medium (paper) and environmental stresses are incorporated in the degradation models. We summarize the conclusions and future work below.

8.1 Conclusions

The conclusions of the dissertation are:

1. In consideration of the catalytic fading induced by halftone printing, we propose a multi-layered state transition diagram for ink fading. The ink area coverage of the states is used as the performance indicator. Assuming constant fading rates, a physics-based first-order reaction rate ink fading model is developed. Further, a vector autoregressive ink diffusion model is derived from the two-dimensional diffusion equation. The two models are integrated into the physics-based degradation model for constant fading and diffusion rates. This model is validated as it predicts the ink fading and diffusion of printed images accurately.

2. We prove that the developed physics-based degradation model with constant fading and diffusion rates is equivalent to a statistics-based Markov process model with

exponential transition time distribution. A more general degradation model with time-varying fading and diffusion rates is then obtained by replacing the exponential distribution with other distributions. Hence, the Markov process model becomes a semi-Markov process model. We provide the method for solving the semi-Markov process model and specifically investigate the case of Weibull state transition time distribution for ink fading and diffusion.

3. Stochastic process models are investigated to provide stochastic area coverage prediction for the ink degradation. We propose a Hull-White/Vasicek (HWV) stochastic ink fading model with a mean-reverting property, which results in a shrinking variance as the ink area coverage approaches zero. The HWV ink fading model is further integrated with a convolution-based ink diffusion model into a spatio-temporal stochastic degradation model. The models are initially developed using constant fading and diffusion rates, but further extended to the case of recurrent as well as non-recurrent time-varying fading and diffusion rates.

4. We develop a general degradation model of ink fading and ink diffusion with ink-paper interactions. Two aspects of the ink-paper interactions are considered, i.e., the effect of paper aging such as depolymerization and yellowing, and the fiber

orientation of the paper, on the ink fading and diffusion rates. The results show that the printed medium (paper) has a major impact on the printed image degradation.

5. The effect of environmental stresses: temperature, humidity, and illumination intensity, on the fading and diffusion rates is studied and an accelerated degradation model is proposed. The design of optimal accelerated degradation test planning for the degradation of printed images is also investigated. The D-optimality criterion is chosen to maximize the estimation accuracy of the model parameters, and a Latin hypercube design is adopted to run the experiments within a reasonable amount of time.

8.2 Future Work

The color degradation of printed images is a subtle yet highly complex process. It is the result of various physical and chemical changes. On the one hand, the proposed degradation models can be validated by the image degradation simulations as well as the experimental results because the model is initially developed from a physics-based perspective. On the other hand, the proposed spatio-temporal multistate models in this dissertation themselves are quite complex, making them capable of incorporating the highly nonlinear degradation process of the printed images. However, the research on the color degradation prediction

of printed images in this dissertation needs future work. We summarize potential areas for future work.

1. The degradation models developed in this dissertation are based on multiple assumptions, which may be violated in some cases. One example is the uniform ink concentration assumption, though it might be compensated by the time-varying fading and diffusion rates. Other phenomena in the degradation of printed images and their degradation modeling deserve further study and experimental validation.

2. The degradation model is nonlinear and contains many parameters. The estimation of the model parameters is difficult to obtain analytically, and sequential estimation is not accurate. A successful attempt to estimate all the parameters together is made in Section 6.1.2 using gradient descent method. Also, accurate estimation of the model parameters needs further study when spatio-temporal correlation exist.

3. Only illumination intensity is considered in the accelerated degradation model. The effect of the spectral distribution of the illumination on the color degradation of printed images needs to be investigated.

APPENDIX

We ignore state 16 W. The area coverage transition rates into the states are

$$r_1(t) = 0$$

$$r_2(t) = k_{1,2}a_1(t)$$

$$r_3(t) = k_{1,3}a_1(t)$$

$$r_4(t) = k_{1,4}a_1(t)$$

$$r_5(t) = k_{1,5}a_1(t)$$

$$r_6(t) = k_{2,6}a_2(t) + k_{3,6}a_3(t)$$

$$r_7(t) = k_{2,7}a_2(t) + k_{4,7}a_4(t)$$

$$r_8(t) = k_{2,8}a_2(t) + k_{5,8}a_5(t)$$

$$r_9(t) = k_{4,9}a_4(t) + k_{5,9}a_5(t)$$

$$r_{10}(t) = k_{3,10}a_3(t) + k_{5,10}a_5(t)$$

$$r_{11}(t) = k_{3,11}a_3(t) + k_{4,11}a_4(t)$$

$$r_{12}(t) = k_{7,12}a_7(t) + k_{8,12}a_8(t) + k_{9,12}a_9(t)$$

$$r_{13}(t) = k_{6,13}a_6(t) + k_{8,13}a_8(t) + k_{10,13}a_{10}(t)$$

$$r_{14}(t) = k_{6,14}a_6(t) + k_{7,14}a_7(t) + k_{11,14}a_{11}(t)$$

$$r_{15}(t) = k_{9,15}a_9(t) + k_{10,15}a_{10}(t) + k_{11,15}a_{11}(t)$$

The differential equation matrix $\boldsymbol{A}$ is

$$\boldsymbol{A} = \begin{bmatrix}
-\kappa_1 & & & & & & & & & & & & & & \\
k_{1,2} & -\kappa_2 & & & & & & & & & & & & & \\
k_{1,3} & & -\kappa_3 & & & & & & & & & & & & \\
k_{1,4} & & & -\kappa_4 & & & & & & & & & & & \\
k_{1,5} & & & & -\kappa_5 & & & & & & & & & & \\
 & k_{2,6} & k_{3,6} & & & -\kappa_6 & & & & & & & & & \\
 & k_{2,7} & & k_{4,7} & & & -\kappa_7 & & & & & & & & \\
 & k_{2,8} & & & k_{5,8} & & & -\kappa_8 & & & & & & & \\
 & & & k_{4,9} & k_{5,9} & & & & -\kappa_9 & & & & & & \\
 & & k_{3,10} & & k_{5,10} & & & & & -\kappa_{10} & & & & & \\
 & & k_{3,11} & k_{4,11} & & & & & & & -\kappa_{11} & & & & \\
 & & & & & & k_{7,12} & k_{8,12} & k_{9,12} & & & -\kappa_{12} & & & \\
 & & & & & k_{6,13} & & k_{8,13} & & k_{10,13} & & & -\kappa_{13} & & \\
 & & & & & k_{6,14} & k_{7,14} & & & & k_{11,14} & & & -\kappa_{14} & \\
 & & & & & & & & k_{9,15} & k_{10,15} & k_{11,15} & & & & -\kappa_{15}
\end{bmatrix}$$

The predicted area coverages of the states are

$$a_1(t) = c_{1,1}e^{-\kappa_1 t}$$

$$a_2(t) = c_{2,1}e^{-\kappa_1 t} + c_{2,2}e^{-\kappa_2 t}$$

$$a_3(t) = c_{3,1}e^{-\kappa_1 t} + c_{3,3}e^{-\kappa_3 t}$$

$$a_4(t) = c_{4,1}e^{-\kappa_1 t} + c_{4,4}e^{-\kappa_4 t}$$

$$a_5(t) = c_{5,1}e^{-\kappa_1 t} + c_{5,5}e^{-\kappa_5 t}$$

$$a_6(t) = c_{6,1}e^{-\kappa_1 t} + c_{6,2}e^{-\kappa_2 t} + c_{6,3}e^{-\kappa_3 t} + c_{6,6}e^{-\kappa_6 t}$$

$$a_7(t) = c_{7,1}e^{-\kappa_1 t} + c_{7,2}e^{-\kappa_2 t} + c_{7,4}e^{-\kappa_4 t} + c_{7,7}e^{-\kappa_7 t}$$

$$a_8(t) = c_{8,1}e^{-\kappa_1 t} + c_{8,2}e^{-\kappa_2 t} + c_{8,5}e^{-\kappa_5 t} + c_{8,8}e^{-\kappa_8 t}$$

$$a_9(t) = c_{9,1}e^{-\kappa_1 t} + c_{9,4}e^{-\kappa_4 t} + c_{9,5}e^{-\kappa_5 t} + c_{9,9}e^{-\kappa_9 t}$$

$$a_{10}(t) = c_{10,1}e^{-\kappa_1 t} + c_{10,3}e^{-\kappa_3 t} + c_{10,5}e^{-\kappa_5 t} + c_{10,10}e^{-\kappa_{10} t}$$

$$a_{11}(t) = c_{11,1}e^{-\kappa_1 t} + c_{11,3}e^{-\kappa_3 t} + c_{11,4}e^{-\kappa_4 t} + c_{11,11}e^{-\kappa_{11} t}$$

$$a_{12}(t) = c_{12,1}e^{-\kappa_1 t} + c_{12,2}e^{-\kappa_2 t} + c_{12,4}e^{-\kappa_4 t} + c_{12,5}e^{-\kappa_5 t} + c_{12,7}e^{-\kappa_7 t} + c_{12,8}e^{-\kappa_8 t} + c_{12,9}e^{-\kappa_9 t} + c_{12,12}e^{-\kappa_{12} t}$$

$$a_{13}(t) = c_{13,1}e^{-\kappa_1 t} + c_{13,2}e^{-\kappa_2 t} + c_{13,3}e^{-\kappa_3 t} + c_{13,5}e^{-\kappa_5 t} + c_{13,6}e^{-\kappa_6 t} + c_{13,8}e^{-\kappa_8 t} + c_{13,10}e^{-\kappa_{10} t} + c_{13,13}e^{-\kappa_{13} t}$$

$$a_{14}(t) = c_{14,1}e^{-\kappa_1 t} + c_{14,2}e^{-\kappa_2 t} + c_{14,3}e^{-\kappa_3 t} + c_{14,4}e^{-\kappa_4 t} + c_{14,6}e^{-\kappa_6 t} + c_{14,7}e^{-\kappa_7 t} + c_{14,11}e^{-\kappa_{11} t} + c_{14,14}e^{-\kappa_{14} t}$$

$$a_{15}(t) = c_{15,1}e^{-\kappa_1 t} + c_{15,3}e^{-\kappa_3 t} + c_{15,4}e^{-\kappa_4 t} + c_{15,5}e^{-\kappa_5 t} + c_{15,9}e^{-\kappa_9 t} + c_{15,10}e^{-\kappa_{10} t} + c_{15,11}e^{-\kappa_{11} t} + c_{15,15}e^{-\kappa_{15} t}$$

The coefficient matrix $\boldsymbol{c}$ is

$$\boldsymbol{c}=\begin{bmatrix}
c_{1,1} & & & & & & & & & & & & & & \\
c_{2,1} & c_{2,2} & & & & & & & & & & & & & \\
c_{3,1} & & c_{3,3} & & & & & & & & & & & & \\
c_{4,1} & & & c_{4,4} & & & & & & & & & & & \\
c_{5,1} & & & & c_{5,5} & & & & & & & & & & \\
c_{6,1} & c_{6,2} & c_{6,3} & & & c_{6,6} & & & & & & & & & \\
c_{7,1} & c_{7,2} & & c_{7,4} & & & c_{7,7} & & & & & & & & \\
c_{8,1} & c_{8,2} & & & c_{8,5} & & & c_{8,8} & & & & & & & \\
c_{9,1} & & & c_{9,4} & c_{9,5} & & & & c_{9,9} & & & & & & \\
c_{10,1} & & c_{10,3} & & c_{10,5} & & & & & c_{10,10} & & & & & \\
c_{11,1} & & c_{11,3} & c_{11,4} & & & & & & & c_{11,11} & & & & \\
c_{12,1} & c_{12,2} & & c_{12,4} & c_{12,5} & & c_{12,7} & c_{12,8} & c_{12,9} & & & c_{12,12} & & & \\
c_{13,1} & c_{13,2} & c_{13,3} & & c_{13,5} & c_{13,6} & & c_{13,8} & & c_{13,10} & & & c_{13,13} & & \\
c_{14,1} & c_{14,2} & c_{14,3} & c_{14,4} & & c_{14,6} & c_{14,7} & & & & c_{14,11} & & & c_{14,14} & \\
c_{15,1} & & c_{15,3} & c_{15,4} & c_{15,5} & & & & c_{15,9} & c_{15,10} & c_{15,11} & & & & c_{15,15}
\end{bmatrix}$$

where

$$c_{i,i}=a_i\left(0\right)-\sum_{h<i}c_{i,h},\ i=1,2,...,15,$$

$$c_{2,1}=\frac{k_{1,2}c_{1,1}}{\kappa_2-\kappa_1},\ c_{3,1}=\frac{k_{1,3}c_{1,1}}{\kappa_3-\kappa_1},c_{4,1}=\frac{k_{1,4}c_{1,1}}{\kappa_4-\kappa_1},\ c_{5,1}=\frac{k_{1,5}c_{1,1}}{\kappa_5-\kappa_1},$$

$$c_{6,1}=\frac{k_{2,6}c_{2,1}+k_{3,6}c_{3,1}}{\kappa_6-\kappa_1},\ c_{6,2}=\frac{k_{2,6}c_{2,2}}{\kappa_6-\kappa_2},\ c_{6,3}=\frac{k_{3,6}c_{3,3}}{\kappa_6-\kappa_3},$$

$$c_{7,1}=\frac{k_{2,7}c_{2,1}+k_{4,7}c_{4,1}}{\kappa_7-\kappa_1},\ c_{7,2}=\frac{k_{2,7}c_{2,2}}{\kappa_7-\kappa_2},\ c_{7,4}=\frac{k_{4,7}c_{4,4}}{\kappa_7-\kappa_4},$$

$$c_{8,1}=\frac{k_{2,8}c_{2,1}+k_{5,8}c_{5,1}}{\kappa_8-\kappa_1},\ c_{8,2}=\frac{k_{2,8}c_{2,2}}{\kappa_8-\kappa_2},\ c_{8,5}=\frac{k_{5,8}c_{5,5}}{\kappa_8-\kappa_5},$$

$$c_{9,1}=\frac{k_{4,9}c_{4,1}+k_{5,9}c_{5,1}}{\kappa_9-\kappa_1},\ c_{9,4}=\frac{k_{4,9}c_{4,4}}{\kappa_9-\kappa_4},\ c_{9,5}=\frac{k_{5,9}c_{5,5}}{\kappa_9-\kappa_5},$$

$$c_{10,1}=\frac{k_{3,10}c_{3,1}+k_{5,10}c_{5,1}}{\kappa_{10}-\kappa_1},\ c_{10,3}=\frac{k_{3,10}c_{3,3}}{\kappa_{10}-\kappa_3},\ c_{10,5}=\frac{k_{5,10}c_{5,5}}{\kappa_{10}-\kappa_5},$$

$$c_{11,1}=\frac{k_{3,11}c_{3,1}+k_{4,11}c_{4,1}}{\kappa_{11}-\kappa_1},\ c_{11,3}=\frac{k_{3,11}c_{3,3}}{\kappa_{11}-\kappa_3},\ c_{11,4}=\frac{k_{4,11}c_{4,4}}{\kappa_{11}-\kappa_4},$$

$$c_{12,1}=\frac{k_{7,12}c_{7,1}+k_{8,12}c_{8,1}+k_{9,12}c_{9,1}}{\kappa_{12}-\kappa_1}\quad,\quad c_{12,2}=\frac{k_{7,12}c_{7,2}+k_{8,12}c_{8,2}}{\kappa_{12}-\kappa_2}\quad,\quad c_{12,4}=\frac{k_{7,12}c_{7,4}+k_{9,12}c_{9,4}}{\kappa_{12}-\kappa_4}\quad,$$

$$c_{12,5}=\frac{k_{8,12}c_{8,5}+k_{9,12}c_{9,5}}{\kappa_{12}-\kappa_5},\ c_{12,7}=\frac{k_{7,12}c_{7,7}}{\kappa_{12}-\kappa_7},\ c_{12,8}=\frac{k_{8,12}c_{8,8}}{\kappa_{12}-\kappa_8},\ c_{12,9}=\frac{k_{9,12}c_{9,9}}{\kappa_{12}-\kappa_9},$$

$$c_{13,1}=\frac{k_{6,13}c_{6,1}+k_{8,13}c_{8,1}+k_{10,13}c_{10,1}}{\kappa_{13}-\kappa_1}\quad,\quad c_{13,2}=\frac{k_{6,13}c_{6,2}+k_{8,13}c_{8,2}}{\kappa_{13}-\kappa_2}\quad,\quad c_{13,3}=\frac{k_{6,13}c_{6,3}+k_{10,13}c_{10,3}}{\kappa_{13}-\kappa_3}\quad,$$

$$c_{13,5}=\frac{k_{8,13}c_{8,5}+k_{10,13}c_{10,5}}{\kappa_{13}-\kappa_5},\ c_{13,6}=\frac{k_{6,13}c_{6,6}}{\kappa_{13}-\kappa_6},\ c_{13,8}=\frac{k_{8,13}c_{8,8}}{\kappa_{13}-\kappa_8},\ c_{13,10}=\frac{k_{10,13}c_{10,10}}{\kappa_{13}-\kappa_{10}},$$

$$c_{14,1}=\frac{k_{6,14}c_{6,1}+k_{7,14}c_{7,1}+k_{11,14}c_{11,1}}{\kappa_{14}-\kappa_1}\quad,\quad c_{14,2}=\frac{k_{6,14}c_{6,2}+k_{7,14}c_{7,2}}{\kappa_{14}-\kappa_2}\quad,\quad c_{14,3}=\frac{k_{6,14}c_{6,3}+k_{11,14}c_{11,3}}{\kappa_{14}-\kappa_3}\quad,$$

$$c_{14,4}=\frac{k_{7,14}c_{7,4}+k_{11,14}c_{11,4}}{\kappa_{14}-\kappa_4},\ c_{14,6}=\frac{k_{6,14}c_{6,6}}{\kappa_{14}-\kappa_6},\ c_{14,7}=\frac{k_{7,14}c_{7,7}}{\kappa_{14}-\kappa_7},\ c_{14,11}=\frac{k_{11,14}c_{11,11}}{\kappa_{14}-\kappa_{11}},$$

$$c_{15,1}=\frac{k_{9,15}c_{9,1}+k_{10,15}c_{10,1}+k_{11,15}c_{11,1}}{\kappa_{15}-\kappa_1}\quad,\quad c_{15,3}=\frac{k_{10,15}c_{10,3}+k_{11,15}c_{11,3}}{\kappa_{15}-\kappa_3}\quad,\quad c_{15,4}=\frac{k_{9,15}c_{9,4}+k_{11,15}c_{11,4}}{\kappa_{15}-\kappa_4}\quad,$$

$$c_{15,5}=\frac{k_{9,15}c_{9,5}+k_{10,15}c_{10,5}}{\kappa_{15}-\kappa_5},\ c_{15,9}=\frac{k_{9,15}c_{9,9}}{\kappa_{15}-\kappa_9},\ c_{15,10}=\frac{k_{10,15}c_{10,10}}{\kappa_{15}-\kappa_{10}},\ c_{15,11}=\frac{k_{11,15}c_{11,11}}{\kappa_{15}-\kappa_{11}},$$ and blank elements are zeros.

The fading transition matrix $\boldsymbol{p}$ is

$$\boldsymbol{p} = \begin{bmatrix}
p_{1,1} & & & & & & & & & & & & & & \\
p_{1,2} & p_{2,2} & & & & & & & & & & & & & \\
p_{1,3} & & p_{3,3} & & & & & & & & & & & & \\
p_{1,4} & & & p_{4,4} & & & & & & & & & & & \\
p_{1,5} & & & & p_{5,5} & & & & & & & & & & \\
 & p_{2,6} & p_{3,6} & & & p_{6,6} & & & & & & & & & \\
 & p_{2,7} & & p_{4,7} & & & p_{7,7} & & & & & & & & \\
 & p_{2,8} & & & p_{5,8} & & & p_{8,8} & & & & & & & \\
 & & & p_{4,9} & p_{5,9} & & & & p_{9,9} & & & & & & \\
 & & p_{3,10} & & p_{5,10} & & & & & p_{10,10} & & & & & \\
 & & p_{3,11} & p_{4,11} & & & & & & & p_{11,11} & & & & \\
 & & & & & & p_{7,12} & p_{8,12} & p_{9,12} & & & p_{12,12} & & & \\
 & & & & & p_{6,13} & & p_{8,13} & & p_{10,13} & & & p_{13,13} & & \\
 & & & & & p_{6,14} & p_{7,14} & & & & p_{11,14} & & & p_{14,14} & \\
 & & & & & & & & p_{9,15} & p_{10,15} & p_{11,15} & & & & p_{15,15}
\end{bmatrix}$$

where $p_{i,i} = 1 - \kappa_i \Delta t$, $p_{i,j} = k_{i,j} \Delta t$, and blank elements are zeros.

The overall diffusion transition matrix is

$$\mathbf{H} = \begin{bmatrix} \mathbf{H}_1 & & & & & & & & & & & & & & \\ & \mathbf{H}_2 & & & & & & & & & & & & & \\ & & \mathbf{H}_3 & & & & & & & & & & & & \\ & & & \mathbf{H}_4 & & & & & & & & & & & \\ & & & & \mathbf{H}_5 & & & & & & & & & & \\ & & & & & \mathbf{H}_6 & & & & & & & & & \\ & & & & & & \mathbf{H}_7 & & & & & & & & \\ & & & & & & & \mathbf{H}_8 & & & & & & & \\ & & & & & & & & \mathbf{H}_9 & & & & & & \\ & & & & & & & & & \mathbf{H}_{10} & & & & & \\ & & & & & & & & & & \mathbf{H}_{11} & & & & \\ & & & & & & & & & & & \mathbf{H}_{12} & & & \\ & & & & & & & & & & & & \mathbf{H}_{13} & & \\ & & & & & & & & & & & & & \mathbf{H}_{14} & \\ & & & & & & & & & & & & & & \mathbf{H}_{15} \end{bmatrix}$$

where $\mathbf{H}_i$ is the diffusion transition matrix of state *i*.

The overall fading-diffusion transition matrix is

$$\boldsymbol{\Pi} = \begin{bmatrix}
\boldsymbol{\Pi}_1 & & & & & & & & & & & & & & \\
p_{1,2}\mathbf{I} & \boldsymbol{\Pi}_2 & & & & & & & & & & & & & \\
p_{1,3}\mathbf{I} & & \boldsymbol{\Pi}_3 & & & & & & & & & & & & \\
p_{1,4}\mathbf{I} & & & \boldsymbol{\Pi}_4 & & & & & & & & & & & \\
p_{1,5}\mathbf{I} & & & & \boldsymbol{\Pi}_5 & & & & & & & & & & \\
 & p_{2,6}\mathbf{I} & p_{3,6}\mathbf{I} & & & \boldsymbol{\Pi}_6 & & & & & & & & & \\
 & p_{2,7}\mathbf{I} & & p_{4,7}\mathbf{I} & & & \boldsymbol{\Pi}_7 & & & & & & & & \\
 & p_{2,8}\mathbf{I} & & & p_{5,8}\mathbf{I} & & & \boldsymbol{\Pi}_8 & & & & & & & \\
 & & & p_{4,9}\mathbf{I} & p_{5,9}\mathbf{I} & & & & \boldsymbol{\Pi}_9 & & & & & & \\
 & & p_{3,10}\mathbf{I} & & p_{5,10}\mathbf{I} & & & & & \boldsymbol{\Pi}_{10} & & & & & \\
 & & p_{3,11}\mathbf{I} & p_{4,11}\mathbf{I} & & & & & & & \boldsymbol{\Pi}_{11} & & & & \\
 & & & & & & p_{7,12}\mathbf{I} & p_{8,12}\mathbf{I} & p_{9,12}\mathbf{I} & & & \boldsymbol{\Pi}_{12} & & & \\
 & & & & & p_{6,13}\mathbf{I} & & p_{8,13}\mathbf{I} & & p_{10,13}\mathbf{I} & & & \boldsymbol{\Pi}_{13} & & \\
 & & & & & p_{6,14}\mathbf{I} & p_{7,14}\mathbf{I} & & & & p_{11,14}\mathbf{I} & & & \boldsymbol{\Pi}_{14} & \\
 & & & & & & & & p_{9,15}\mathbf{I} & p_{10,15}\mathbf{I} & p_{11,15}\mathbf{I} & & & & \boldsymbol{\Pi}_{15}
\end{bmatrix}$$

where $\boldsymbol{\Pi}_i$ is obtained by substituting the diagonal values of $\mathbf{H}_i$, $1-n_s\dfrac{\delta_i}{(\Delta s)^2}\Delta t$, by $1-\kappa_i\Delta t-n_s\dfrac{\delta_i}{(\Delta s)^2}\Delta t$, $p_{i,j}$ is defined in the fading transition matrix ***p***, and **I** is identity matrix.

REFERENCES

Ahmed, J., Kaur, A. and Shivhare, U. 2002. Color degradation kinetics of spinach, mustard leaves, and mixed puree. *Journal of Food Science,* 67, 1088-1091.

Bae, S. J., Kim, S. J., Kim, M. S., Lee, B. J. and Kang, C. W. 2008. Degradation analysis of nano-contamination in plasma display panels. *IEEE Transactions on Reliability,* 57, 222-229.

Bae, S. J., Kuo, W. and Kvam, P. H. 2007. Degradation models and implied lifetime distributions. *Reliability Engineering and System Safety,* 92, 601-608.

Bae, S. J. and Kvam, P. H. 2004. A nonlinear random-coefficients model for degradation. *Technometrics,* 46, 460-469.

Bahadori, L., Chakrabarti, M. H., Manan, N. S. A., Hashim, M. A., Mjalli, F. S., AlNashef, I. M. and Brandon, N. 2015. The effect of temperature on kinetics and diffusion coefficients of metallocene derivatives in polyol-based deep eutectic solvents. *PLoS ONE,* 10.

Baumann, E. and Hofmann, R. 2003. The characterization of humidity sensitivity of ink-jet prints. *International Conference on Digital Printing Technologies*. 402-405.

Baumann, E. and Hofmann, R. 2004. The equivalence of light sources in light stability testing. *International Conference on Digital Printing Technologies*. 699-704.

Berger, M. and Wilhelm, H. 2003. Comparison of different methods for estimating the sensitivity of inkjet images to gas fading. *International Conference on Digital Printing Technologies*. 438-443.

Berger, M. and Wilhelm, H. 2004. Evaluating the ozone resistance of inkjet prints: Comparisons between two types of accelerated ozone tests and ambient air exposure in a home. *International Conference on Digital Printing Technologies*. 740-745.

Bian, L. and Gebraeel, N. Z. 2012. Computing and updating the first-passage time distribution for randomly evolving degradation signals. *IIE Transactions,* 44, 974-987.

Blayo, A., Murie, C. and Pineaux, B. 2003. Contribution of spectroscopic techniques to the analysis of permanence properties of ink-jet printed materials. *International Conference on Digital Printing Technologies*. 434-437.

Boulanger, M. and Escobar, L. A. 1994. Experimental design for a class of accelerated degradation tests. *Technometrics,* 36, 260-272.

Brown, P. E., Karesen, K. F., Roberts, G. O. and Tonellato, S. 2000. Blur-generated non-separable space-time models. *Journal of the Royal Statistical Society: Series B (Statistical Methodology),* 62, 847-860.

Bugner, D. E., LaBarca, J., Phillips, J. and Kaltenbach, T. 2006. A survey of environmental conditions relative to the storage and display of photographs in consumer homes. *Journal of Imaging Science and Technology,* 50, 309-319.

Bugner, D. E., LaBarca, J., Phillips, J., Kaltenbach, T., Bush, A. and Kapecki, J. 2005. Survey of environmental conditions relative to display of photographs in consumer homes - phase II. *Archiving Conference*. 179-183.

Bugner, D. E. and Lindstrom, B. L. 2005. A closer look at the effects of temperature and humidity on inkjet photographic prints. *International Conference on Digital Printing Technologies*. 348-352.

Bugner, D. E. and Lindstrom, B. L. 2006. Further investigations into accelerated light fade reciprocity of inkjet photographic prints. *International Conference on Digital Printing Technologies*. 235-238.

Burns, P. D. and Berns, R. S. 1996. Analysis of multispectral image capture. *Fourth Color Imaging Conference: Color Science, Systems and Applications*. 19-22.

Cameletti, M., Lindgren, F., Simpson, D. and Rue, H. 2013. Spatio-temporal modeling of particulate matter concentration through the SPDE approach. *AStA Advances in Statistical Analysis,* 97, 109-131.

Campbell, K., Miller, N., Books, L. and Burns, K. 2007. Simulating accelerated commercial in-window display: Predicted print longevity for pigment ink systems on a range of media types. *International Conference on Digital Printing Technologies*. 734-738.

Carter, H. A. 1996a. The chemistry of paper preservation part 1. the aging of paper and conservation techniques. *Journal of Chemical Education,* 73, 417-420.

Carter, H. A. 1996b. The chemistry of paper preservation part 2. the yellowing of paper and conservation bleaching. *Journal of Chemical Education,* 73, 1068-1073.

Chang, H. T., Wu, N. and Zhu, F. 2000. A kinetic model for photocatalytic degradation of organic contaminants in a thin-film TiO2 catalyst. *Water Research,* 34, 407-416.

Chen, D. and Ray, A. K. 1998. Phtodegradation kinetics of 4-nitrophenol in TiO2 suspension. *Water Research,* 32, 3223-3234.

Chen, Z. and Zheng, S. 2005. Lifetime distribution based degradation analysis. *IEEE Transactions on Reliabiltiy,* 54, 3-10.

Chryssaphinou, O., Limnios, N. and Malefaki, S. 2011. Multi-state reliability systems under discrete time semi-Markovian hypothesis. *IEEE Transactions on Reliability,* 60, 80-87.

Clifton, A. A. and Nugent, N. 2000. Lightfastness performance in digital imaging: the role of dye-dye and dye-polymer interactions. *International Conference on Digital Printing Technologies.*

Compare, M., Baraldi, P., Bani, I., Zio, E. and Mc Donnell, D. 2017. Development of a Bayesian multi-state degradation model for up-to-date reliability estimations of working industrial components. *Reliability Engineering and System Safety.*

Crk, V. 2000. Reliability assessment from degradation data. *Annual Reliability and Maintainability Symposium.*

De Rossi, U., Litz, U. and Blendl, C. 2003. Activation energy of dye degradation processes on different inkjet papers. *International Conference on Digital Printing Technologies*. 450-453.

Deshpande, K., Green, P. and Pointer, M. R. 2014. Colour separation of n-colour printing process using inverse printer models. *Color and Imaging Conference*. 194-199.

Dewar, M., Scerri, K. and Kadirkamanathan, V. 2009. Data-driven spatio-temporal modeling using the integro-difference equation. *IEEE Transactions on Signal Processing,* 57, 83-91.

Ding, H. Z. and Wang, Z. D. 2008. On the degradation evolution equations of cellulose. *Cellulose,* 15, 205-224.

Doksum, K. A. and Hoyland, A. 1992. Models for variable-stress accelerated life testing experiments based on Wiener processes and the inverse Gaussian distribution. *Technometrics,* 34, 74-82.

Drouin, B. and Gagnon, R. 1993. Optical measurement of paper fiber orientation. *Optical Engineering,* 32, 2138-2142.

Einstein, A. 1905. Über die von der molekularkinetischen Theorie der Wärme geforderte Bewegung von in ruhenden Flüssigkeiten suspendierten Teilchen. *Annalen der Physik,* 322, 549-560.

Elsayed, E. A. 2012. *Reliability Engineering, 2nd Edition.* Hoboken, NJ: John Wiley & Sons.

Elsayed, E. A. and Zebib, A. 1979. A reparable multistate device. *IEEE Transactions on Reliability,* R-28, 81-82.

Emsley, A. M., Heywood, R. J., Ali, M. and Eley, C. M. 1997. On the kinetics of degradation of cellulose. *Cellulose,* 4, 1-5.

Emsley, A. M., Heywood, R. J. and Xiao, X. 2000. Degradation of cellulosic insulation in power transformers. part 4: effects of ageing on the tensile strength of paper. *IEE Proceedings - Science, Measurement and Technology,* 147, 285-290.

Eryilmaz, S. 2015. Dynamic assessment of multi-state systems using phase-type modeling. *Reliability Engineering and System Safety,* 140, 71-77.

Eryilmaz, S. 2016. A reliability model for a three-state degraded system having random degradation rates. *Reliability Engineering and System Safety.*

Escobar, L. A. and Meeker, W. Q. 2006. A review of accelerated test models. *Statistical Science,* 21, 552-577.

Feng, J., Kvam, P. H. and Tang, Y. 2016. Remaining useful lifetime prediction based on the damage-marker bivariate degradation model: A case study on lithium-ion batteries used in electric vehicles. *Engineering Failure Analysis,* 70, 323-342.

Fryberg, M. 2005. Dyes for ink-jet printing. *Review of Progress in Coloration and Related Topics,* 35, 1-30.

Gagliardi, M., Lenarda, P. and Paggi, M. 2017. A reaction-diffusion formulation to simulate EVA polymer degradation in environmental and accelerated ageing conditions. *Solar Energy Materials & Solar Cells,* 164, 93-106.

Gebraeel, N. Z. 2006. Sensory-updated residual life distributions for components with exponential degradation patterns. *IEEE Transcations on Automation Science and Engineering,* 3, 382-393.

Gebraeel, N. Z., Elwany, A. and Pan, J. 2009. Residual life predictions in the absence of prior degradation knowledge. *IEEE Transactions on Reliability,* 58, 106-117.

Gebraeel, N. Z., Lawley, M. A., Li, R. and Ryan, J. K. 2005. Residual-life distributions from component degradation signals: A Bayesian approach. *IIE Transactions,* 37, 543-557.

Gebraeel, N. Z. and Pan, J. 2008. Prognostic degradation models for computing and updating residual life distributions in a time-varying environment. *IEEE Transcations on Reliability,* 57, 539-550.

Gschwind, R. 1989. Restoration of faded color photographs by digital image processing. *Proc. SPIE 1135, Image Processing III*. SPIE, 27-30.

Guo, S. and Miller, N. 2001. Estimating light-fastness of inkjet images: Accounting for reciprocity failure. *International Conference on Digital Printing Technologies*. 186-191.

Guo, S., Miller, N. and Weeks, D. 2002. Assessing humid permanence of inkjet photos. *International Conference on Digital Printing Technologies*. 319-325.

Haberman, R. 1987. *Elementary Applied Partial Differential Equations with Fourier Series and Boundary Value Problems.* Englewood Cliffs, New Jersey, USA: Prentice Hall.

Hill, D. J. T., Le, T. T., Darveniza, M. and Saha, T. 1995. A study of degradation of cellulosic insulation materials in a power transformer. part 2: tensile strength of cellulose insulation paper. *Polymer Degradation and Stability,* 49, 429-435.

Hill, P., Suitor, K. and Artz, P. 2000. Measurement of humidity effects on the dark keeping properties of inkjet photographic prints. *International Conference on Digital Printing Technologies*. 70-73.

Hodgson, A. and Jackson, A. M. 2004a. The differences in characteristics of dye based inkjet images subjected to gas and light fading. *International Conference on Digital Printing Technologies*. 734-739.

Hodgson, A. and Jackson, A. M. 2004b. The light fading of dye based inkjet images - a multidimensional issue. *Archiving Conference*. 43-48.

Hofmann, R. and Reber, J. 2009. Humidity diffusion of dye-based IJ prints. *International Conference on Digital Printing Technologies*. 126-129.

Honda, C. 1998. A new method of predicting the oxidative discoloration of silver images. *Journal of Imaging Science and Technology*, 42, 148-152.

Hooten, M. B. and Wikle, C. K. 2008. A hierarchical Bayesian non-linear spatio-temporal model for the spread of invasive species with application to the Eurasian collared-dove. *Environmental and Ecological Statistics,* 15, 59-70.

Howard, R. A. 1964. System analysis of semi-Markov processes. *IEEE Transactions on Military Electronics*, 8, 114-124.

Howard, R. A. 1971. *Dynamic Probabilistic Systems, Vol. 1: Markov Models*. New York, USA: John Wiley and Sons.

Image Permanence Institute. 2004. A consumer guide to traditional and digital print stability. Available: https://www.imagepermanenceinstitute.org/webfm_send/313.

Image Permanence Institute. 2009. A consumer guide to understanding permanence testing. Available: https://www.imagepermanenceinstitute.org/webfm_send/311.

Image Permanence Institute. 2010. A consumer guide to materials for preservation framing and the display of photographic images. Available: https://www.imagepermanenceinstitute.org/webfm_send/312.

Immergut, E. H., Schurz, J. and Mark, H. 1953. Viskositätszahl-Molekulargewichts-Beziehung für Cellulose und Untersuchungen von Nitrocellulose in verschiedenen Lösungsmitteln. *Monatshefte für Chemie,* 84, 219-249.

International Standards Office. 2006. *Photography - processed photographic colour films and paper prints - methods for measuring image stability*.

Jin, G. and Matthews, D. 2014. Measurement plan optimization for degradation test design based on the bivariate Wiener process. *Quality and Reliability Engineering International,* 30, 1215-1231.

Johnson, M. E., Moore, L. M. and Ylvisaker, D. 1990. Minimax and maximin distance designs. *Journal of Statistical Planning and Inference,* 26, 131-148.

Johnston-Feller, R., Feller, R. L., Bailie, C. W. and Curran, M. 1984. The kinetics of fading: Opaque paint films pigmented with alizarin lake and titanium dioxide. *Journal of the American Institute for Conservation,* 23, 114-129.

Joseph, V. R. and Yu, I.-T. 2006. Reliability improvement experiments with degradation data. *IEEE Transactions on Reliability,* 55, 149-157.

Kallen, M. J. and van Noortwijk, J. M. 2005. Optimal maintenance decisions under imperfect inspection. *Reliability Engineering and System Safety,* 90, 177-185.

Kao, E. P. C. 1973. Optimal replacement rules when changes of state are semi-Markovian. *Operations Research,* 21, 1231-1249.

Kimmel, B. W. and Baranoski, G. V. G. 2016. Practical acceleration strategies for the predictive visualization of fading phenomena. *International Conference on Computer Animation and Social Agents*. 45-52.

Kimmel, B. W., Baranoski, G. V. G., Chen, T. F., Yim, D. and Miranda, E. 2013. Spectral appearance changes induced by light exposure. *ACM Transactions on Graphics,* 32, 10:1-10:13.

Kuniewski, S. P., van der Weide, J. A. M. and van Noortwijk, J. M. 2009. Sampling inspection for the evaluation of time-dependent reliability of deteriorating systems under imperfect defect detection. *Reliability Engineering and System Safety,* 94, 1480-1490.

Kunii, T. L., Nosovskij, G. V. and Hayashi, T. 1995. A diffusion model for computer animation of diffuse ink painting. *Proceedings Computer Animation*. 98-102.

Lawless, J. F. and Crowder, M. J. 2004. Covariates and random effects in a gamma process model with application to degradation and failure. *Lifetime Data Analysis,* 10, 213-227.

Li, N., Taylor, L. S. and Mauer, L. J. 2011. Degradation kinetics of catechins in green tea powder: effects of temperature and relative humidity. *Journal of Agricultural and Food Chemistry,* 59, 6082-6090.

Li, Y. and Nilkitsaranont, P. 2009. Gas turbine performance prognostic for condition-based maintenance. *Applied Energy,* 86, 2152-2161.

Liao, C. and Tseng, S. 2006. Optimal design for step-stress accelerated degradation tests. *IEEE Transactions on Reliability,* 55, 59-66.

Liao, H. and Elsayed, E. A. 2006. Reliability inference for field conditions from accelerated degradation testing. *Naval Research Logistics,* 53, 576-587.

Liao, H. and Tian, Z. 2013. A framework for predicting the remaining useful life of a single unit under time-varying operating conditions. *IIE Transactions,* 45, 964-980.

Lim, H. and Yum, B. 2011. Optimal design of accelerated degradation tests based on Wiener process models. *Journal of Applied Statistics,* 38, 309-325.

Lisnianski, A. 2007. Extended block diagram method for a multi-state system reliability assessment. *Reliability Engineering and System Safety,* 92, 1601-1607.

Lisnianski, A. and Levitin, G. 2003. *Multi-State System Reliability: Assessment, Optimization and Applications.* World Scientific.

Liu, X., Yeo, K., Hwang, Y., Singh, J. and Kalagnanam, J. 2016. A statistical modeling approach for air quality data based on physical dispersion processes and its application to ozone modeling. *The Annals of Applied Statistics,* 10, 756-785.

Liu, Y.-W. and Kapur, K. C. 2006. Reliability measures for dynamic multistate nonrepairable systems and their applications to system performance evaluation. *IIE Transactions,* 38, 511-520.

Liu, Y.-W. and Kapur, K. C. 2008. New patient-centered models of quality-of-life measures for evaluation of interventions for multi-stage diseases. *IIE Transactions*, 40, 870-879.

Liu, Y. and Huang, H. 2010. Optimal replacement policy for multi-state system under imperfect maintenance. *IEEE Transactions on Reliability*, 59, 483-495.

Liu, Y., Zuo, M., Li, Y. and Huang, H. 2015. Dynamic reliability assessment for multi-state systems utilizing system-level inspection data. *IEEE Transactions on Reliability*, 64, 1287-1299.

Lu, C. J. and Meeker, W. Q. 1993. Using degradation measures to estimate a time-to-failure distribution. *Technometrics*, 35, 161-174.

Lu, D., Pandey, M. D. and Xie, W. 2013. An efficient method for the estimation of parameters of stochastic gamma process from noisy degradation measurements. *Proceedings of the Institution of Mechanical Engineers, Part O: Journal of Risk and Reliability*, 227, 425-433.

Lu, J., Park, J. and Yang, Q. 1997. Statistical inference of a time-to-failure distribution derived from linear degradation data. *Technometrics*, 39, 391-400.

LuValle, M. J., Welsher, T. L. and Svoboda, K. 1988. Acceleration transforms and statistical kinetic models. *Journal of Statistical Physics*, 52, 311-330.

Mahy, M. 1998. Insight into the solutions of the Neugebauer equations. *Proceedings of the SPIE - The International Society for Optical Engineering*. 76-85.

Mahy, M. and Delabastita, P. 1996. Inversion of the Neugebauer equations. *Color Research and Application*, 21, 404-411.

Malmberg, A., Arellano, A., Edwards, D. P., Flyer, N., Nychka, D. and Wikle, C. K. 2008. Interpolating fields of carbon monoxide data using a hybrid statistical-physical model. *The Annals of Applied Statistics*, 2, 1231-1248.

Manzocco, L., Panozzo, A. and Calligaris, S. 2012. Accelerated shelf life testing (ASLT) of oils by light and temperature exploitation. *Journal of the American Oil Chemists' Society*, 89, 577-583.

Mao, C. Q. 2001. *Local rewetting and distortion of paper*. Thesis (MS), University of Toronto.

Marseguerra, M., Zio, E. and Podofillini, L. 2002. Condition-based maintenance optimization by means of genetic algorithms and Monte Carlo simulation. *Reliability Engineering and System Safety*, 77, 151-166.

McCormick-Goodhart, M. and Wilhelm, H. 2000. Humidity-induced color changes and ink migration effects in inkjet photographs in real-world environmental conditions. *International Conference on Digital Printing Technologies*. 74-77.

McCormick-Goodhart, M. and Wilhelm, H. 2001. The influence of relative humidity on short-term color drift in inkjet prints. *International Conference on Digital Printing Technologies*. 179-185.

McCormick-Goodhart, M. and Wilhelm, H. 2003a. The correlation of line quality degradation with color changes in inkjet prints exposed to high relative humidity. *International Conference on Digital Printing Technologies*. 420-425.

McCormick-Goodhart, M. and Wilhelm, H. 2003b. A new test method based on CIELAB colorimetry for evaluating the permanence of pictorial images. Available: http://wilhelm-imaging.com/pdf/WIR_CIELAB_TEST_2003_07_25.pdf.

McCormick-Goodhart, M. and Wilhelm, H. 2005. New test methods for evaluating the humidity-fastness of inkjet prints. *The Annual Conference of the Imaging Society of Japan*. 95-98.

McPherson, J. W. 2010. *Reliability Physics and Engineering: Time-to-Failure Modeling.* New York: Springer.

Medley, J. 2009. Semiempirical predictive kinetic model of light induced magenta dye-based ink jet ink fading on polymer-coated photomedia. *Journal of Imaging Science and Technology,* 53, 40501-1-40501-6.

Meeker, W. Q. and Escobar, L. A. 1998. *Statistical Methods for Reliability Data.* New York: John Wiley & Sons.

Meeker, W. Q., Escobar, L. A. and Lu, C. J. 1998. Accelerated degradation tests: Modeling and analysis. *Technometrics,* 10, 89-99.

Meeker, W. Q. and LuValle, M. J. 1995. An accelerated life test model based on reliability kinetics. *Technometrics,* 37, 133-146.

Mehrotra, K., Yablonsky, G. S. and Ray, A. K. 2003. Kinetic studies of photocatalytic degradation in a TiO2 slurry system: distinguishing working regimes and determining rate dependences. *Industrial & Engineering Chemistry Research,* 42, 2273-2281.

Menart, E., De Bruin, G. and Strlic, M. 2011. Dose-response functions for historic paper. *Polymer Degradation and Stability,* 96, 2029-2039.

Morris, M. D. and Mitchell, T. J. 1995. Exploratory designs for computational experiments. *Journal of Statistical Planning and Inference,* 43, 381-402.

Nash, E., Benson, R., White, G., Holbert, R. M. and Wilhelm, H. G. 2007. *Nash Editions: photography and the art of digital printing.* New Riders.

Naversnik, K. and Jurecic, R. 2016. Humidity-corrected Arrhenius equation: the reference condition approach. *International Journal of Pharmaceutics,* 500, 360-365.

Nelson, W. 1990. *Accelerated Testing: Statistical Models, Test Plans, and Data Analysis.* New York: John Wiley & Sons.

Neugebauer, H. E. J. 1937. Die Theoretischen Grundlagen des Mahrfarbenbuchdrucks. *Zeitschrift fur Wissenschaftliche Photographie Photophysik und Photochemie,* 36, 73-89.

Nicolai, R. P., Budai, G., Dekker, R. and Vreijing, M. 2004. Modeling the deterioration of the coating on steel structures: a comparison of methods. *IEEE International Conference on Systems, Man and Cybernetics.*

Nicolai, R. P., Dekker, R. and van Noortwijk, J. M. 2007. A comparison of models for measurable deterioration: An application to coatings on steel structures. *Reliability Engineering and System Safety,* 92, 1635-1650.

Nunn, W. R. and Desiderio, A. M. 1977. Semi-Markov processes: An introduction. Center for Naval Analyses.

Oldfield, D. J., Pino, G., Segur, R. K., Odell, S. F. and Twist, J. P. 2004. Assessment of the current light-fade endpoint metrics used in the determination of print life - part I. *Journal of Imaging Science and Technology,* 48, 495-501.

Pan, D., Liu, J. and Cao, J. 2016. Remaining useful life estimation using an inverse Gaussian degradation model. *Neurocomputing,* 185, 64-72.

Pan, Z. and Balakrishnan, N. 2011. Reliability modeling of degradation of products with multiple performance characteristics based on gamma processes *Reliability Engineering and System Safety*, 96, 949-957.

Pan, Z., Balakrishnan, N. and Sun, Q. 2011. Bivariate constant-stress accelerated degradation model and inference. *Communications in Statistics - Simulation and Computation*, 40, 247-257.

Park, C. and Padgett, W. J. 2005. Accelerated degradation models for failure based on geometric Brownian motion and gamma processes. *Lifetime Data Analysis,* 11, 511-527.

Park, C. and Padgett, W. J. 2006. Stochastic degradation models with several accelerating variables. *IEEE Transactions on Reliability,* 55, 379-390.

Park, N. C., Oh, W. W. and Kim, D. H. 2013. Effect of temperature and humidity on the degradation rate of multicrystalliine silicon photovoltaic module. *International Journal of Photoenergy*.

Peck, D. S. 1986. Comprehensive model for humidity testing correlation. *International Reliability Physics Symposium*. IEEE, 44-50.

Peng, C. 2015. Inverse Gaussian processes with random effects and explanatory variables for degradation data. *Technometrics,* 57, 100-111.

Peng, C. and Hsu, S. 2012. A note on a Wiener process with measurement error. *Applied Mathematics Letters,* 25, 729-732.

Peng, C. and Tseng, S. 2009. Mis-specification analysis of linear degradation models. *IEEE Transactions on Reliability,* 58, 444-455.

Peng, C. and Tseng, S. 2013. Statistical lifetime inference with skew-Wiener linear degradation models. *IEEE Transactions on Reliability,* 62, 338-350.

Peng, W., Li, Y., Mi, J., Yu, L. and Huang, H. 2016a. Reliability of complex systems under dynamic conditions: A Bayesian multivariate degradation perspective. *Reliability Engineering and System Safety*, 153, 75-87.

Peng, W., Li, Y., Y., Y., Mi, J. and Huang, H. 2017. Bayesian degradation analysis with inverse Gaussian process models under time-varying degradation rates. *IEEE Transactions on Reliability,* 66, 84-96.

Peng, W., Li, Y., Yang, Y., Huang, H. and Zuo, M. 2014. Inverse Gaussian process models for degradation analysis: A Bayesian perspective *Reliability Engineering and System Safety* 130, 175-189.

Peng, W., Li, Y., Yang, Y., Zhu, S. and Huang, H. 2016b. Bivariate analysis of incomplete degradation observations based on inverse Gaussian processes and copulas *IEEE Transactions on Reliability,* 65, 624-639.

Pugh, S. L. and Guthrie, J. T. 2001. The development of light fastness testing and light fastness standards. *Review of Progress in Coloration,* 31, 42-56.

Pugh, S. L. and Guthrie, J. T. 2002. Some characteristics of pigments that affect the kinetics of fading of prints made from water-based liquid ink formulations. *Dyes and Pigments,* 55, 109-121.

Roberts, J. C. 2007. *The Chemistry of Paper*. Cambridge: Royal Society of Chemistry.

Robinson, M. E. and Crowder, M. J. 2000. Bayesian methods for a growth-curve degradation model with repeated measures. *Lifetime Data Analysis,* 6, 357-374.

Sahu, S. K., Gelfand, A. E. and Holland, D. M. 2007. High-resolution space-time ozone modeling for assessing trends. *Journal of the American Statistical Association*, 102, 1221-1234.

Salesin, E. and Burge, D. 2014. The determination of humidity limits to prevent colorant bleed in inkjet prints. *Digital Fabrication and Digital Printing*. 79-83.

Sari, J. K., Newby, M. J., Brombacher, A. C. and Tang, L. C. 2009. Bivariate constant stress degradation model: LED lighting system reliability estimation with two - stage modelling. *Quality and Reliability Engineering International*, 25, 1067-1084.

Scerri, K., Dewar, M. and Kadirkamanathan, V. 2009. Estimation and model selection for an IDE-based spatio-temporal model. *IEEE Transactions on Signal Processing*, 57, 482-492.

Sheu, S. and Zhang, Z. 2013. An optimal age replacement policy for multi-state systems. *IEEE Transactions on Reliability*, 62, 722-735.

Shi, X. and Lu, D. 2005. Colorimetric and chemical modeling based aging simulation of Dunhuang murals. *International Conference on Computer and Information Technology*.

Shibahara, Y., Machida, M., Ishibashi, H. and Ishizuka, H. 2004. Endpoint criteria for print life estimation. *International Conference on Digital Printing Technologies*. 673-679.

Shu, M., Hsu, B. and Kapur, K. C. 2010. Dynamic performance measures for tools with multi-state wear processes and their applications for tool design and selection. *International Journal of Production Research*, 48, 4725-4744.

Si, X., Chen, M., Wang, W., Hu, C. and Zhou, D. 2013a. Specifying measurement errors for required lifetime estimation performance. *European Journal of Operational Research*, 231, 631-644.

Si, X., Wang, W., Chen, M., Hu, C. and Zhou, D. 2013b. A degradation path-dependent approach for remaining useful life estimation with an exact and closed-form solution. *European Journal of Operational Research*, 226, 53-66.

Si, X., Wang, W., Hu, C., Chen, M. and Zhou, D. 2013c. A Wiener-process-based degradation model with a recursive filter algorithm for remaining useful life estimation. *Mechanical Systems and Signal Processing*, 35, 219-237.

Si, X., Wang, W., Hu, C. and Zhou, D. 2011. Remaining useful life estimation: A review on the statistical data driven approaches. *European Journal of Operational Research*, 213, 1-14.

Sigrist, F., Künsch, H. R. and Stahel, W. A. 2011. An autoregressive spatio-temporal precipitation model. *Procedia Environmental Sciences.*

Sigrist, F., Künsch, H. R. and Stahel, W. A. 2012. A dynamic nonstationary spatio-temporal model for short term prediction of precipitation. *The Annals of Applied Statistics*, 6, 1452-1477.

Sigrist, F., Künsch, H. R. and Stahel, W. A. 2015. Stochastic partial differential equation based modelling of large space-time data sets. *Journal of the Royal Statistical Society: Series B (Statistical Methodology)*, 77, 3-33.

Son, K. L., Fouladirad, M. and Barros, A. 2016. Remaining useful lifetime estimation and noisy gamma deterioration process. *Reliability Engineering and System Safety*, 149, 76-87.

Soro, I. W., Nourelfath, M. and Ait-Kadi, D. 2010. Performance evaluation of multi-state degraded systems with minimal repairs and imperfect preventive maintenance. *Reliability Engineering and System Safety,* 95, 65-69.

Stroud, J. R., Stein, M. L., Lesht, B. M., Schwab, D. J. and Beletsky, D. 2010. An ensemble Kalman filter and smoother for satellite data assimilation. *Journal of the American Statistical Association,* 105, 978-990.

Taplin, L. A. 2001. *Spectral modeling of a six-color inkjet printer.* Thesis (MS), Rochester Institute of Technology.

Tsai, T., Lin, C., Sung, Y., Chou, P., Chen, C. and Lio, Y. 2012. Inference from lumen degradation data under Wiener diffusion process *IEEE Transactions on Reliability,* 61, 710-718.

Tzeng, D. 1999. *Spectral-based color separation algorithm development for multiple-ink color reproduction.* Thesis (PhD), Rochester Institute of Technology.

Tzeng, D. and Berns, R. S. 1998. Spectral-based ink selection for multiple-ink printing I. colorant estimation of original objects. *The Sixth Color Imaging Conference: Color Science, Systems, and Applications*. 106-111.

Urban, P., Rosen, M. R. and Berns, R. S. 2007. Accelerating spectral-based color separation within the Neugebauer subspace. *Journal of Electronic Imaging,* 16, 043014-1-043014-11.

van Noortwijk, J. M. 2009. A survey of the application of gamma processes in maintenance. *Reliability Engineering and System Safety,* 94, 2-21.

van Noortwijk, J. M., van der Weide, J. A. M., Kallen, M. J. and Pandey, M. D. 2007. Gamma processes and peaks-over-threshold distributions for time-dependent reliability. *Reliability Engineering and System Safety,* 92, 1651-1658.

Veeramany, A. and Pandey, M. D. 2011. Reliability analysis of nuclear piping system using semi-Markov process model. *Annals of Nuclear Energy,* 38, 1133-1139.

Vikman, K. 2004. *Studies on fastness properties of ink jet prints on coated papers.* Thesis (PhD), Helsinki University of Technology.

Wang, W., Carr, M., Xu, W. and Kobbacy, K. 2011. A model for residual life prediction based on Brownian motion with an adaptive drift. *Microelectronics Reliability,* 51, 285-293.

Wang, W., Scarf, P. A. and Smith, M. A. J. 2000. On the application of a model of condition-based maintenance. *Journal of the Operational Research Society,* 51, 1218-1227.

Wang, X.-L., Balakrishnan, N. and Guo, B. 2015a. Residual life estimation based on nonlinear-multivariate Wiener processes. *Journal of Statistical Computation and Simulation,* 85, 1742-1764.

Wang, X.-L., Balakrishnan, N., Guo, B. and Jiang, P. 2015b. Residual life estimation based on bivariate non-stationary gamma degradation process. *Journal of Statistical Computation and Simulation,* 85, 405-421.

Wang, X.-L., Guo, B. and Cheng, Z. 2014a. Residual life estimation based on bivariate Wiener degradation process with time-scale transformations. *Journal of Statistical Computation and Simulation,* 84, 545-563.

Wang, X.-L., Jiang, P., Guo, B. and Cheng, Z. 2014b. Real-time reliability evaluation with a general Wiener process-based degradation model. *Quality and Reliability Engineering International,* 30, 205-220.

Wang, X. 2010. Wiener processes with random effects for degradation data. *Journal of Multivariate Analysis,* 101, 340-351.

Wang, X. and Xu, D. 2010. An inverse Gaussian process model for degradation data. *Technometrics*, 52, 188-197.

Whitmore, G. A. 1995. Estimating degradation by a Wiener diffusion process subject to measurement error. *Lifetime Data Analysis*, 1, 307-319.

Whitmore, G. A., Crowder, M. J. and Lawless, J. F. 1998. Failure inference from a marker process based on a bivariate Wiener model. *Lifetime Data Analysis,* 4, 229-251.

Whitmore, G. A. and Schenkelberg, F. 1997. Modelling accelerated degradation data using Wiener diffusion with a time scale transformation. *Lifetime Data Analysis,* 3, 27-45.

Wikle, C. K. 1999. A dimension-reduced approach to space-time Kalman filtering. *Biometrika,* 86, 815-829.

Wikle, C. K. 2002. A kernel-based spectral model for non-Gaussian spatio-temporal processes. *Statistical Modelling,* 2, 299-314.

Wikle, C. K. 2003. Hierarchical Bayesian models for predicting the spread of ecological processes. *Ecology*, 84, 1382-1394.

Wikle, C. K., Berliner, L. M. and Cressie, N. 1998. Hierarchical Bayesian space-time models. *Environmental and Ecological Statistics,* 5, 117-154.

Wikle, C. K., Berliner, L. M. and Milliff, R. F. 2003. Hierarchical Bayesian approach to boundary value problems with stochastic boundary conditions. *Monthly Weather Review,* 131, 1051-1062.

Wilhelm, H. 2002. How long will they last? an overview of the light-fading stability of inkjet prints and traditional color photographs. *International Symposium on Photofinishing Technology*. 32-37.

Wilhelm, H. 2003a. Light-induced and thermally-induced yellowish stain formation in inkjet prints and traditional chromogenic color photographs. *The Annual Conference of the Imaging Society of Japan*. 213-216.

Wilhelm, H. 2003b. Yellowish stain formation in inkjet prints and traditional silver-halide color photographs. *International Conference on Digital Printing Technologies*. 444-449.

Wilhelm, H. 2004. A review of accelerated test methods for predicting the image life of digitally-printed photographs. *The Annual Conference of the Imaging Society of Japan*. 81-84.

Wilhelm, H. 2007. A survey of print permanence in the 4×6-inch consumer digital print market in 2004-2007. *IS&T's International Symposium on Technologies for Digital Fulfillment*. 43-47.

Wilhelm, H., Armah, K., Shklyarov, D., Stahl, B. and Tasev, D. 2007. A study of "unprotected ozone resistance" of photographs made with inkjet and other digital printing technologies. *Imaging Conference JAPAN*. 137-140.

Wilhelm, H., Boydston, K., Armah, K. and Stahl, B. C. 2011. Use of a multispectral camera system and very small, comprehensive "micropatch" test targets for full tonal scale colorimetric evaluation of the permanence of digitally-printed color and B&W photographs. *Imaging Conference JAPAN*. 131-134.

Wilhelm, H. and Brower, C. 1993. *The Permanence and Care of Color Photographs: Traditional and Digital Color Prints, Color Negatives, Slides, and Motion Pictures.* Grinnell, IA, USA: Preservation Publishing Company.

Wilhelm, H. and McCormick-Goodhart, M. 2000. An overview of the permanence of inkjet prints compared with traditional color prints. *International Symposium on Photofinishing Technology*. 34-39.

Wilhelm, H. and McCormick-Goodhart, M. 2001. Reciprocity behavior in the light stability testing of inkjet photographs. *International Conference on Digital Printing Technologies*. 197-202.

Wu, J. and Berland, K. M. 2008. Propagators and time-dependent diffusion coefficients for anomalous diffusion. *Biophysical Journal,* 95, 2049-2052.

Wyble, D. R. and Berns, R. S. 2000. A critical review of spectral models applied to binary color printing. *Color Research and Application,* 25, 4-19.

Xiao, X. and Ye, Z. 2016. Optimal design for destructive degradation tests with random initial degradation values using the Wiener process. *IEEE Transactions on Reliability,* 65, 1327-1342.

Xu, K. and Wikle, C. K. 2007. Estimation of parameterized spatio-temporal dynamic models. *Journal of Statistical Planning and Inference,* 137, 567-588.

Xu, K., Wikle, C. K. and Fox, N. I. 2005. A kernel-based spatio-temporal dynamical model for nowcasting weather radar reflectivities. *Journal of the American Statistical Association,* 100, 1133-1144.

Xue, J. and Yang, K. 1995. Dynamic reliability analysis of coherent multistate systems. *IEEE Transactions on Reliability,* 44, 683-688.

Yang, C. F., Crosby, C. M., Eusufzai, A. R. K. and Mark, R. E. 1987. Determination of paper sheet fiber orientation distributions by a laser optical diffraction method. *Journal of Applied Polymer Science,* 34, 1145-1157.

Ye, Z. and Chen, N. 2014. The inverse Gaussian process as a degradation model. *Technometrics,* 56, 302-311.

Ye, Z., Chen, N. and Tsui, K. 2015. A Bayesian approach to condition monitoring with imperfect inspections. *Quality and Reliability Engineering International,* 31, 513-522.

Ye, Z., Wang, Y., Tsui, K. and Pecht, M. G. 2013. Degradation data analysis using Wiener processes with measurement errors. *IEEE Transactions on Reliability,* 62, 772-780.

Ye, Z. and Xie, M. 2015. Stochastic modelling and analysis of degradation for highly reliable products. *Applied Stochastic Models in Business and Industry,* 31, 16-32.

Yin, M., Angus, J. E. and Trivedi, K. S. 2013. Optimal preventive maintenance rate for best availability with hypo-exponential failure distribution. *IEEE Transactions on Reliability,* 62, 351-361.

Yu, H. 2006. Designing an accelerated degradation experiment with a reciprocal Weibull degradation rate. *Journal of Statistical Planning and Inference,* 136, 282-297.

Yuan, X. and Pandey, M. D. 2009. A nonlinear mixed-effects model for degradation data obtained from in-service inspections. *Reliability Engineering and System Safety,* 94, 509-519.

Yule, J. A. C. and Neilsen, W. J. 1951. The penetration of light into paper and its effect on halftone reproduction. *TAGA Proceedings*. 65-76.

Zhang, S., Zhou, W. and Qin, H. 2013. Inverse Gaussian process-based corrosion growth model for energy pipelines considering the sizing error in inspection data. *Corrosion Science,* 73, 309-320.

Zhang, Z., Si, X., Hu, C. and Lei, Y. 2018. Degradation data analysis and remaining useful life estimation: A review on Wiener-process-based methods. *European Journal of Operational Research,* 271, 775-796.

Zhou, R., Serban, N. and Gebraeel, N. Z. 2014. Degradation-based residual life prediction under different environments. *The Annals of Applied Statistics,* 8, 1671-1689.

Zhou, Y., Sun, Y., Mathew, J., Wolff, R. and Ma, L. 2011. Latent degradation indicators estimation and prediction: A Monte Carlo approach. *Mechanical Systems and Signal Processing,* 25, 222-236.

Zou, X., Gurnagul, N., Uesaka, T. and Bouchard, J. 1994. Accelerated aging of papers of pure cellulose: mechanism of cellulose degradation and paper embrittlement. *Polymer Degradation and Stability,* 43, 393-402.

Zuo, M., Jiang, R. and Yam, R. C. M. 1999. Approaches for reliability modeling of continuous-state devices. *IEEE Transactions on Reliability,* 48, 9-18.